

POLITECNICO DI TORINO

Dipartimento di Ingegneria Meccanica e Aerospaziale

Tesi di Laurea Magistrale in Automotive Engineering



EFFECT OF THERMALLY EXPANDABLE PARTICLE ADDITIVES ON THE MECHANICAL PERFORMANCE OF MIXED MATERIAL ADHESIVE JOINTS

Academic Supervisor:
Prof. Giovanni Belingardi

Co-Supervisors:
Dr. Sayed A. Nassar (Oakland University)

Candidate:
Giulio Piazza

ACADEMIC YEAR 2019 - 2020

© Giulio Piazza, 2020
All rights are reserved

To my beloved family, girlfriend and friends

ACKNOWLEDGMENTS

Firstly, I would like to thank my advisor, Professor Sayed Nassar, for all the help and support that has provided me to learn and improve myself, inside and outside the academic environment. This journey has been successful thanks to you and in the way the FAJRI works as a group.

I would also like to thank Professor Giovanni Belingardi and the Politecnico of Turin, that allow students like me to be part of this kind of experience, that is useful to apply what has been study in the past years.

I am also deeply grateful to my FCA advisors Gabriele Ciaccio and David Biernat, which have demonstrated his interest on my research. David has been crucial for the realization of my thesis, together with the amazing guys at DuPont: Arthur F. Cawley, Brad Limberg and Raymond F. Bis. Without their expertise, this research would have required much more time and effort. Furthermore, I would like to offer my special thanks to the Hugh Foran of Teijin Continental Structural Plastic, for their great help in providing the carbon fibers substrates, necessary for the study.

Marco Gerini Romagnoli deserves a special mentioning too, He has been an important point of reference inside the FAJRI labs, but mainly outside it. He helped me to adapt in a different country and to learn from it. If it wasn't for him, I will be still sleeping on an air mattress on the floor.

ABSTRACT

EFFECT OF THERMALLY EXPANDABLE PARTICLE ADDITIVES ON THE MECHANICAL PERFORMANCE OF MIXED MATERIAL ADHESIVE JOINTS

By

Giulio Piazza

Supervisor: Prof. Giovanni Belingardi

This research investigates the effect of the addition of Thermally Expandable Particles (TEP) to a commercially available adhesive on the mechanical performance of bonded mixed material Single Lap Joints (SLJs) in lap shear tests.

Investigated variables include additive concentration by weight (from 5 to 20%) and particulate size (ranging between 6 and 16 micrometers), for their effect on joint static and fatigue strength, as well as reversibility performance, as compared to those of SLJs bonded with the baseline adhesive with no additives.

Each test joint is made by one Aluminum 6061 substrate that is adhesively-bonded to a composite substrate made of woven carbon fiber reinforced plastic 0/90/0 with epoxy matrix. The test samples are bonded using a commercially available epoxy adhesive that has been modified using two types of polymeric TEP additives with gaseous core.

Lap shear tests are conducted to evaluate the maximum static Load Transfer Capacity (LTC), and fatigue S-N curves for a selected level of mean stress are drawn. Results show that particle enrichment is detrimental to the baseline adhesive performance in both static and fatigue scenarios.

Reversibility performance is assessed using a charged RF coil that heats the substrate bondline by induction, causing significant volumetric expansion of the additive particles (TEP's) that leads to complete debonding of the adhesive joint. The time to complete debonding is used for assessing adhesive reversibility performance as affected by the concentration and the particulate size of the additive.

TABLE OF CONTENTS

ACKNOWLEDGMENTS	iv
ABSTRACT	v
LIST OF TABLES	ix
LIST OF FIGURES	x
NOMENCLATURE	xvi
CHAPTER ONE	
INTRODUCTION AND LITERATURE SURVEY	1
1.1. Introduction	1
1.2. Adhesive Bonding	5
1.3. Objectives	13
CHAPTER TWO	
EXPERIMENTAL SET UP AND TEST PROCEDURE	15
2.1. Material Selection and Sample Preparation	15
2.2. Selection of Baseline Adhesive and Additives	18
2.2.1. Adhesive Selection	18
2.2.2. Additives Selection	20
2.3. Scanning Electron Microscopy Imaging of Additive Materials	22
2.4. Lap Shear Tests	26
2.4.1. Static Lap Shear Test Procedure	26
2.4.2. Fatigue Testing	26
2.4.3. Adopted Statistical Approach	29
2.5. Debonding Test Set up	30

TABLE OF CONTENTS – Continued

CHAPTER THREE	
RESULTS AND DISCUSSION	34
3.1. Static Strength	34
3.1.1. Baseline Static Performance	34
3.1.2. Effect of Additive Concentration on Static Strength	35
3.1.3. Particulate size Effect on Lap Shear Strength	44
3.2. Fatigue Test Data and Analysis	48
3.2.1. Fatigue Performance of Baseline adhesive SLJs	49
3.2.2. Effect of Additive Concentration on Fatigue Performance	50
3.3. Debonding Test	72
3.3.1 Effect of Particle Enrichment on Debonding Performance	73
3.3.2 Residual Strength Analysis	76
CHAPTER FOUR	
CONCLUSIONS	78
APPENDICES	79
A. COPIRIGHT PERMISSION LETTER	79
REFERENCES	82

LIST OF TABLES

Table 2.1	Substrates Material Properties	15
Table 2.2	Thermally Expandable Particle Characteristics	21
Table 3.1	Chosen Alternating Stress levels for Fatigue Tests	51

LIST OF FIGURES

Figure 1.1	Mass produced Vehicles Weight Features from 1975 to 2010	2
Figure 1.2	Evolution of Lightweight Material Use in Passenger Vehicles [adapted from 7]	4
Figure 1.3	Sample of (partial) galvanic corrosion chart	5
Figure 1.4	Example of Heating Setup for Debonding Test	13
Figure 1.5	Illustration of particle volume expansion due to RF heating in debonding	14
Figure 2.1	Surface topography of aluminum coupons	16
Figure 2.2	3D Surface topology of aluminum coupons	17
Figure 2.3	Surface topology of carbon fiber coupons	17
Figure 2.4	3D Surface Topology of Carbon Fiber Coupons	18
Figure 2.5	Adhesive Screening Strength Comparison	19
Figure 2.6	Adhesive and Particles a) Before mixing, b) After two stage mixing	21
Figure 2.7	Curing Schedule Temperature Profile	22
Figure 2.8	SEM images of 031DU40 and 461DU20 particles	24
Figure 2.9	Polarized reflected light images of 031DU40 and 461DU20 particles mixed with Betamate 73326/73327 M	24
Figure 2.10	SEM images of adhesive cross-section 031DU40 particles before and after heating	25
Figure 2.11	SEM images of adhesive cross-section 461DU20 particles before and after heating	25
Figure 2.12	MTS 810 Material test system	27
Figure 2.13	a) Single Lap Joint dimensions (mm)	27
Figure 2.14	Illustration of applied fatigue load parameters	28

LIST OF FIGURES – Continued

Figure 2.15	Baseline fatigue results for different mean stress levels	28
Figure 2.16	RDO Model HFI - 3.0 kW RF Heating System 135-400 KHz	31
Figure 2.17	Induction RF Coil Dimensions	31
Figure 2.18	Sample Positioning inside RF coil	32
Figure 2.19	Schematic of Debonding Fixture	33
Figure 3.1	Static Performance Tests Data for Baseline Betamate (73326/73327 M)	35
Figure 3.2	5% Concentration Large Size Particles (031DU40) Betamate 73326/77327M Static Test Data	37
Figure 3.3	5% Concentration Small Size Particles (461DU20) Betamate 73326/77327M Static Test Data	37
Figure 3.4	5% Additive Concentration vs Baseline Adhesive Stress-Displacement Curves	38
Figure 3.5	Effect of Additive Size on Baseline Adhesive Static Performance (5% Concentration)	38
Figure 3.6	10% Concentration Large Size Particles (031DU40) Betamate 73326/77327M Static Test Data	40
Figure 3.7	10% Concentration Small Size Particles (461DU20) Betamate 73326/77327M Static Test Data.	40
Figure 3.8	10% Additive Concentration vs Baseline Adhesive Stress-Displacement Curves	41
Figure 3.9	Effect of Additive Size on Baseline Adhesive Static Performance (10% Concentration)	41
Figure 3.10	FEA model of multi-material joint	42
Figure 3.11	Peel Stress Gradient along the adhesive thickness: a) Carbon Fiber Side b) Aluminum Side	42

LIST OF FIGURES – Continued

Figure 3.12	Illustration of failure mode change due to particle enrichment	43
Figure 3.13	20% Concentration Large Size Particles (031DU40) Betamate 73326/77327M Static Test Data	45
Figure 3.14	20% Concentration Small Size Particles (461DU20) Betamate 73326/77327M Static Test Data.	45
Figure 3.15	20% Additive Concentration vs Baseline Adhesive Stress-Displacement Curves	46
Figure 3.16	Effect of Additive Size on Baseline Adhesive Static Performance (20% Concentration)	46
Figure 3.17	Lap Shear Strength Variation Betamate 73326/73327M for Different Additive Concentrations	47
Figure 3.18	Baseline Betamate (73326/73327M) Fatigue Performance (S-N curve)	49
Figure 3.19	5% Concentration Small Particle (461DU20) Fatigue performance (S-N curve)	52
Figure 3.20	5% Concentration Large Particle (031DU40) Fatigue performance (S-N curve)	53
Figure 3.21	Fatigue Data for 5% Additive Concentration vs Baseline Prediction Intervals (Small Particle 461DU20)	53
Figure 3.22	Fatigue Data for 5% Additive Concentration vs Baseline Confidence Intervals (Small Particle 461DU20)	54
Figure 3.23	Fatigue Data for 5% Additive Concentration vs Baseline Prediction Intervals (Small Particle 461DU20, non-normalized)	54
Figure 3.24	Fatigue Data for 5% Additive Concentration vs Baseline Confidence Intervals (Small Particle 461DU20, non-normalized)	55

LIST OF FIGURES – Continued

Figure 3.25	Fatigue Data for 5% Additive Concentration vs Baseline Prediction Intervals (Large Particle 031DU40)	55
Figure 3.26	Fatigue Data for 5% Additive Concentration vs Baseline Confidence Intervals (Large Particle 031DU40)	56
Figure 3.27	Fatigue Data for 5% Additive Concentration vs Baseline Prediction Intervals (Large Particle 031DU40, non-normalized)	56
Figure 3.28	Fatigue Data for 5% Additive Concentration vs Baseline Confidence Intervals (Large Particle 031DU40, non-normalized)	57
Figure 3.29	5% Concentration vs. Baseline Static and Fatigue Performance (at 10^5 cycles)	57
Figure 3.30	10% Concentration Small Particle (461DU20) Fatigue performance (S-N curve)	59
Figure 3.31	10% Concentration Large Particle (031DU40) Fatigue performance (S-N curve)	59
Figure 3.32	Fatigue Data for 10% Additive Concentration vs Baseline Prediction Intervals (Small Particle 461DU20)	60
Figure 3.33	Fatigue Data for 10% Additive Concentration vs Baseline Confidence Intervals (Small Particle 461DU20)	60
Figure 3.34	Fatigue Data for 10% Additive Concentration vs Baseline Prediction Intervals (Small Particle 461DU20, non-normalized)	61
Figure 3.35	Fatigue Data for 10% Additive Concentration vs Baseline Confidence Intervals (Small Particle 461DU20, non-normalized)	61
Figure 3.36	Fatigue Data for 10% Additive Concentration vs Baseline Prediction Intervals (Large Particle 031DU40)	62
Figure 3.37	Fatigue Data for 10% Additive Concentration vs Baseline Confidence Intervals (Large Particle 031DU40)	62

LIST OF FIGURES – Continued

Figure 3.38	Fatigue Data for 10% Additive Concentration vs Baseline Prediction Intervals (Large Particle 031DU40, non-normalized)	63
Figure 3.39	Fatigue Data for 10% Additive Concentration vs Baseline Confidence Intervals (Large Particle 031DU40, non-normalized)	63
Figure 3.40	10% Concentration vs. Baseline Static and Fatigue Performance (at 10^5 cycles)	64
Figure 3.41	20% Concentration Small Particle (461DU20) Fatigue performance (S-N curve)	66
Figure 3.42	20% Concentration Large Particle (031DU40) Fatigue performance (S-N curve)	66
Figure 3.43	Fatigue Data for 20% Additive Concentration vs Baseline Prediction Intervals (Small Particle 461DU20)	67
Figure 3.44	Fatigue Data for 20% Additive Concentration vs Baseline Confidence Intervals (Small Particle 461DU20)	67
Figure 3.45	Fatigue Data for 20% Additive Concentration vs Baseline Prediction Intervals (Small Particle 461DU20, non-normalized)	68
Figure 3.46	Fatigue Data for 20% Additive Concentration vs Baseline Confidence Intervals (Small Particle 461DU20, non-normalized)	68
Figure 3.47	Fatigue Data for 10% Additive Concentration vs Baseline Prediction Intervals (Large Particle 031DU40)	69
Figure 3.48	Fatigue Data for 10% Additive Concentration vs Baseline Confidence Intervals (Large Particle 031DU40)	69
Figure 3.49	Fatigue Data for 20% Additive Concentration vs Baseline Prediction Intervals (Large Particle 031DU40, non-normalized)	70

LIST OF FIGURES – Continued

Figure 3.50	Fatigue Data for 20% Additive Concentration vs Baseline Confidence Intervals (Large Particle 031DU40, non-normalized)	70
Figure 3.51	20% Concentration vs. Baseline Static and Fatigue Performance (at 10^5 cycles)	71
Figure 3.52	Substrate Temperature vs Time	73
Figure 3.53	Substrate Temperature Profile for varies additive concentration Large Particle (031DU40)	74
Figure 3.54	Substrate Temperature Profile for varies additive concentration Small Particle (461DU20)	74
Figure 3.55	Time to Debond vs Additive Concentration	76
Figure 3.56	Residual Strength After Heating	77

NOMENCLATURE

σ_a	Alternating Stress
σ_m	Mean Stress
σ_{max}	Maximum Stress
σ_{min}	Minimum Stress
S_i	Stress Range
N_i	Endurance in Cycles
$\text{Log}(A)$	First Coefficient of Regression Line
m	Second Coefficient of Regression Line
t	Student's t Distribution Coefficient
$\hat{\sigma}^2$	Best Estimate Variance
f	Number of Degree of Freedom
n	Number of Element in Studied Population

CHAPTER ONE

INTRODUCTION AND LITERATURE SURVEY

1.1 Introduction

Fuel economy requirements, emissions regulations, environmental impact associated with the increasing use of multi-material design on the End-of-Life phase (EoL) and the push for energy independence are key factors driving the industry towards the increase of the vehicle efficiency. Environmental demands for reducing carbon emissions are driving the need to improve vehicle fuel economy, while increasing, on the other hand, the vehicle performance and passenger comfort [1]. Over the past several decades the weight of vehicle's structural components has been steadily reduced, although, the added components necessary to meet the more stringent safety standards and emission regulations have caused an increase of the overall vehicle weight [2,3]; as illustrated by Figure 1.1 for the US automotive industry.

Similarly, in the European Union, the 2030 target of emission reduction is at least 40% of greenhouse gas emission (from 1990 levels), with a target improvement of at least 32.5% in energy efficiency. As a result, the use of light-weighting and composites materials has been steadily increasing in mass produced passenger vehicles [4]. This trend leads to the introduction of various joining techniques that face the complications that are introduced by the joining of dissimilar materials, particularly between metals and non-metals or composites. The amount of techniques for joining dissimilar materials is limited.

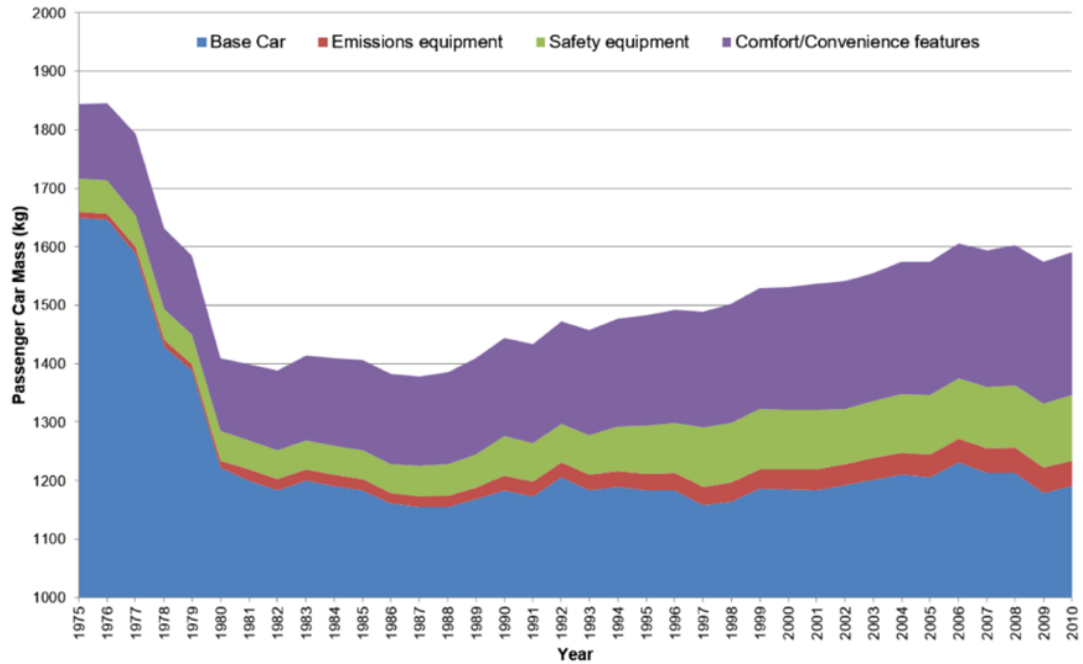


Figure 1.1 Mass Produced Vehicles Weight features from 1975 to 2010
 Note: From “Automotive Features Mass Impact and Deployment Characterization”
 Copyright 2020 by Zoepf, S. M. Reprinted with permission

Few choices such as adhesive bonding and mechanical fastening are currently available, while welding remain applicable for really particular application on steel-aluminum substrates. Same waste management and environmental requirements now require higher rates of reuse, recycling, and recovery. For example, the European Commission’s has recently increased the reuse, recovery and recycling rate to 95% and 85%, respectively [5].

The use of polymer and composite materials complicates the recycling process. The use of multi-material bonded structural components makes material recycling at End of Life (EoL) using traditional techniques, such as shredder-based recycling process, difficult due to the complexity of separating the different material

types while maintaining high level of purity [2]. This difficulty may be explained as follows.

Firstly, the separation process necessary to decouple composites, polymers and metals is labor intensive and expensive. Even though the industry has made significant progress on recycling technology, the shift to lightweight material makes the recycling process more challenging. The main joining technique for polymers and composites is adhesive bonding as it generally outperforms traditional joining techniques when joining dissimilar materials and non-metal materials, but it incurs more problem during the recycling process at EoL.

Secondly, the recycling and recovering process of composite materials is difficult due to their physical and chemical makeup. The recycling of carbon fiber constituents in reinforced composites has been a source of heated debate, due to its environmental impact. Facing the recycling challenges, many have suggested that design for disassembly is now an essential requirement of the design process. Specifically, a new joining technology that enables rapid disassembly is of great interest [6].

The choice of lightweight materials that depends greatly on the weight reduction potential, crash performance and material manufacturing costs lead to the utilization of new multi materials and composite structures. The use of advanced materials has a big impact on the weight of the vehicle and on fuel economy, for every 10% reduction in vehicle mass, fuel economy is improved by 6%, which illustrates the significant leverage of vehicle weight. Over the past 30 years, the automotive industry has reduced the vehicle structural components weight by about 30%. That weight reduction came from smarter design and materials substitutions. A large range of materials is now being developed and will significantly change the

nature of materials usage in vehicles [7] as shown in Figure 1.2. The implementation of adhesive joining processes is the best candidate for those new materials. However, joining dissimilar materials can present challenges, because of the mismatch in the mechanical, physical and chemical properties of the components that are joined [8].

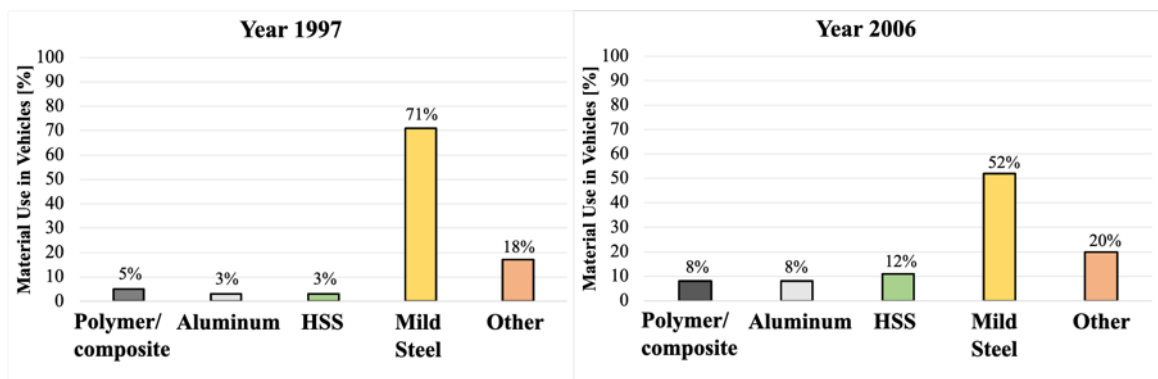


Figure 1.2 Evolution of lightweight material use in passenger vehicles

The most recurring issue, when dealing with dissimilar materials, is galvanic (or bimetallic) corrosion. For a galvanic couple, the anode and cathode are determined by their relative position in the galvanic series (Figure 1.3). The automotive industry uses metallic materials such as steel, aluminum and magnesium as well as carbon-fiber composites. When joining dissimilar materials together, galvanic corrosion may occur due to the electro-potential differences between the two substrates. For example, the graphite present in Carbon-Fiber Reinforced Plastics (CFRP) is electro-positive to most of the materials used in modern vehicles. As a result, when CFRP is coupled with metals, galvanic corrosion in the more cathodic metallic element is induced.

Designers need to make efforts to isolate the joint between conventional materials and CFRP, and the use of adhesive bonding as joining technique offers a great advantage, avoiding direct contact between the two dissimilar components [8].

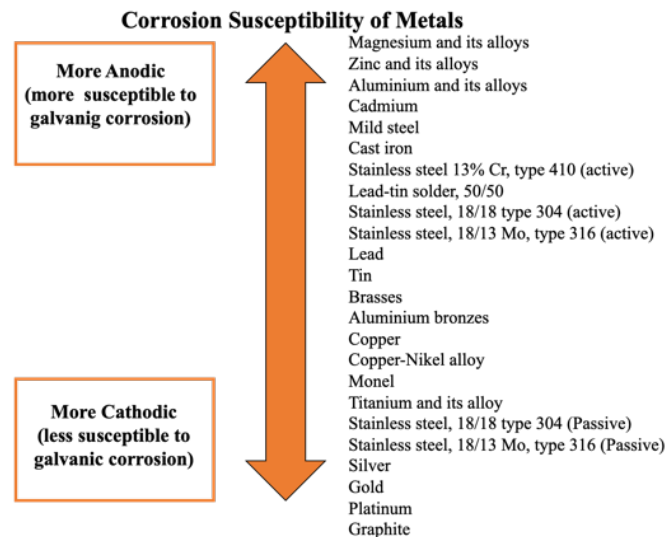


Figure 1.3 Sample of (partial) galvanic corrosion chart

1.2 Adhesive Bonding

Adhesive bonding is already extensively adopted in the industry; a vast selection of adhesives exists for very specific applications and requirements. This makes adhesive joining a strong candidate for particularly difficult material combinations such as metals to composites and/or polymers [9].

Adhesives have a long list of advantages for mixed material applications such as their ability to join materials with dramatically different melting points while also sealing and separating dissimilar substrates, which in other cases would cause corrosion.

The choice of the adhesive is directly connected to the type of application for which they are needed. Epoxy-based, Polyurethane-based and Acrylic-based adhesives are mainly used as structural adhesives with high bearing capacity and high tensile strength. Differently, thermoplastic adhesives, such as Hot-melt and polymers-based adhesives, are typically the best option for non-structural applications. Adhesive bonding has many advantages: firstly, it allows to have significant weight reduction in the structure, while allowing better distribution of stresses, increased fatigue life and high impact resistance.

Secondly, all solid can be joined, also dissimilar materials, with consequently improved corrosion resistance. Additionally, films, thin sheets and delicate parts (such as electronic components) can be joined. On the other hand, the choice of this joining technique will cause some drawback. Indeed, adhesives are difficult to manage, requiring special surface treatment, and can be characterized by slow curing time, not optimal for industrial process due to increased cycle time. Additionally, adhesives are generally difficult to disassemble. A wide variety of applications are available in the literature, both scientific papers and industrial applications have demonstrated that this type of joining technology can lead to great performance while maintaining the efficiency in costs and timing. In the Automotive industry many types of adhesives are used for different purposes, structural adhesives are used for bonding applications or to increase the stiffness of a structure, while non-structural adhesives can be used as sealing elements.

For example, acrylic and epoxy adhesives are often used for door hem bonding which provides rigid connection between inner and outer panels. Hemming techniques are used to prevent relative movement between two layers and resist corrosion from within the crimp joint. It also adds overall panel stiffness to

allow for metal thickness reduction. In many cases this may be used on dissimilar metal combinations, where a magnesium inner panel is bonded to an aluminum outer panel or a polypropylene inner panel is bonded to a plastic outer panel (TPO).

Multiple automotive adhesive and sealant applications in the car body structure, might use chemical and/or physical foaming additives to the adhesive matrix, in order to strengthen the substrate adhesion as the vehicle body goes through the oven, during the painting process. The volume of these additives expands when exposed to high temperatures, their presence inside the adhesive will guarantee a perfect stitching of the parts improving the corrosion protection keeping the vehicle sealed. The scientific community investigated multiple aspects of the adhesive bonding for different applications:

Banea et al. [10] have analyzed multiple material applications in order to optimize the performance of different families of materials, in particular composites and metals. They found that the increase of the overlap length results in a nonlinear increase in load bearing capacity, while increasing the adherend thickness (in particular for CFRP/HS combinations) caused no significant variation of the joint strength, allowing favorable weight reductions. Other studies are currently exploring the effects of the modification of the base line adhesive by addition of particles in the adhesive matrix, therefore modifying the adhesive behavior.

Nassar et al. [11] have studied the effect of the addition of Silicon Oxide and Aluminum oxide nano-powders on the static load transfer capacity and failure mode on bonded multi material applications. The study investigated joints made of lightweight materials, magnesium and steel in particular, and how different nano powders material, concentrations and particulate size, can affect the joint performance. The experiments showed that mixing the adhesive with silica

nanoparticles, would generally increase the Load Transfer Capacity of most of the joints, as compared to using alumina nanoparticles.

The adhesive bonding research is recently going through some major changes. In the last years, studies have focused on the achievement of the reversibility of adhesively-bonded joints. The reversible joint adhesive Technology will be further discussed in the next chapter. In order to have recyclable parts it may be necessary to separate the different material components. Heating the joined substrates can achieve the thermal softening of the adhesive (exceeding the adhesive Glass temperature) or can lead to thermal decomposition of the adhesive layer (exceeding the temperature of flammability-in air or autoignition point).

Certain solvent or acid immersion techniques can also facilitate the adhesive disassembly process, but the chemical composition of some adhesives may cause toxic gases emission during the disassembly process, harmful for human beings. To overcome those problems the possibility to add in the adhesive matrix some particles that may facilitate the disassembly when triggered by some physical or chemical factors is currently analyzed. The reversibility is obtained by modification of a baseline adhesive by means of additives that allow to reach the separation of the adherends without damaging the components (cohesive failure within the bondline).

Many studies have been conducted using different types of adhesive matrix, substrates (such as metallic non-metallic and composites) and additives combinations. Some of those additives can be electromagnetically triggered in order to increase the temperature of the adhesive; others are thermally activated in order to cause mechanical substrates separation.

Ciardiello et al. [12] have studied the effect of the particulate size of iron-based particles on the mechanical properties of single lap joints. Their work evaluated

the mechanical behavior of Hot-Melt Adhesives (HMA) when Epoxy-based substrates were used. They discovered that the HMA that was modified using the smallest iron particles showed no significant strength reduction compared to the pristine adhesive. The use of iron-oxide particles gave better results in terms of heating and mechanical properties. Overall, the adhesive maintained good mechanical properties.

Banea et al. [13] and Veloso [14] studied the effect of the addition of different weight percentages of Thermally Expandable Particles (TEPs) in two different adhesive matrices, using metallic substrates. They found that joints mechanical performance would strongly depend on the TEPs concentration in the adhesive. The temperature needed for debonding resulted dependent on the added weight percentage, and could be lowered increasing the TEPs content.

Banea et al. [15] have studied the effect of moisture uptake on the behavior of a structural adhesive modified with TEPs. Due to the effect of ageing, both the elastic modulus and tensile strength of the studied TEPs-modified adhesive have been reduced, thus, the physical properties have been damaged. On the other hand, the strain to failure increased, indicating that moisture increases the flexibility and ductility of the adhesive.

Hutchinson et al. [16] have studied the effect of the addition of five different physical foaming agents and four different chemical foaming agents in three different automotive structural epoxy-based adhesives. They discovered that the one-time reversibility of a structural adhesive is possible with the use of thermally labile functional additives. However, it has been shown that each adhesive matrix will react in a very unique way to the presence of such additives, anyway the joint strength will be typically reduced by the presence of such elements.

Giulia Spezzanti et al. [17] were able to use new joining technologies with Hot-Melt adhesive modified with electromagnetic sensitive particles, this new technique was used to bond and debond the lower tail gate of a passenger vehicle. The magnetite nanoparticles embedded in the adhesive were activated by an electromagnetic field, this was characterized by properly conceived power and frequency that had made the assembly/disassembly process faster and easier. The total assembly/disassembly time varied depending on the amount of concentration of particles in the adhesive matrix. Demonstrating the feasibility of a robust process for bonding/debonding of plastic components in the automotive industry.

Those are just some example of the studies that have been done on this topic, further developments will be necessary in order to complete its understanding and applying those techniques in a more intense rate.

The principal advantage in using reversible adhesive bonding techniques is obviously the possibility to disassemble the substrates when needed for maintenance, repair or recycling. This can become a fundamental requirement if future legislations will require more stringent measures for recovery of materials. The innovation in this field is fundamental since the use of particle in the adhesive matrix cause, in most of the cases, a reduction of the adhesive strength or an increase of the brittleness of the adhesive matrix, and the time that is usually required for disassembly is not feasible for industrial applications. The evaluation of the mechanical and chemical characteristic of the joint is made following some specific criteria.

However, the focus of the tests for reversibility purposes are different respect to the classical mechanical characterization for adhesive bonding. In this particular application, indeed the tests are done to understand how the presence of the added

particles is modifying the mechanical and chemical properties of the adhesive, commonly a comparison respect to the pristine adhesive is made.

The first aspect that has to be checked when a modified adhesive is used is how the particles are distributed inside the adhesive matrix, achieve a homogenous distribution of particles within the bond line is fundamental to ensure proper stress distributions along the bond line. The particle distribution is usually checked using optical microscopes, and can be easily achieved in vacuum conditions, in order to avoid air bubbles incursions inside the adhesive, using mixers which have a temperature controller that allow to set a precise level of viscosity for the adhesive.

Secondly, debonding tests are required to analyze the reversibility performance of modified adhesives. Those tests are usually performed at high temperatures for faster disassembly. The joints adhesive layer needs to be heated up to a temperature that allow to reach the thermal softening and achieve the separation, this temperature may vary for different application and additive types. The use of electromagnetic induction allows to optimize the heating procedure; the use of this technology makes possible to heat the substrates only in a localized section near the bondline.

When the electromagnetic field induction is used, the typical set up consists in a coil system in which the specimens (usually single or double lap joints) can be inserted as showed in Figure 1.4. Doing so is possible to achieve localized heating near the adhesive avoiding the possibility of damaging the substrates using an oven as heating source. The specimens are usually tested using a weight in order to apply a constant shear force on the adhesives that is possible to cause the failure of the joint and study the failure mode.

The parameter of most interest in those tests are the time to debond and the temperature at which the separation of the substrates occurs. Those main parameters are coupled with others connected to the additive material such as: the additive weight concentration, the particulate size and the nature of the additives. The physics of the induction process can vary drastically according to the chosen materials and particles used. Two major scenarios can be considered:

Scenario I (non-metallic, plastic composites, substrates and ferromagnetic particles addition in the adhesive): when the two substrates are non-conductive materials the electromagnetic field will be exciting only the ferromagnetic particles. The heating source will be mainly inside the adhesive and the thermal softening will be created by the wasted energy in the particles. [12].

Scenario II (Metallic substrates and TEP addition in the adhesive): when the substrates are made of metallic materials they will inevitably react to the presence of the electromagnetic field and they will start to waste energy under thermal energy release. In this case is possible to use the heat delivered by the substrates to trigger the particles that are mixed with the adhesive. An example could be the use of Thermally Expandable Particles (TEPs), those particles are capable to increase their volume when their triggering temperature is reached, this temperature varies according to the type of particle used.

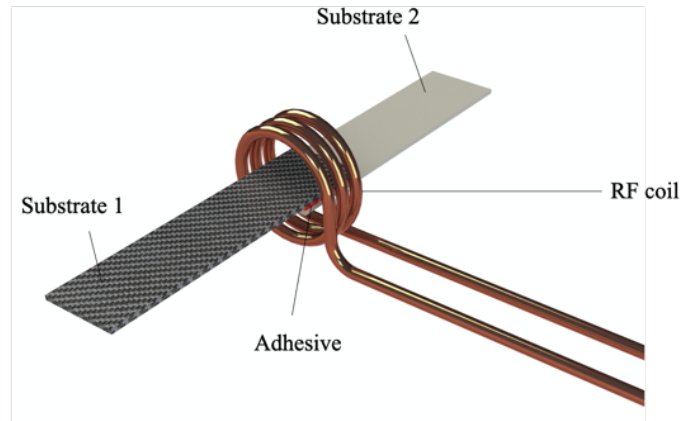


Figure 1.4 Example of Heating Setup for Debonding Test

1.3 Objectives

The objective of the research is to use TEPs (thermally expandable particles) in order to achieve the reversibility of an adhesive bonded multi-material Single Lap Joint (SLJ). The main assumption is that the reversibility can be achieved using an electromagnetic field to heat the two substrates so that the heat, transferred to the TEPs, will simplify the joint separation process (metallic substrates and non-ferromagnetic particles addition in the adhesive configuration).

When the substrates are made of metallic materials, they will inevitably react to the presence of the electromagnetic field starting to waste energy under thermal energy release. In this case is possible to use the heat delivered by the substrates, under form of conduction exchange, to trigger the particles that are mixed with the adhesive. The use of Thermally Expandable Particles (TEPs) allows to reach the reversibility of the bond, those particles are indeed capable to increase their volume when their triggering temperature is reached, as showed in Figure 1.5 (triggering temperature varies according to the type of particle).

The heat delivered by the substrates is used to trigger the particles that are mixed with the adhesive, the expansion and the thermal softening of the adhesive, due to high temperature, will cause the joint separation when a constant load of 100N is applied. Moreover, the effect of the particle enrichment on the static and fatigue performance of the joints will be analyzed, since the presence of voids inside the adhesive matrix is expected to reduce significantly the load transfer capacity of the joint.

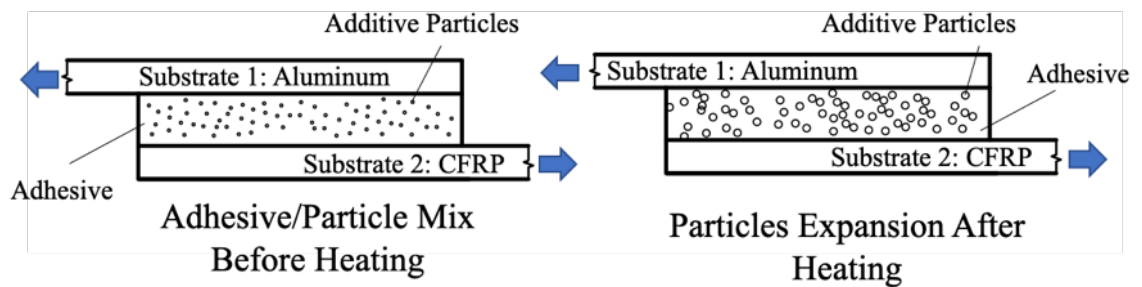


Figure 1.5 Illustration of particle volume expansion due to RF heating in debonding

CHAPTER TWO.

EXPERIMENTAL SET UP AND TEST PROCEDURE

In this section will be presented how the tests have been conducted and which is the method used to select and prepare the sample, to enrich the adhesive with TEPs, how the adhesive is crafted and how the tests have been conducted.

2.1 Material Selection and Sample Preparation

In order to follow the recent trend of light weight material use two substrates have been selected. One of the two substrates is made of Aluminum 6061-T6 with a thickness of 1/16” (1.6 mm), while the second one is made of woven carbon fiber (CFRP 0-90-0, aligned with the SLJ axes) with a thickness of 1/16” (1.6 mm). The data of the material are listed in the Table 2.1. The selection of a woven reinforced carbon fiber is not casual. The substrates have to be able to respond to the induction heating caused by an electromagnetic field.

Table 2.1: Substrates material properties

Material	Young Modulus (GPa)	Tensile Strength (MPa)	Elongation at Break (%)
ALUMINUM 6061T6	70	276	12
CFRP 0-90-0 (SLJ axes)	32.5	553	1.7

It is necessary that the wavelength of the oscillating electromagnetic field is comparable to the specimen species. The sample surfaces are prepared differently according to the material that is considered, however both follows a two steps surface preparation procedure prior to bonding. Aluminum substrate's surface is prepared using a drill-operated wired brush for consistent roughness of all tested samples. As measured by an optical profilometer, an average surface roughness (Ra) of 3.57 μm has been recorded (Figure 2.1 and Figure 2.2).

The Carbon Fiber coupons are hand scuffed to avoid fiber tear on the coupons, and an average surface roughness (Ra) of 2.01 μm is obtained (Figure 2.3 and Figure 2.4). After the first step both the materials are cleaned using Acetone in order to remove the presence of grease and oil on the surface and to avoid the presence of residual dust due to the scuffing procedure.

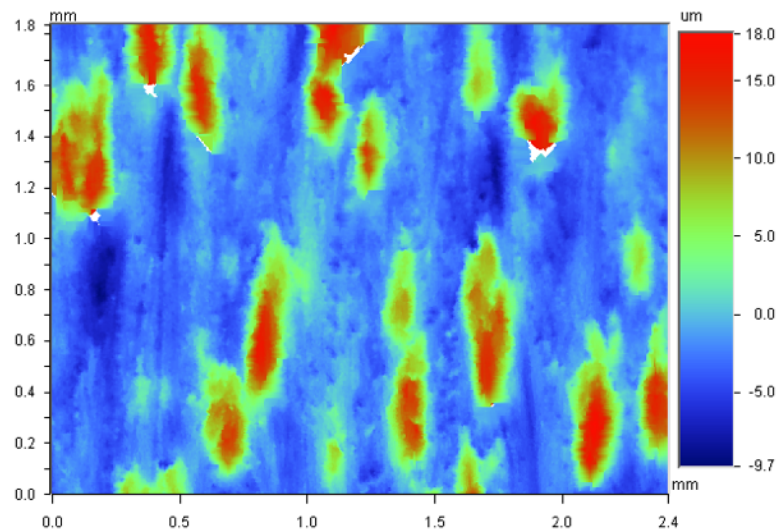


Figure 2.1 Surface topography of aluminum coupons

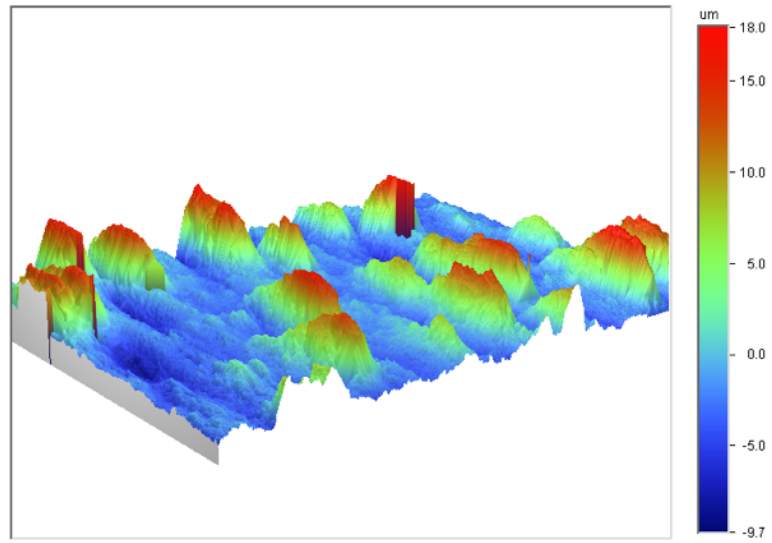


Figure 2.2 3D Surface topology of aluminum coupons

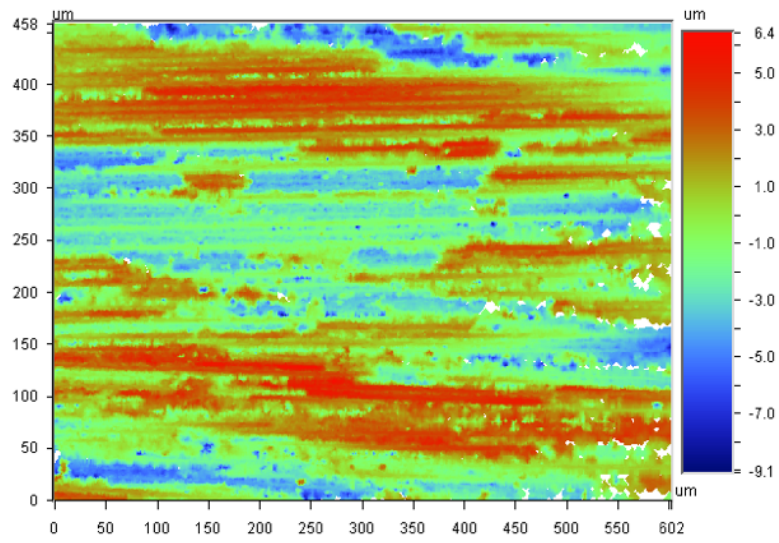


Figure 2.3 Surface topology of carbon fiber coupons

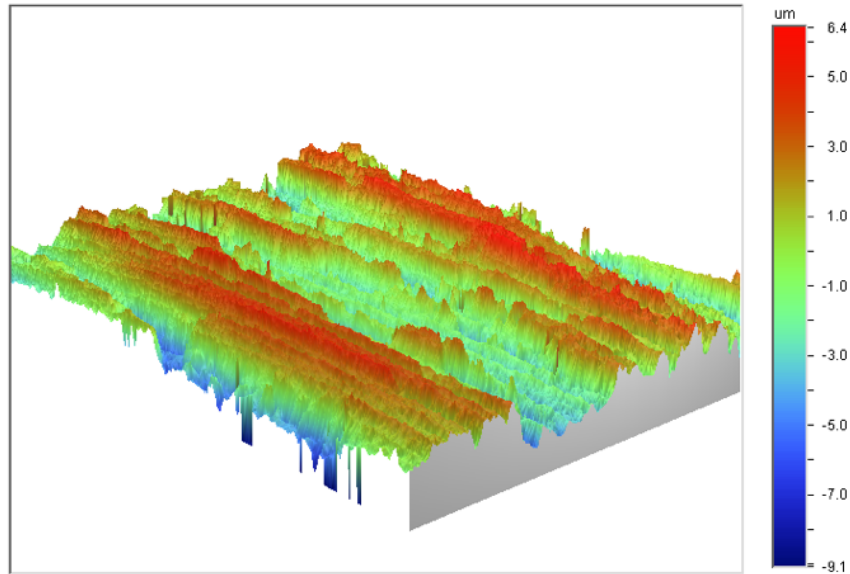


Figure 2.4 3D Surface topology of carbon fiber coupons

2.2 Selection of Baseline Adhesive and Additives

In this section the methodology adopted in the selection of the baseline adhesive and of the additives used is reported. Moreover, the procedures followed to mix the adhesive and the additives and to cure the modified adhesive are presented.

2.2.1 Adhesive Selection

The adhesive selection is a fundamental process, in order to choose the most compatible adhesive for the selected substrates, a screening of different adhesives has been done.

The comparison will be made using the same substrates combination of aluminum and carbon fiber while three different adhesives will be tested. Those are respectively: the Betamate 73326/73327M (epoxy adhesive), the Betamate 2098 (epoxy adhesive) and the Betaforce 20850 (polyurethane adhesive). Must be specified that to guarantee

proper adhesion for the Betaforce20850, prior to the application of the adhesive, the surfaces of the substrates were treated using different primers.

The aluminum was treated in two steps, the first primer used was the Dupont 43521 and the second one was the Dupont 43132; the CFRP substrates were treated using just one layer of Dupont 43532. The Betamate 2098L reaches the highest Lap Shear strength, however, this resulted in the fiber tear of the carbon fiber substrate. The Betaforce 2850L resulted to fail because of failure at primer/surface interface, this caused a considerable reduction of the LTC (load transfer capacity) of the joint. According to the previous results (Figure 2.5), the selected adhesive is the Betamate 73326/73327 M that showed a perfectly cohesive adhesive failure for all the repetitions while resulting in high LTC.

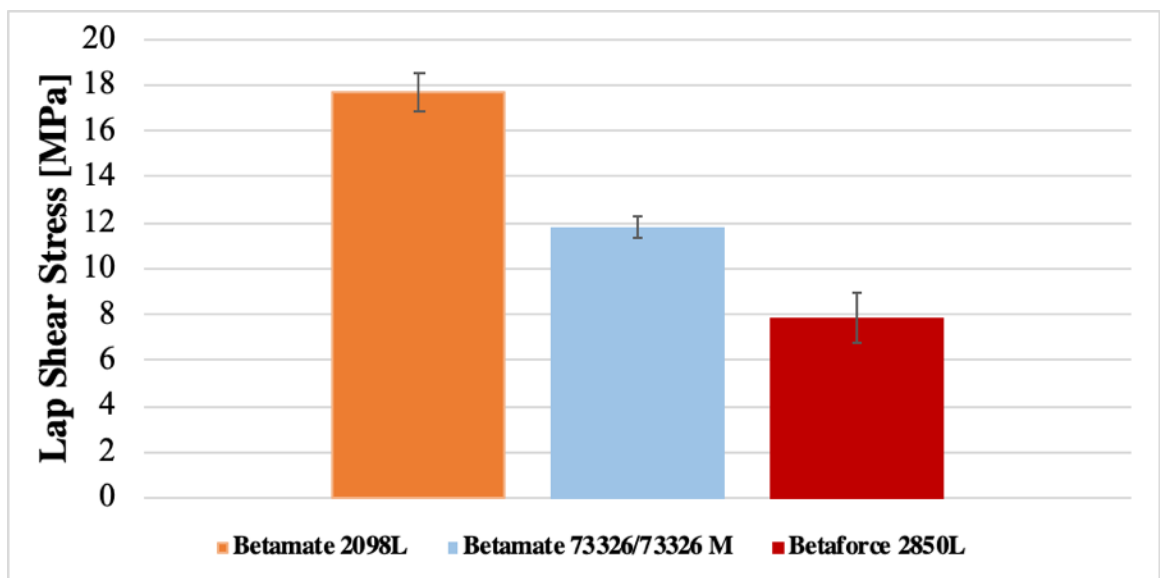


Figure 2.5 Adhesive Screening Strength Comparison

2.2.2 Additives Selection

Two different types of Thermally Expandable Particle will be used in order to study the effect of different particulate size and different values of triggering temperature. The particles that are going to be used and their characteristics are listed in Table 2.2:

The particle will be added inside both the component of the Betamate 73326/73327 M in three different weight concentrations 5,10 and 20%. In order to guarantee that the mix between the adhesive and the particle does not introduce air inside the mix, and that the particle dispersion inside the adhesive is as homogeneous as possible, a multiple step procedure has been followed.

Firstly, the particles have been mixed using an automated mixer (model DAC600FVZ). In order to avoid excessive increase in temperature, due to the heat that is generated during the mixing at high speed, this phase has been divided in two steps, a first one at 2100 rpm for 2 minutes (recorded Temperature 52°C) and a second one at same rotational speed but for 1 minute. After this first stage a second stage of mixing has been done. During this second stage the aim is to remove the presence of air that can be inside the adhesive, in order to ensure that the mix is bubble free a vacuum mixer has been used (model DAC6002VACLR).

As mentioned before to avoid that the heat generated by the mixing procedure may trigger the TEPs the mix strategy has been divided in two different steps, a first one at 1000rpm for 2 minutes followed by a faster step at 1775rpm for 1 minute and 30 seconds (in vacuum conditions). The mixture results to be homogeneous after the adopted procedure (Figure 2.6), after the mixing has been finished the enriched adhesive has been inserted inside two component cartridges.

Table 2.2 Thermally Expandable Particle Characteristics

Particle	Particulate Size (μm)	T _{start} ($^{\circ}\text{C}$)	Max T _{expansion} ($^{\circ}\text{C}$)
031DU40	10 - 16	80 - 95	120 - 135
461DU40	6 - 9	100 - 106	143 - 150

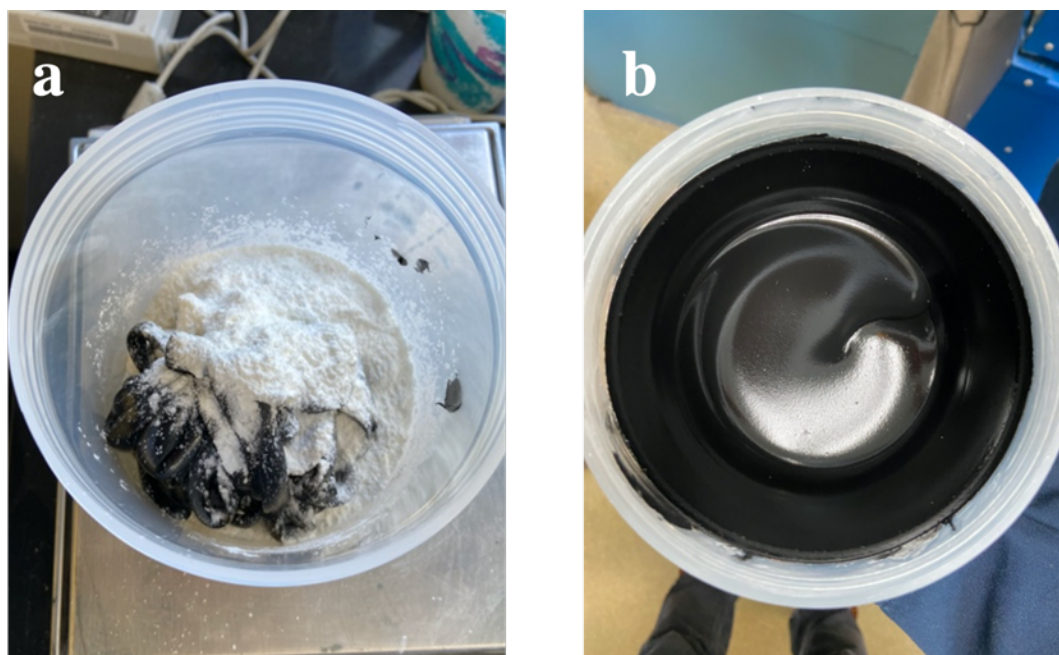


Figure 2.6 Adhesive and Particles a) Before mixing, b) After two stage mixing

Once the particles have been mixed with the adhesive, an oven accelerated curing of the adhesive is advised by the manufacturer specifications. However, the curing schedule of the Betamate 73326/73327 M has been modified to accommodate the additive by ensuring that the TEPs would not expand (or burst) during the curing procedure. The modified procedure is to let the prepared sample rest at room temperature for 30 minutes after manufacturing. Immediately after, the samples follow an oven curing at 65°C for four hours (Figure 2.7) with a final rest period of 24h at room temperature.

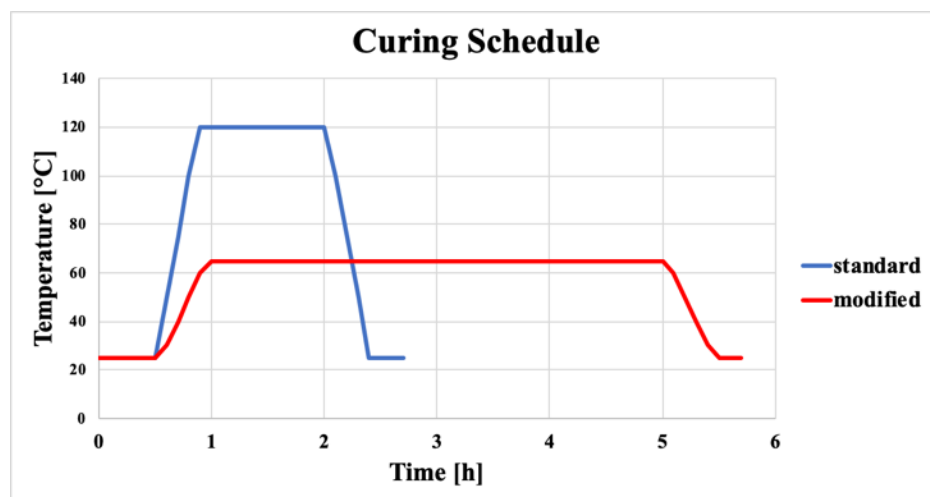


Figure 2.7: Curing Schedule Temperature Profile

2.3 Scanning Electron Microscopy imaging of Additive materials

The efficiency of the mixing strategy and the particle interaction within the adhesive matrix has been evaluated using Scanning Electron Microscopy (SEM) with different techniques.

Two main aspects have been evaluated, the particles dispersion in the adhesive and the particle expansion capability when mixed in the adhesive. Several different samples have been studied. Firstly, the particles have been studied when not mixed with the adhesive, then samples of enriched adhesive have been analyzed.

The surface of each sample was examined using two different techniques, the Back Scattered Electrons (BSE) and the Ultra Variable Detector (UVD) both have been performed using a Scanning Electron Microscopy (SEM).

Moreover, when studying the sample cross section, those were mounted and polished in accordance to ASTM E2015.

Since the material resulted to be translucent to standard white light, providing difficulties to focus on the plane of polish, images of the cross sections were taken using reflected light, polarized reflected light, and Scanning Electron Microscopy (SEM). In Figure 2.8 are visible both large (031DU40) and small (461DU20) particles when not mixed in the adhesive.

It is noticeable that both are characterized by variable particle dimension, respecting in average the dimension that are declared by the manufacturer. In Figure 2.9 are reported images that have been taken using polarized reflected light, those are useful to see how the particle were mixed with the adhesive. It is evident that the particle results to be evenly dispersed in the adhesive.

Lastly, in order to evaluate the particle capability to expand when mixed with the adhesive, images of the adhesive cross section have been taken using SEM. As showed in Figure 2.10 and Figure 2.11 the two particles are able to expand when a heat source is provided, also when they are trapped inside the adhesive matrix.

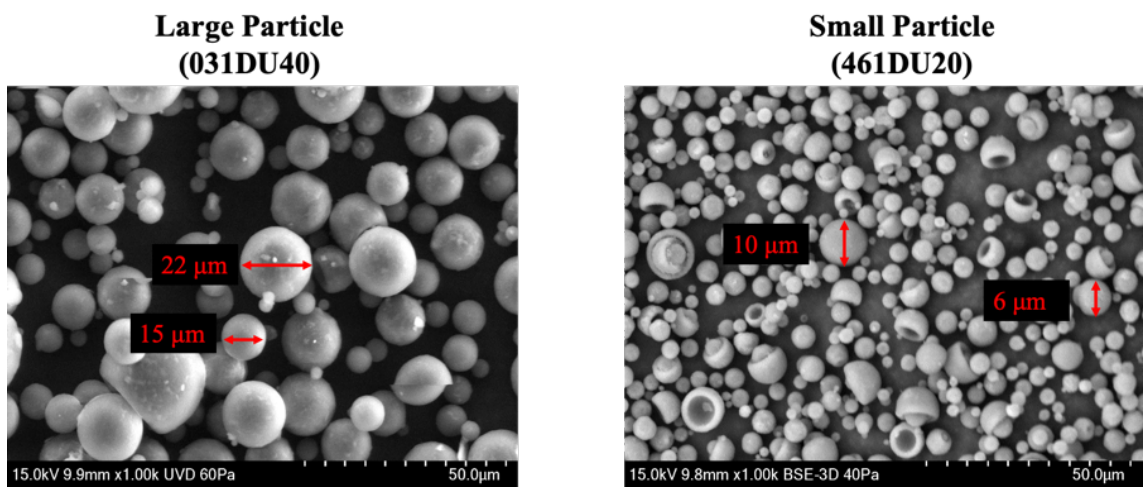


Figure 2.8 SEM images of 031DU40 and 461DU20 particles

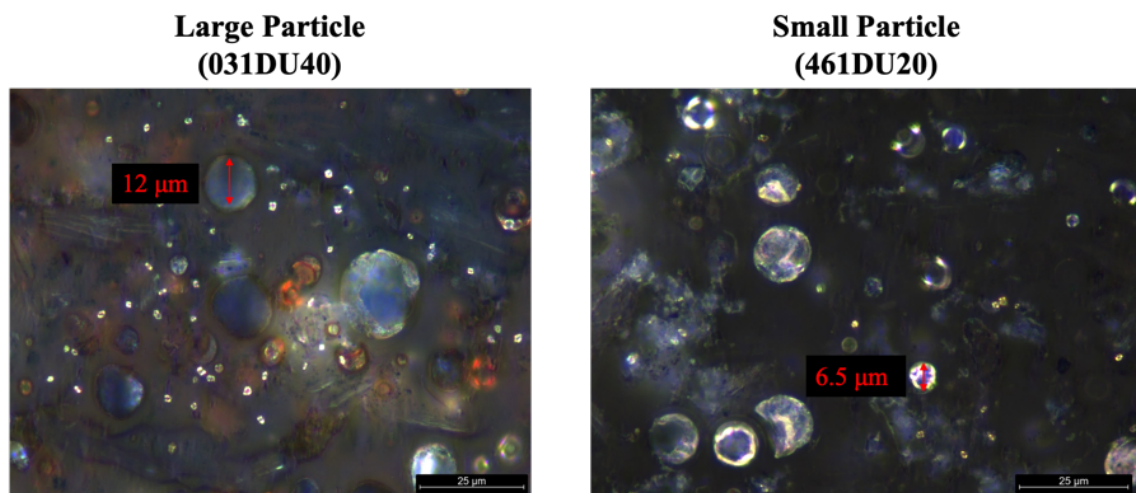


Figure 2.9 Polarized reflected light images of 031DU40 and 461DU20 particles mixed with Betamate 73326/73327 M

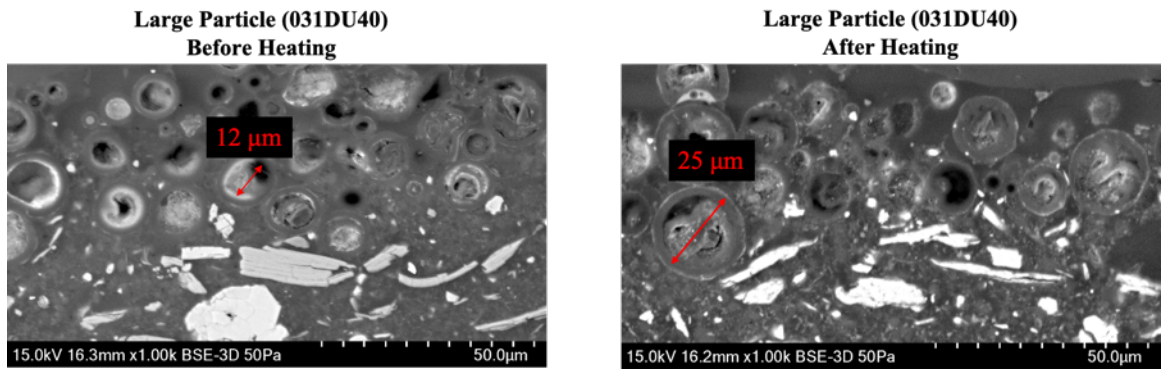


Figure 2.10 SEM images of adhesive cross-section 031DU40 particles before and after heating

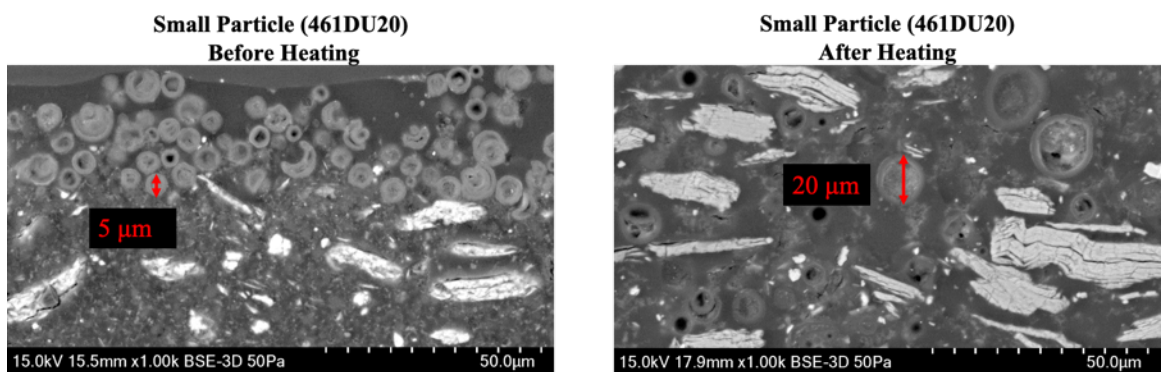


Figure 2.11 SEM images of adhesive cross-section 461DU20 particles before and after heating

2.4 Lap Shear Tests

In this section the methodology adopted for the Lap Shear tests is presented for static and fatigue loading scenarios. Additionally, the adopted statistical approach is discussed and analyzed.

2.4.1 Static Lap Shear Test Procedure

The specimens are tested according a slightly modified version of the ASTM Standards Test method for lap shear Adhesion for Fiber Reinforced Plastic bonding (D5968_01) [18]. The main difference from the standard procedure is the bond line thickness that is reduced from 0.76 mm (0.03”) to 0.2mm (0.079”) in order to use the most commonly used thickness in automotive applications. The specimens loading rate is 13mm/min (0.5”/min). Tests will be conducted using an MTS machine (Figure 2.12).

The used joint dimensions are specified in the Figure 2.13. The substrates are 25.4 mm (1”) wide and 101.6 mm (4”) long, the overlap between the substrates is 6.45 cm square (1sq. Inch).

2.4.2 Fatigue Testing

Experimental Fatigue data is collected using an 810 MTS testing system. The tests samples are cycled to failure at one mean stress level and three different alternating stresses (Figure 2.14). Screening tests have been performed using three different levels of mean stress equal to 30% 35% and 40% of the baseline static LTC. Three different amplitude levels are used to generate the S-N curves (Figure 2.15). The mean stress level that has been chosen for the study continuation is equal to the 35% of the maximum LTC. This value will be used for all the different adhesive/additive combinations.



Figure 2.12 MTS 810 Material test system

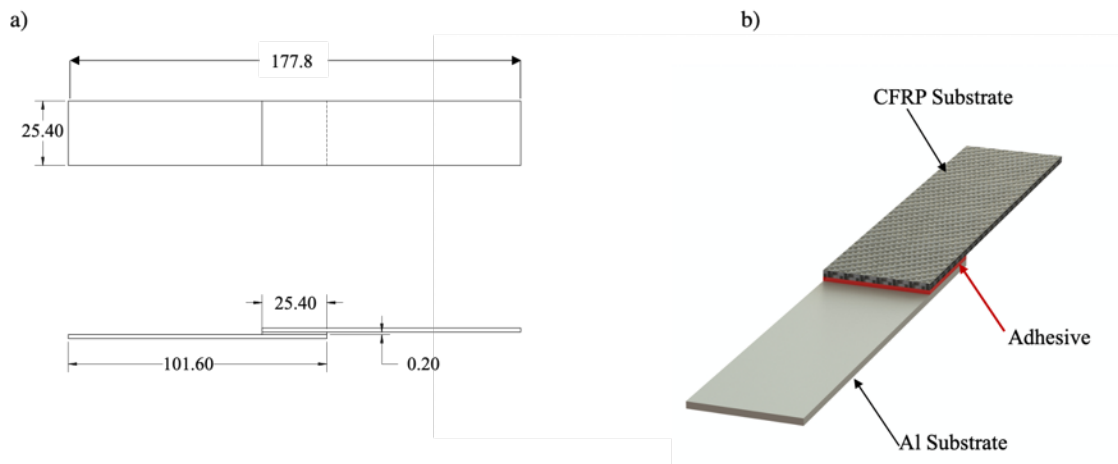


Figure 2.13 Single Lap Joint dimensions (mm)

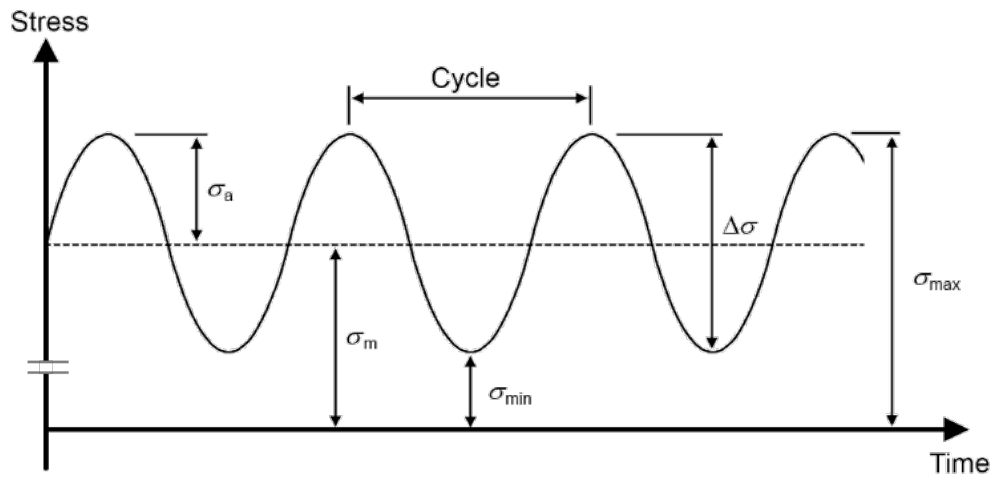


Figure 2.14 Illustration of applied fatigue load parameters

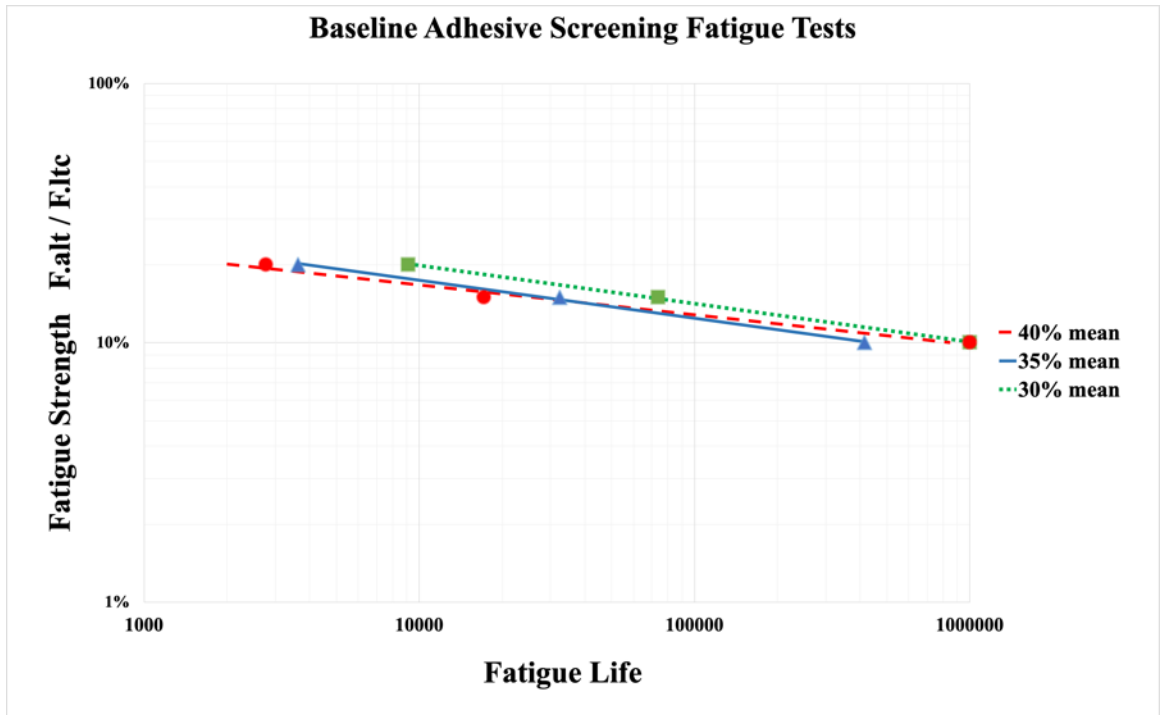


Figure 2.15 Baseline fatigue results for different mean stress levels

2.4.3 Adopted Statistical Approach

Statistical methods are available to assist in this analysis of experimental data and recommendations for their use are found in the literature [19, 20]. Two statistical methods are used for analyzing fatigue test data; namely the 95% confidence interval and 95% prediction interval. The first interval defines the limits inside which a given proportion (95%) of the coefficients of the regression line (which generates the S-N line) fall. The second bound, instead, establish the limits between which a given proportion (95%) of all the data lie. The two bands will be used to compare different distributions; if the bands of two different set of data are overlapping the behaviors of the two compared samples are considered statistically equivalent. Those bands will be determined respectively using the following relations:

$$\log N_{p\%}^{\pm} = (\log A + m \log S) \pm t\hat{\sigma} \sqrt{\frac{1}{n} + \frac{(\log S - \overline{\log S})^2}{\sum_{i=1}^n (\log S_i - \overline{\log S})^2}} \quad (1)$$

$$\log N_{p\%}^{\pm} = (\log A + m \log S) \pm t\hat{\sigma} \sqrt{1 + \frac{1}{n} + \frac{(\log S - \overline{\log S})^2}{\sum_{i=1}^n (\log S_i - \overline{\log S})^2}} \quad (2)$$

where: $\log A$ and m are the coefficients of the regression line through the n data points ($\log S_i, \log N_i$); $\log S$ is the mean of the n values of $\log S_i$. t is the appropriate percentage point of Student's t distribution, with f degrees of freedom, $\hat{\sigma}^2$ is the best estimate of the variance of the data about the regression line, which is equal to the sum of squared residuals divided by the number of degrees of freedom f , that is equal to $n - 2$ in the case where the two coefficients of the regression line have both been estimated from the data.

2.5 Debonding Test Set up

The debonding tests are necessary to verify if the adhesive enrichment is effective to speed up the debonding procedure. A comparison will be made between the base line adhesive and the different concentrations. Two main factors will be evaluated in order to compare the various combinations: the time to debond, when the specimens are loaded with constant force and the temperature at which the debonding occurs.

Test joints are heated using a commercially available RF Heating System 135-400 KHz solid state induction power supply, shown in Figure 2.16. The use of induction heating would cause localized heating of bonded substrates segments. During screening tests three custom-designed single-position multi-turn coils were built to generate the desired heating schedule, the selected coil design is showed in Figures 2.17-2.18. Frequency of 330kHz at 210W power were selected for this study. Substrate temperature was controlled both, an optical thermometer and indicating paint that dissolves when the substrate reaches the target temperature.

It was observed that it took 3 minutes to heat the sample up to 200°C for all the adopted heating solutions. The adopted coil design is the helical coil configuration, its dimensions are specified in Figure 2.17.

Debonding test set up is shown in Figures 2.18 and 2.19. Localized heating is guaranteed by the specimens positioning inside the helical RF coil. The sample is pulled using a constant force of 100N, while has been heated using the RF machine. As shown in Figure 2.19, the sample is clamped on the CFRP side to the fixture, while the load is applied to the Al side by means of a rope/pulley system. During the tests time and temperature will be recorded in order to evaluate the debonding capabilities of the joints.



Figure 2.16 RDO Model HFI - 3.0 kW RF Heating System 135-400 KHz

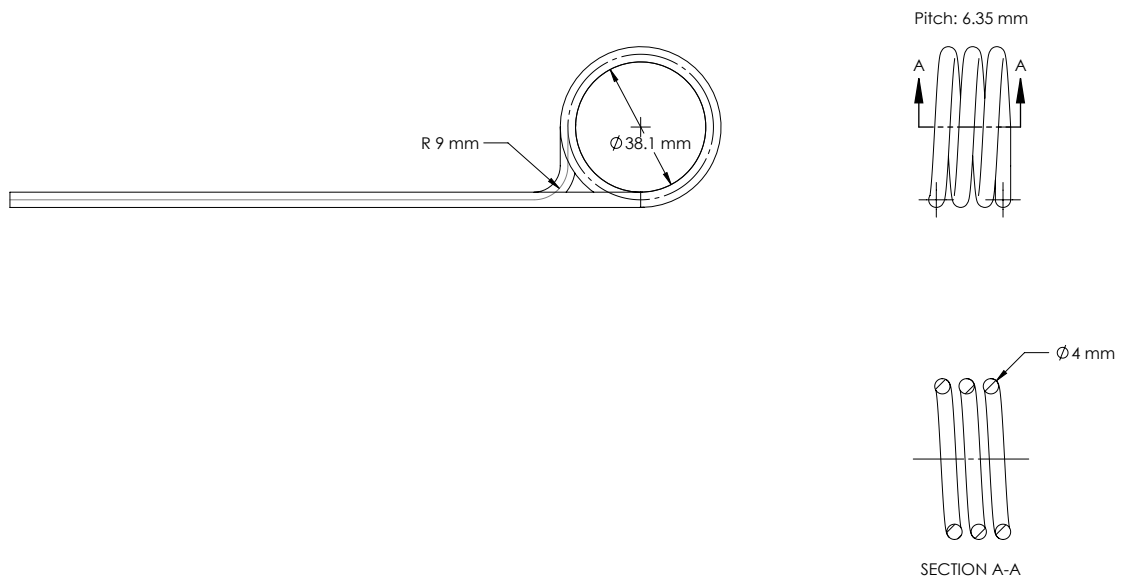


Figure 2.17 Induction RF Coil Dimensions

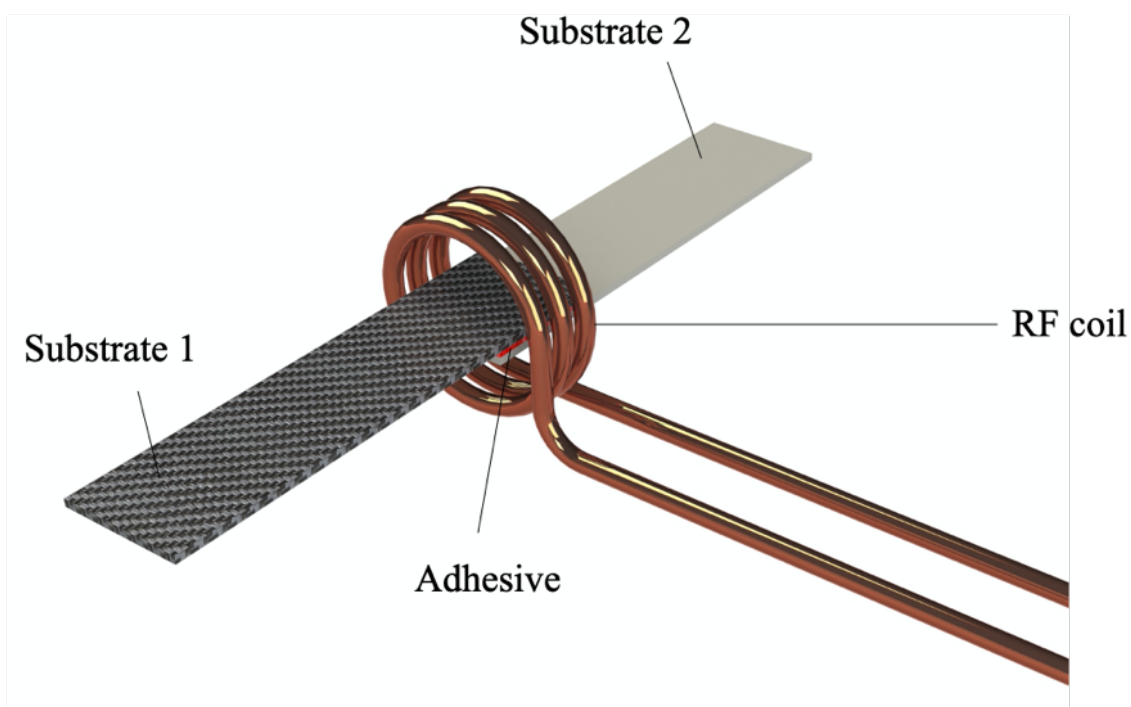
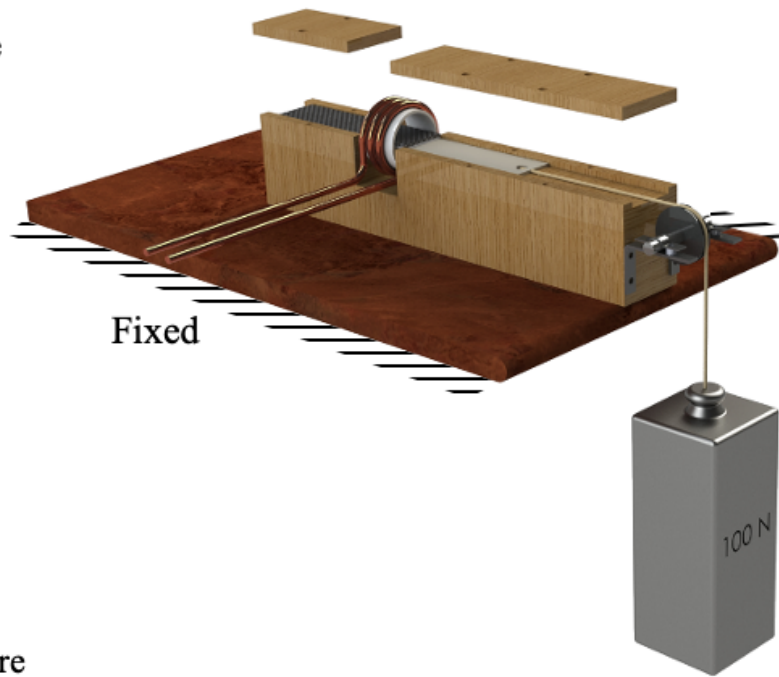


Figure 2.18 Sample Positioning inside RF coil

a) Open fixture



b) Closed fixture

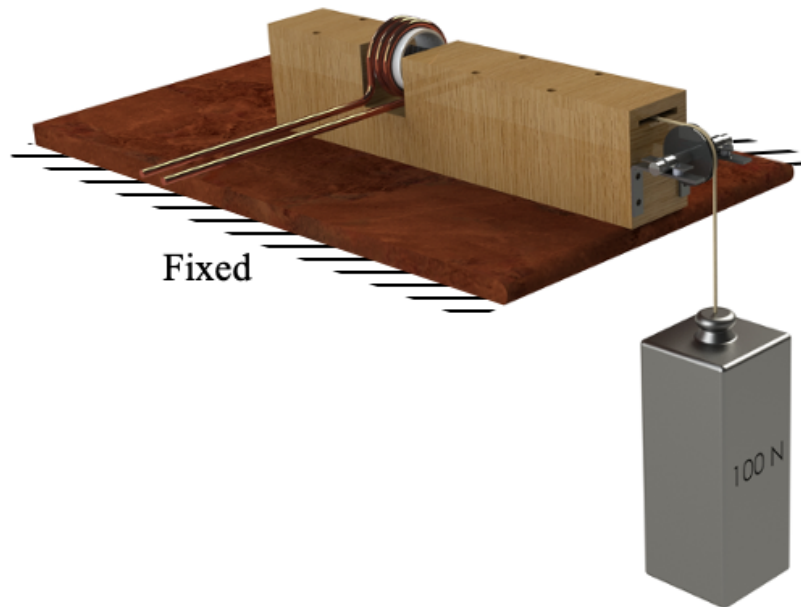


Figure 2.19 Schematic of Debonding Fixture

CHAPTER THREE.

RESULTS AND DISCUSSION

In this chapter, an analysis of the static and fatigue results will be done, this consists in a comparison between the baseline adhesive and the enriched adhesives. The Load Transfer Capacity, the statistical distribution on the S-N plane of different set of data and the different failure modes will be analyzed. At the end of the chapter a study on the debonding performance of the joint is done for all the seven studied combinations.

3.1 Static Strength

In this section, the static performance of seven different adhesive/additive combinations will be analyzed. It results that the particle enrichment, for all the analyzed concentrations, is causing a decrease of the joint Load Transfer Capacity of the adhesive. This result is obtained for both particle dimensions. Results will be reported considering one concentration at a time, in the following order: baseline performance and 5wt% enriched adhesive, 10wt% enriched adhesive, 20wt% enriched adhesive performance.

3.1.1 Baseline Static Performance

In order to define the starting baseline Betamate 73326/73327M performance tests replicas were made following standard ASTM D5968_01. Static tests results are showed in Figure 3.1. Stress elongation data show that joint stiffness remains consistent below the maximum Lap Shear Strength of all test replicas. Joints failure remains cohesive for all the tested joints. However, the maximum Lap Shear Stress varies slightly for various replicas. Total displacement at failure varies as well.

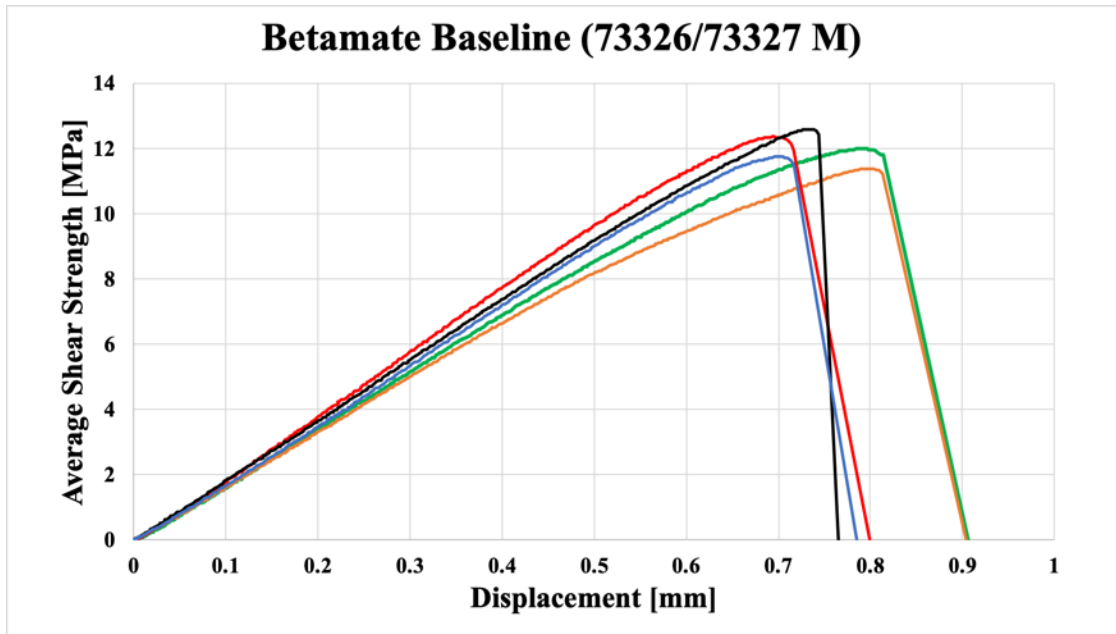


Figure 3.1 Static Performance Tests Data for Baseline Betamate (73326/73327 M)

3.1.2 Effect of Additive Concentration on Static Strength

This section reports the static strength results of the different weight concentrations enriched adhesives, using different grades of Expancel particles, especially larger particulate size (031DU40) and smaller particulate size (461DU20). For all combinations different repetitions have been made using the same procedure followed with the baseline adhesive. The static strength results for 5wt% enriched samples are reported in Figures 3.2-3.5. The stress/displacement curves of the modified adhesives are reported in Figures 3.2 and 3.3. The adhesive that was modified with larger particulate size (031DU40) shows evident reduction in Lap Shear Strength, averaging 7.5% reduction from baseline strength. Differently, the adhesive enriched with the smaller particulate size (461DU20) caused a more severe 12.7% strength reduction.

The stress/displacement curves of the modified adhesives are compared respect to the baseline adhesive (Figure 3.4), it is observed that the particle enrichment is not affecting the joint stiffness. It is evident that slope of the curves is similar. It is also noticeable that the elongation at failure is not significantly affected by the use of additives at 5wt% concentration.

The maximum deformation ranges between 0.75mm to 0.8. The average Lap Shear Strength results are reported in Figure 3.5. The smaller particle 461DU20 resulted in a more significant strength reduction with respect to the bigger particle size 031DU40, averaging 10.9 MPa and 11.5 MPa, respectively. The failure mode remains fully cohesive, without any significant variation in the fracture surface when compared to the baseline adhesive.

The static strength results for 10wt% enriched samples are reported from Figure 3.6 to 3.9. The stress/displacement curves of the modified adhesives are reported in Figures 3.6 and 3.7. Looking at the results, the adhesive modified with larger particulate size (031DU40) is evident that there is a reduction in Lap Shear Strength, averaging 8.7% reduction compared to the baseline. Differently, the adhesive enriched with the smaller particulate size (461DU20) caused a more severe 19% strength reduction.

The stress/displacement curves of the modified adhesives are compared respect to the baseline adhesive (Figure 3.8), it is observed that the particle enrichment is not affecting the joint stiffness. It is evident that slope of the curves is similar. The elongation at failure is not significantly affected by the use of additives at 10wt% concentration. The maximum deformation ranges between 0.7mm to 0.82. The average Lap Shear Strength results are reported in Figure 3.5.

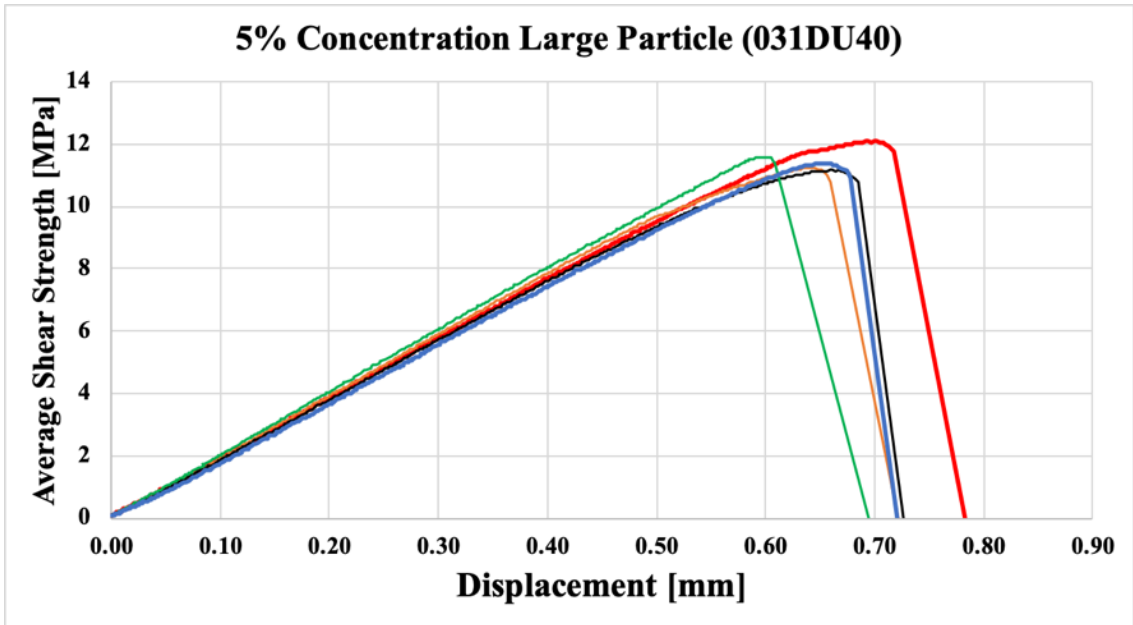


Figure 3.2 5% Concentration Large Size Particles (031DU40) Betamate
73326/77327M Static Test Data

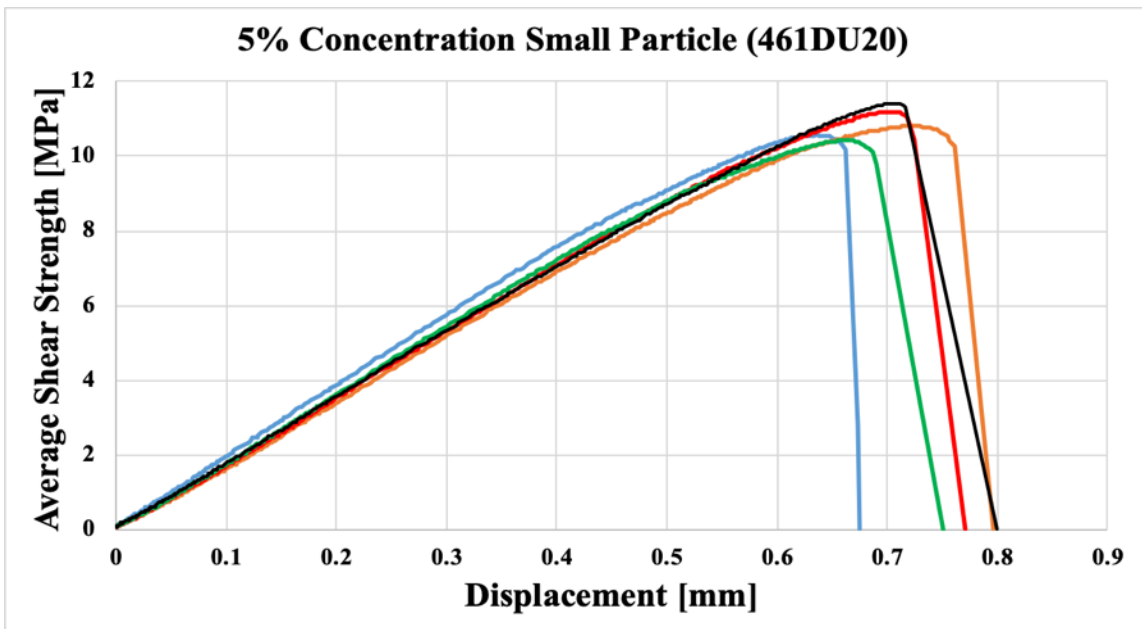


Figure 3.3 5% Concentration Small Size Particles (461DU20) Betamate
73326/77327M Static Test Data

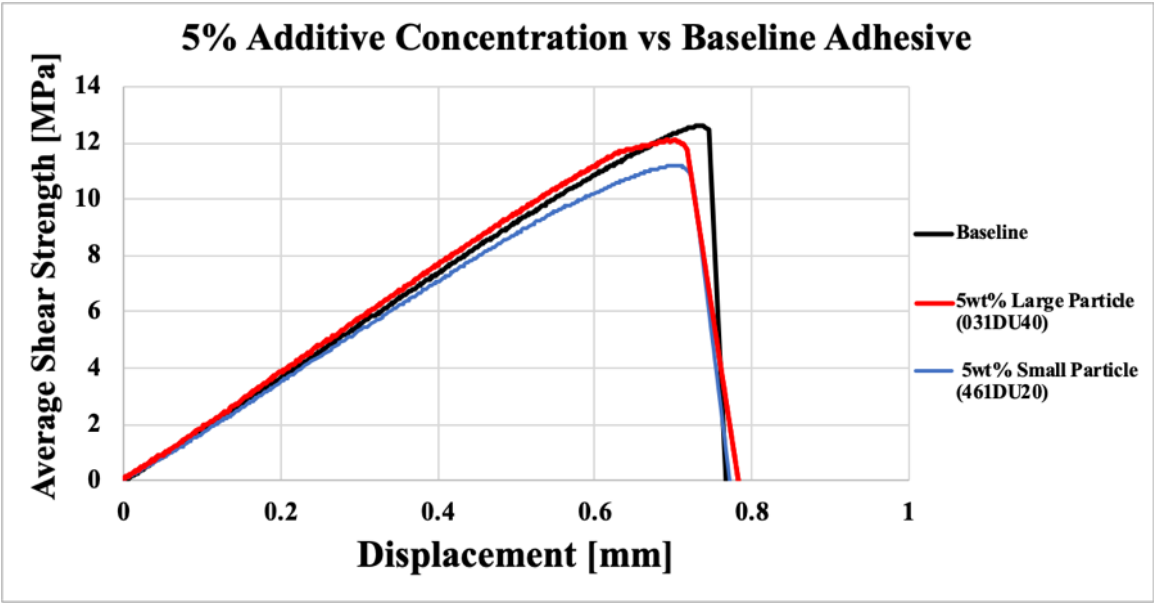


Figure 3.4 5% Additive Concentration vs Baseline Adhesive Stress-Displacement Curves

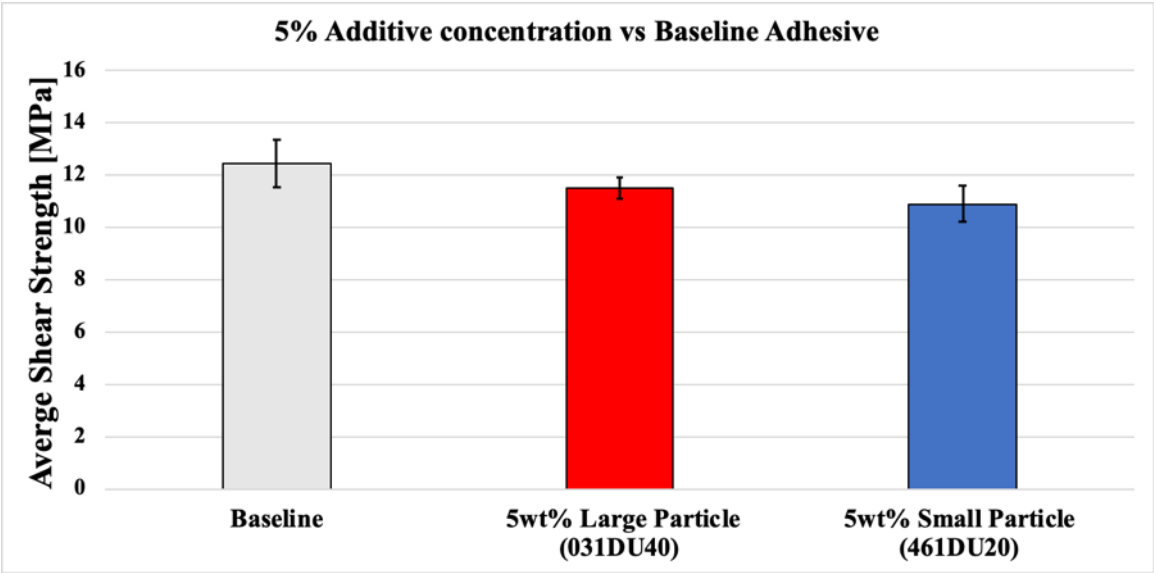


Figure 3.5 Effect of Additive Size on Baseline Adhesive Static Performance (5% Concentration)

The smaller particle 461DU20 resulted in a more significant strength reduction with respect to the larger particle size (031DU40), averaging 10.2 MPa and 11.4 MPa, respectively. The failure mode remains fully cohesive. However, some changes in the failure mechanism are visible in the area where the peel stress is at its peak. The variation of the failure fracture surface appears to be caused by two main factors, the first is the difference in flexural rigidity between the carbon fiber and the aluminum substrates, the second is the reduction in strength of the adhesive.

In order to understand why the different flexural rigidities are affecting the fracture surface, a FEA model has been developed in ABAQUS. A fixed constraint is placed at one end of the 2D model (Figure 3.10) and a displacement of 1mm has been imposed to the other side. The maximum peel stress is located at the two extremes of the overlap area, respectively at the tips of the substrates [22].

The variation of the peel stress along the adhesive thickness has been studied. The stress gradient through the adhesive thickness is measured at “Point A” and “Point B” (Figure 3.11).

The peel stress gradient at the two sides of the structure is plotted in Figure 11 and it is highest at the end of the aluminum substrate (Point B). The variation in the fracture surface has been observed in correspondence to Point B because of the variation of peel stress along the adhesive thickness and its absolute value, are much more accentuated in that area when compared to the opposite side. In that section is possible to observe that the fracture surface shifts from the middle of the bondline towards the aluminum adherend. A sharp step in the fractured adhesive is observed in the maximum peel stress area (Figure 3.12).

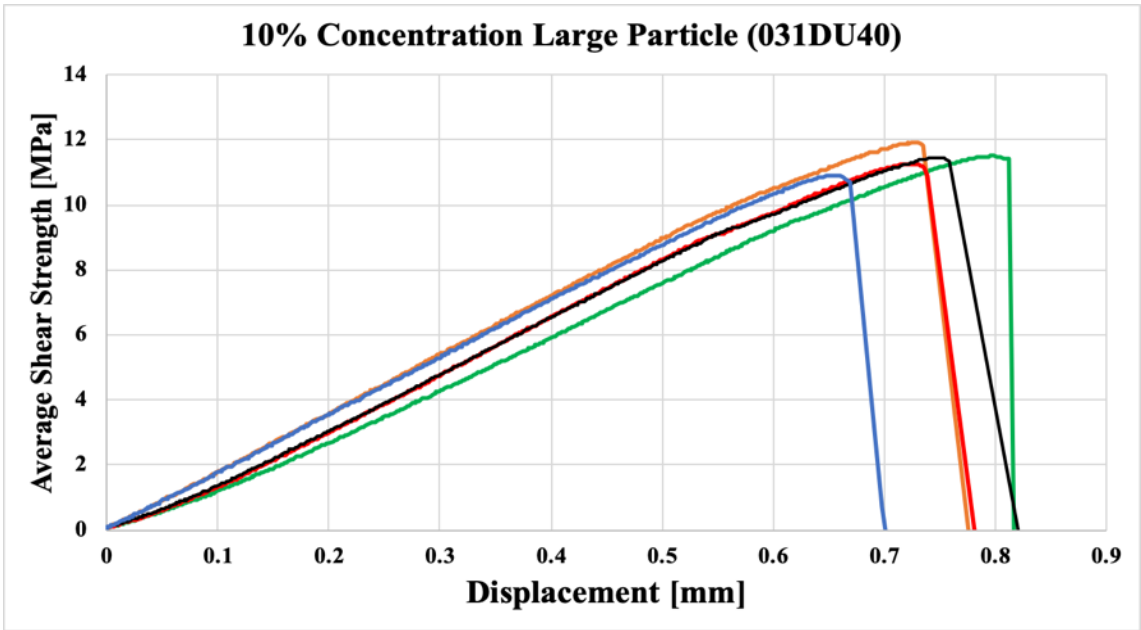


Figure 3.6 10% Concentration Large Size Particles (031DU40) Betamate 73326/77327M Static Test Data

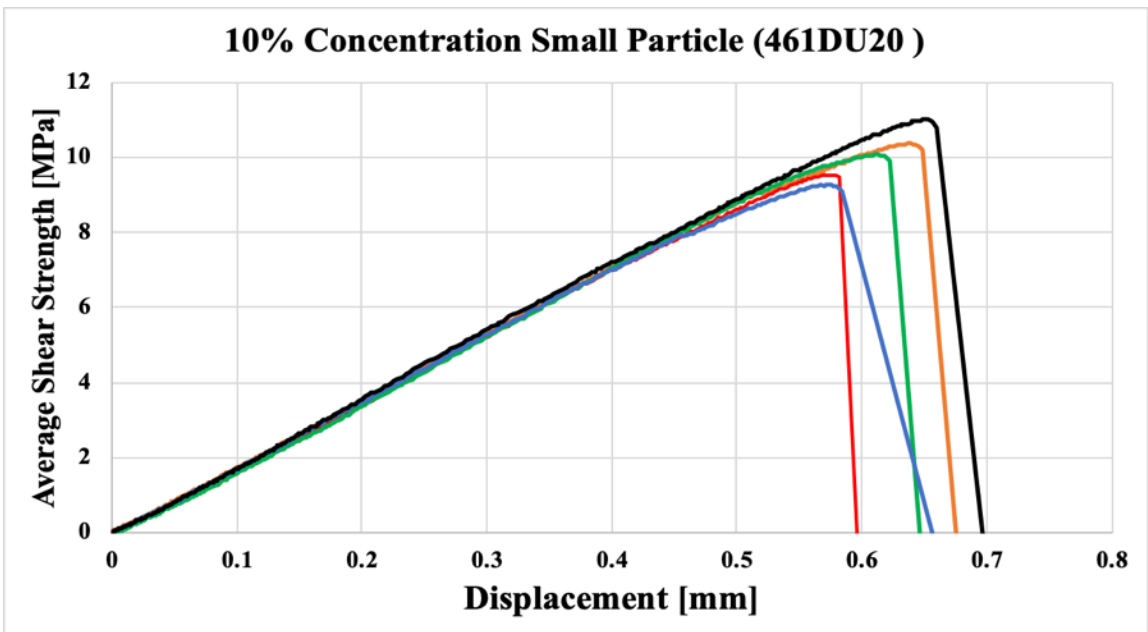


Figure 3.7 10% Concentration Small Size Particles (461DU20) Betamate 73326/77327M Static Test Data

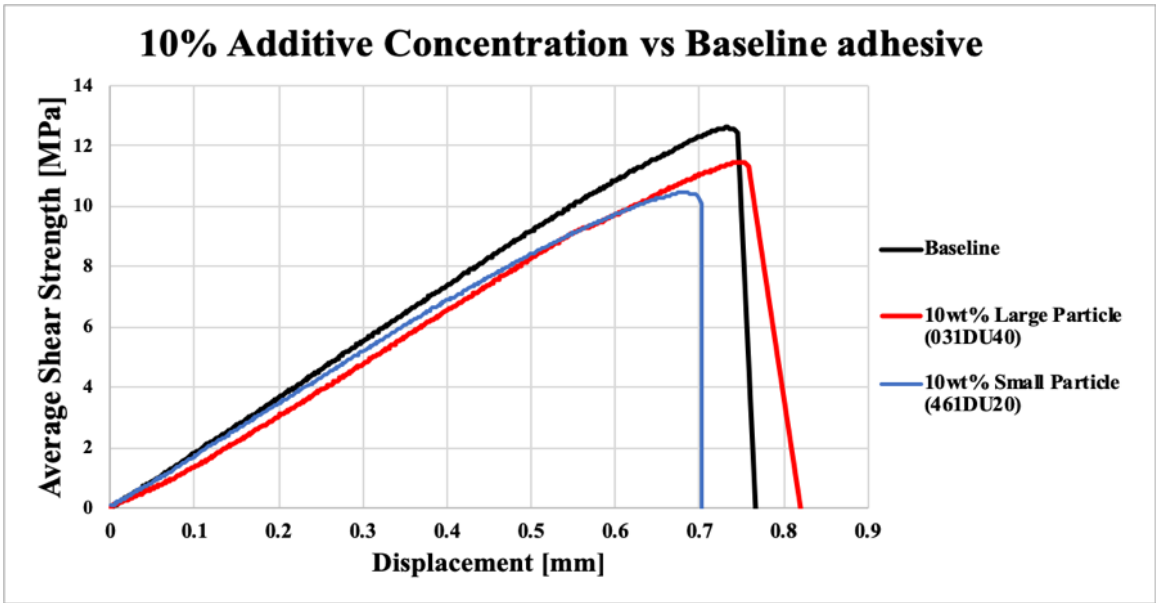


Figure 3.8 10% Additive Concentration vs Baseline Adhesive Stress-Displacement Curves

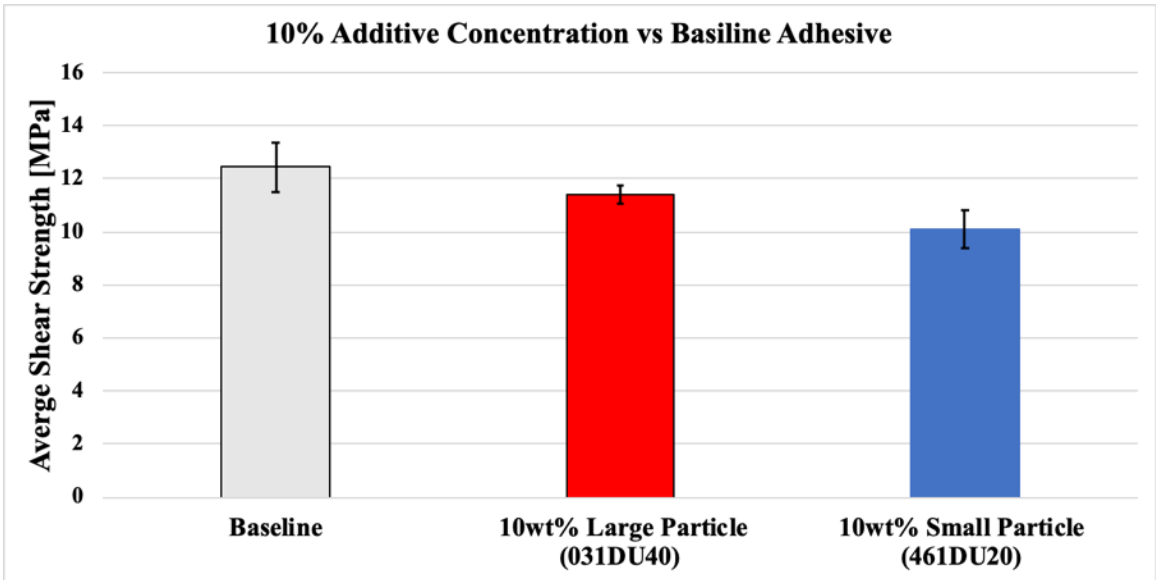


Figure 3.9 Effect of Additive Size on Baseline Adhesive Static Performance (10% Concentration)



Figure 3.10 FEA model of multi-material joint

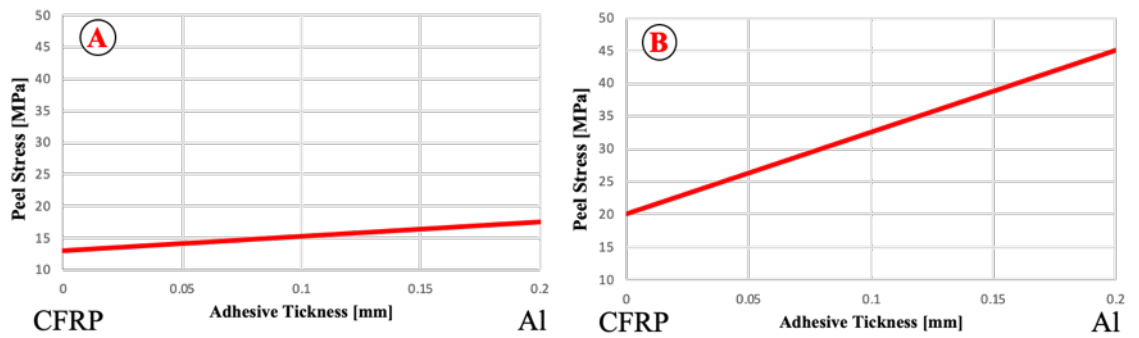
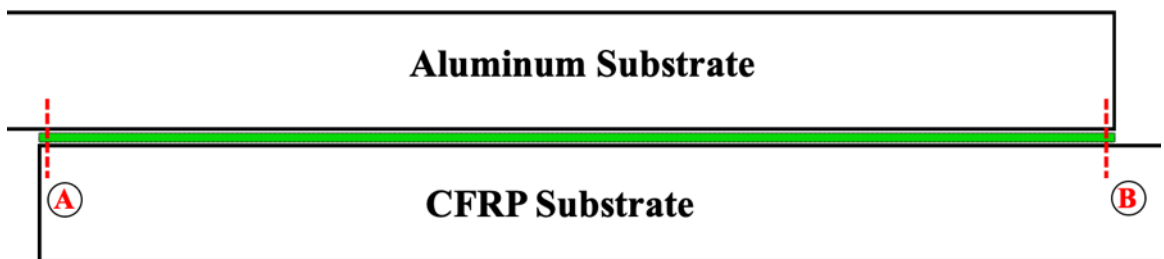


Figure 3.11 Peel Stress Gradient along the adhesive thickness:
 a) Carbon Fiber Side b) Aluminum Side

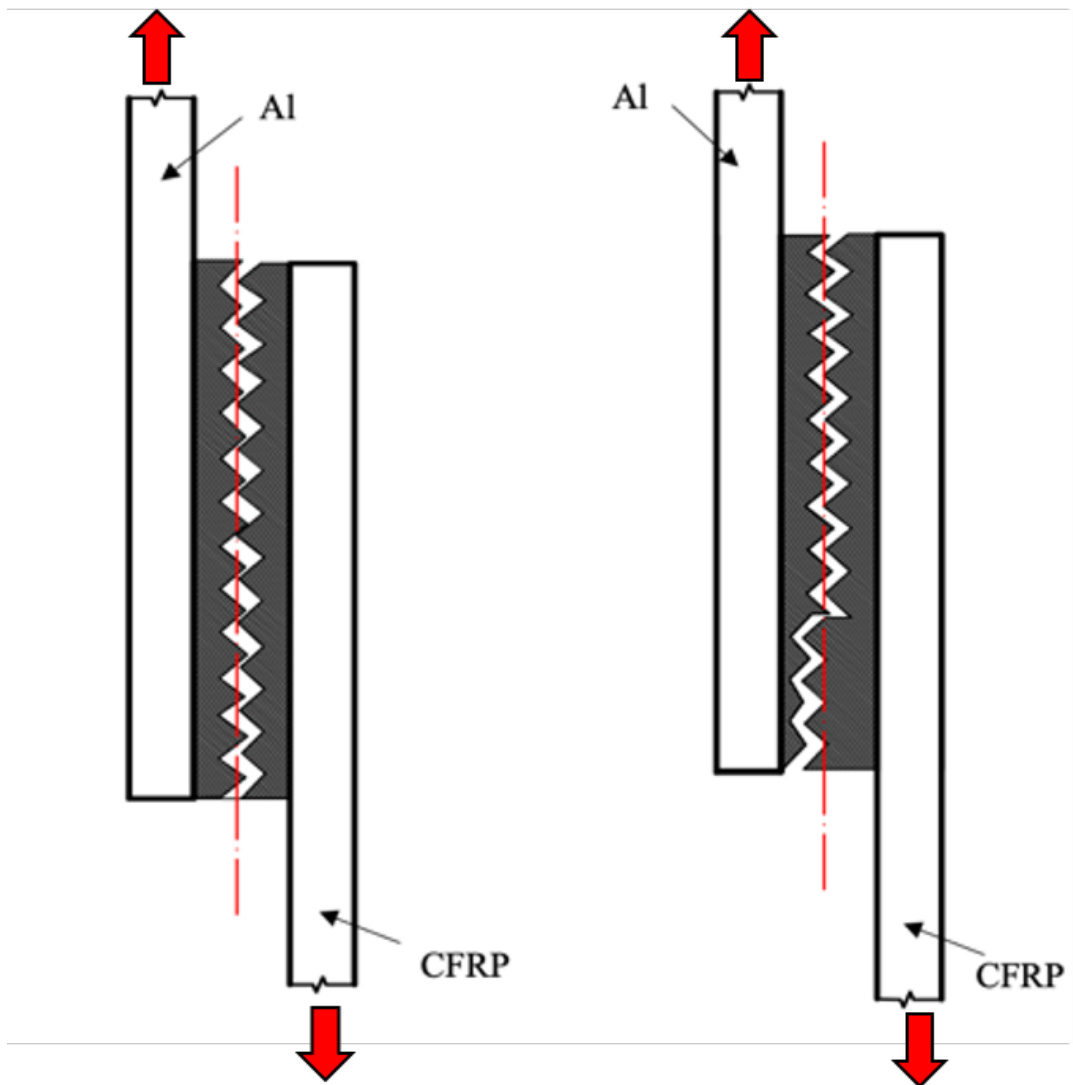


Figure 3.12 Illustration of failure mode change due to particle enrichment

The static strength results for 20wt% enriched samples are reported from Figure 3.13 to 3.16. The stress/displacement curves of the modified adhesives are reported in Figures 3.13 and 3.14. Differently from the previously obtained results the adhesive enriched with the larger particulate size (031DU40) is experiencing a more severe reduction in Load Transfer Capacity when compared with respect to the smaller particulate size (461DU20), respectively 41% and 19% strength reduction (Figure 3.15). Additionally, it is observed that the particle enrichment is not affecting the joint stiffness. It is evident that slope of the curves is similar. The average Lap Shear Strength results are reported in Figure 3.16. The larger particle (031DU40) resulted in a more significant strength reduction with respect to the smaller particle size 461DU20, averaging 7.4 MPa and 10.4 MPa, respectively. The failure mode remains fully cohesive. It is worth mentioning that the fracture surface appears to experience the same variation registered with the specimens tested at 10wt% concentration. The fracture surface shifts from the middle of the bondline towards the aluminum adherend, presenting, again, a sharp step in the fractured adhesive.

3.1.3 Particulate size Effect on Lap Shear Strength

In this section, a summary of the effect of the particle size on the adhesive Lap Shear strength is analyzed. Both the particles cause a decrease in adhesive strength when added to adhesive matrix. However, different additives result in different adhesive behavior. It is interesting to notice that the larger particle dimension (031DU40) is experiencing a constant decreasing trend for increasing concentration, while the smaller particle size (461DU20) experience a first decrease followed by a saturation. Passing from 10wt% to 20wt% the adhesive result to maintain its mechanical strength (Figure 3.17).

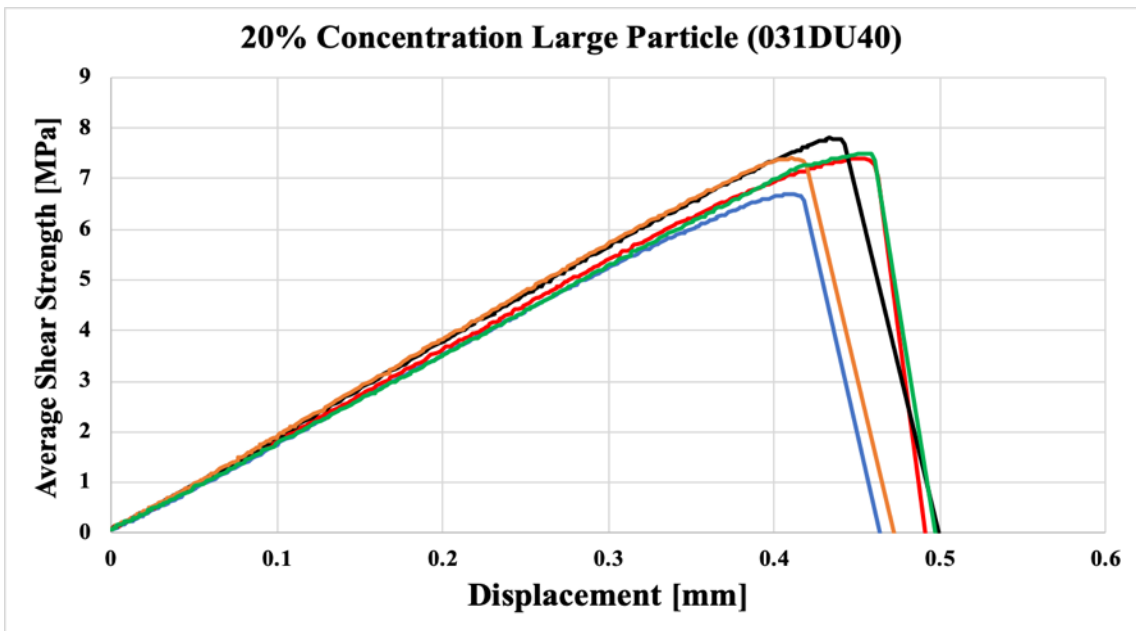


Figure 3.13 20% Concentration Large Size Particles (031DU40) Betamate
73326/77327M Static Test Data

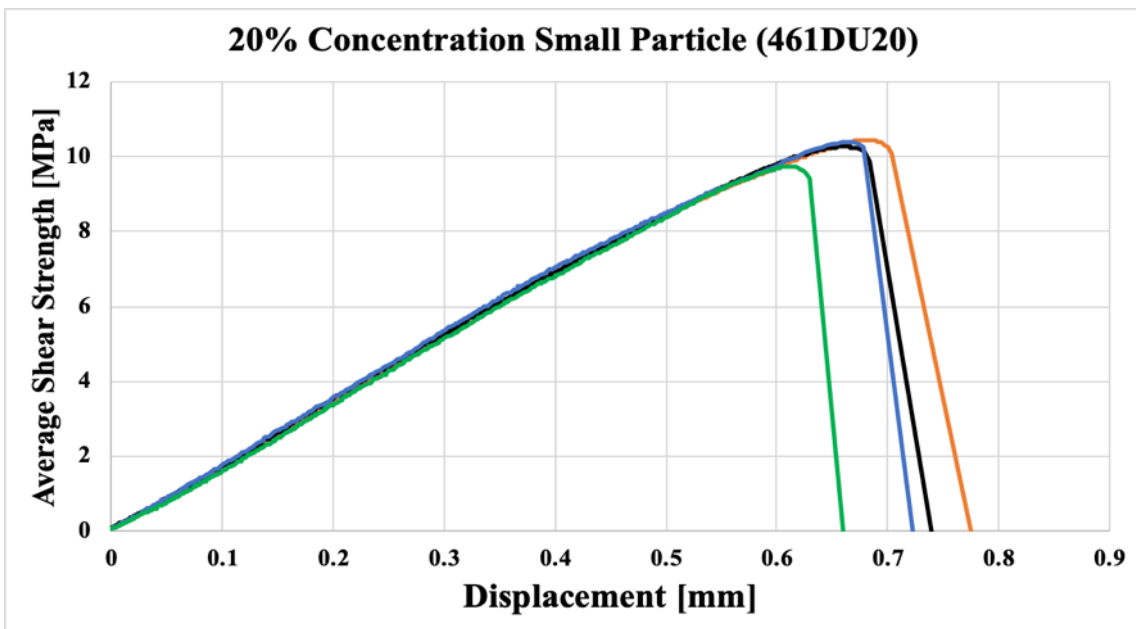


Figure 3.14 20% Concentration Small Size Particles (461DU20) Betamate
73326/77327M Static Test Data

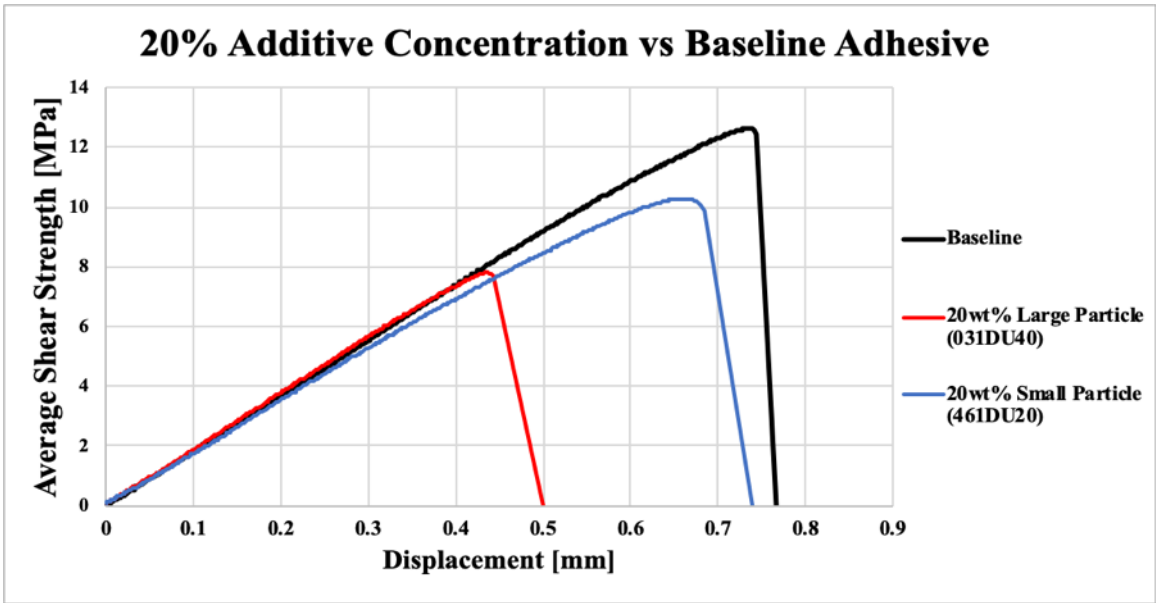


Figure 3.15 20% Additive Concentration vs Baseline Adhesive Stress-Displacement Curves

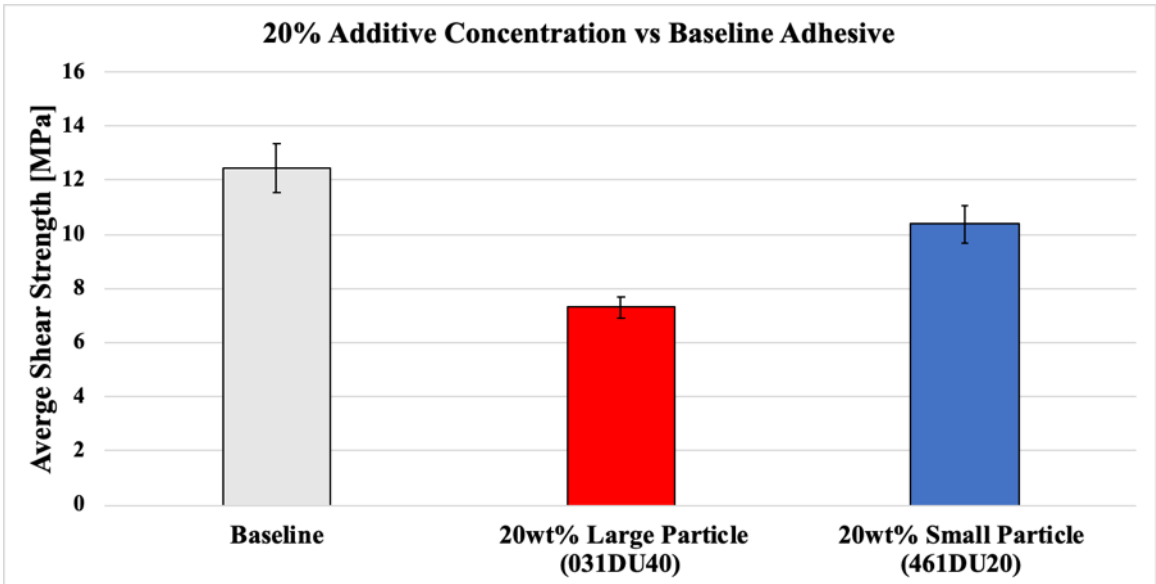


Figure 3.16 Effect of Additive Size on Baseline Adhesive Static Performance (20% Concentration)

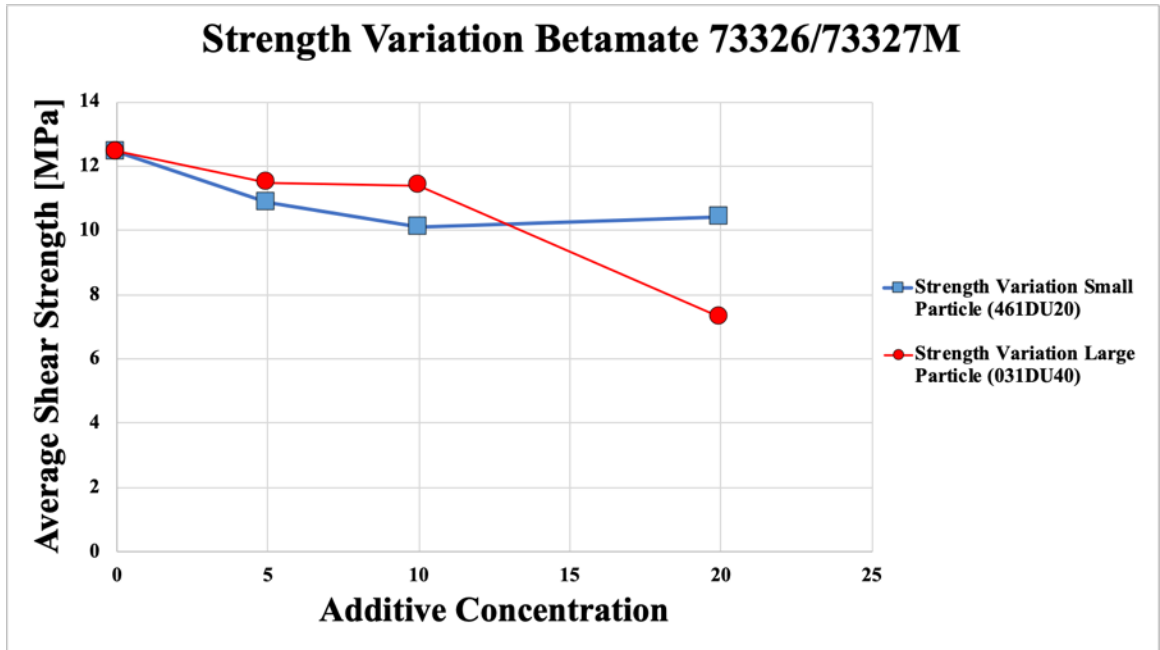


Figure 3.17 Lap Shear Strength Variation Betamate 73326/73327M for Different Additive Concentrations

The observed opposite trend at 20wt% additive concentration can be explained by considering two different factors. The number of particles that are dispersed inside the adhesive matrix and the mechanical properties of the added particles. The modified adhesive characterized by low additives concentration (5wt% and 10wt%) appear to be more affected by the amount of localized stress concentration caused by the particles.

At a given enrichment percentage, joints modified with smaller additive particles (461DU20) contain a larger number of particles than test samples modified with larger diameter 031DU40 additives. This, coupled with the smaller diameter of the particles, results in a higher amount of localized stress concentration (the adhesive's mechanical behavior is almost perfectly elastic, and it is therefore

reasonable to consider the effect of stress concentration even in quasi-static applications, which is normally neglected for elasto-plastic materials).

However, the particles themselves can be responsible for a share of the load bearing capacity of the joints. This effect is more significant for samples with higher additives concentration, in which the particles occupy a significant portion of the adhesive matrix. Smaller particles are characterized by higher strength, and the effect of the spheres' radius on their mechanical performance has been extensively studied in the literature [23-25]. The positive effect of the smaller particles' higher mechanical strength overshadows the negative contribution that these same particles have on the stress concentration in the adhesive matrix, when the additives weight concentration reaches 20wt%.

3.2 Fatigue Test Data and Analysis

In this section the fatigue performance of seven different adhesive/particle combinations are analyzed. Moreover, in order to have a reliable analysis a statistical approach will be used. The results and analysis will be reported considering one concentration at a time.

For this study, two different set of graphs will be used to compare the different adhesive performance. A first set of graphs normalized respect to their maximum LTC and a set of non-normalized graphs. The normalized set will be used to understand if the presence of the particles inside the adhesive emphasizes crack propagation and crack initiation due to localized stress. On the other hand, the non-normalized set will be useful to understand if the absolute fatigue performance of the modified adhesive is reduced (or not) respect to the baseline.

3.2.1 Fatigue Performance of baseline adhesive SLJs

As previously described, three different repetitions for each level of alternating stress at one mean stress level are used to create the S-N curve. For this study the mean stress level has been fixed at 35% of the maximum LTC value. The resulting S-N line, 95% Confidence and 95% prediction intervals are shown in Figure 3.18.

It is noticeable that one of the three samples that were tested at 35% mean stress and 10% alternate load survived up to 1 million cycles. All the tests in which a sample survives up to one million cycles are interrupted.

However, as demonstrated by the ASTM practice for statistical analysis and Schneider et al. [20, 21], it is still possible to use those data in the estimation of the best fit S-N curve.

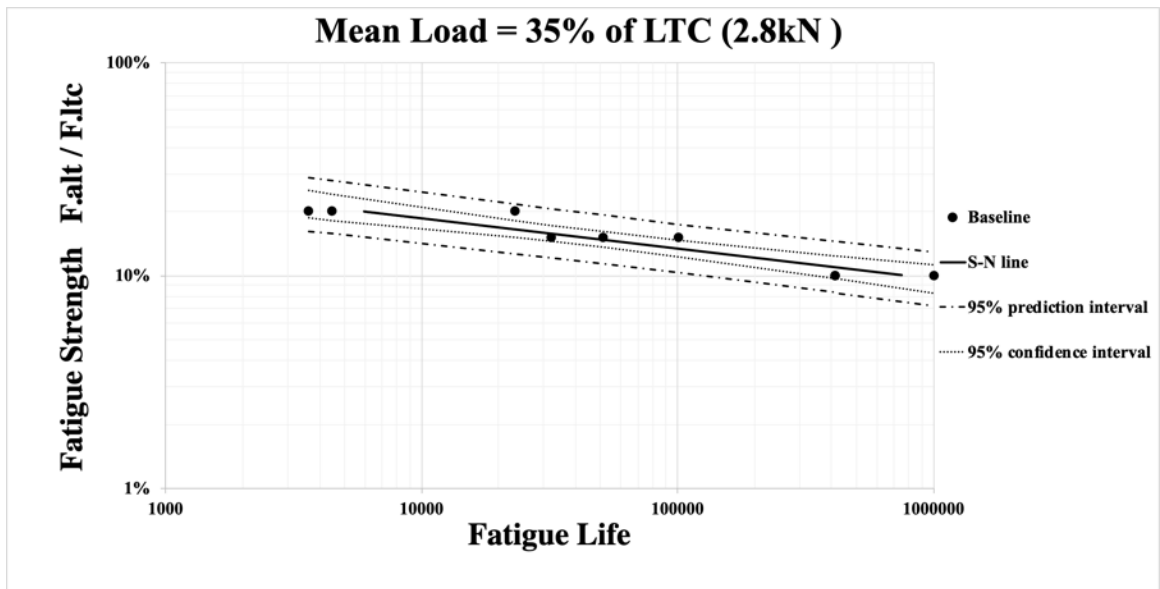


Figure 3.18 Baseline Betamate (73326/73327M) Fatigue Performance (S-N curve)

3.2.2 Effect of Additive Concentration on Fatigue Performance

In this section the fatigue performance of enriched specimens is analyzed. Figures 3.19 to 3.51 show the results of the fatigue tests of 5,10 and 20wt% modified adhesives, with both grades of Expancel additives (031DU40 and 461DU20). For all concentrations the absolute fatigue strength is significantly reduced by the presence of additives within the adhesive matrix.

When the same results are normalized with respect to their own LTC, no statistically significant difference in fatigue strength is observed, comparing baseline with enriched specimens. This allows to infer that the fatigue failure mechanism is not affected by the presence of the additives. When comparing different sets of results, the different data points, 95% confidence intervals, and 95% prediction intervals are shown on the same graphs as in Figures 3.21-3.25.

The alternating stress levels were selected for each combination in order to cause specimens failure within the desired high cycle fatigue (HCL) range, and therefore may vary slightly among weight concentrations. Regardless of the chosen stress amplitudes, the three levels have regular steps from one to the other. The selected stress amplitude for all concentrations are shown in Table 3.1.

Fatigue results for 5wt% additive concentration are shown in Figures 3.19-3.29. S-N curves were drawn for smaller (461DU20) and larger (031DU40) additive particles, these are shown in Figures 3.19 and 3.20, respectively. Two samples enriched with larger 031DU40 survived the 10^6 cycles mark, while none of the specimens made with the smaller 461DU20 enriched adhesive survived. As shown in Figure 3.21, the two predictions bands are overlapped, for the majority of their interval.

Table 3.1 Chosen alternating stress levels for fatigue tests

Additive Concentration	Particle type and size	Alternating Stress (% of LTC)
5wt%	Smaller (461DU20)	25, 20, 15
	Larger (031DU40)	20, 15, 10
10wt%	Smaller (461DU20)	24, 18, 12
	Larger (031DU40)	20, 15, 10
20wt%	Smaller (461DU20)	20, 15, 10
	Larger (031DU40)	20, 15, 10

The confidence intervals show partial overlap only in the lower range of the HCF field, Figure 3.22. The two adhesives have therefore distinct S-N-lines. The slope of the confidence band for the baseline adhesive is slightly steeper than for the 5% enriched joints. The confidence interval of the enriched adhesive in Figure 3.22 does not translate to higher absolute fatigue strength: mean and alternate stress are normalized with respect to the LTC of the enriched SLJs, which is significantly lower than for the baseline adhesive. Confidence and prediction bands for the non-normalized (absolute) fatigue results for specimens enriched with smaller 461DU20 particles are shown in Figures 3.23-3.24, respectively. The two data sets have different mean stress values, with the baseline mean stress being 300N higher than the modified adhesive. The same procedure was applied for the 5wt% larger particles (031DU40) enriched adhesive; confidence and prediction intervals for the normalized

set of data are shown in Figures 3.25-3.26, respectively. Both sets of bands overlap for the entire range.

The same pattern is observed for non-normalized data sets as shown in Figures 3.27-3.28. Similarly, to the previous combination the mean stress at which the enriched specimens were tested is lower than the baseline by 285N.

Finally, a summary of the joints static and fatigue performance (for 100k fatigue life cycles) is reported in Figure 3.29. The graph shows that the baseline is outperforming the modified adhesives in both static and fatigue performance. The adhesive enriched with the smaller particles shows the largest reduction in mechanical strength when compared with respect to the adhesive modified with larger particulate size.

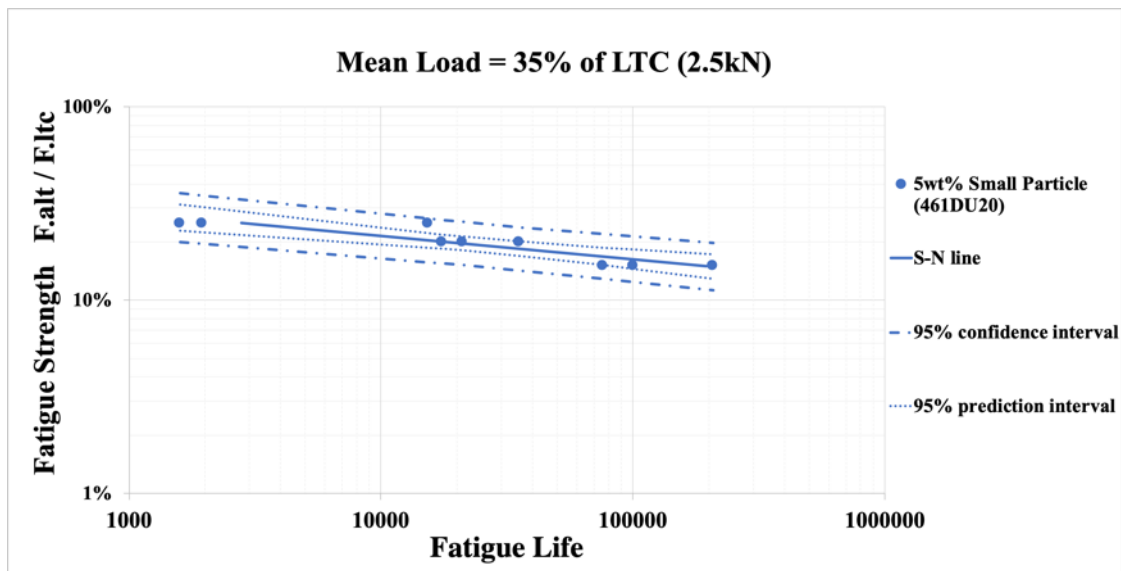


Figure 3.19 5% Concentration Small Particle (461DU20) Fatigue performance (S-N curve)

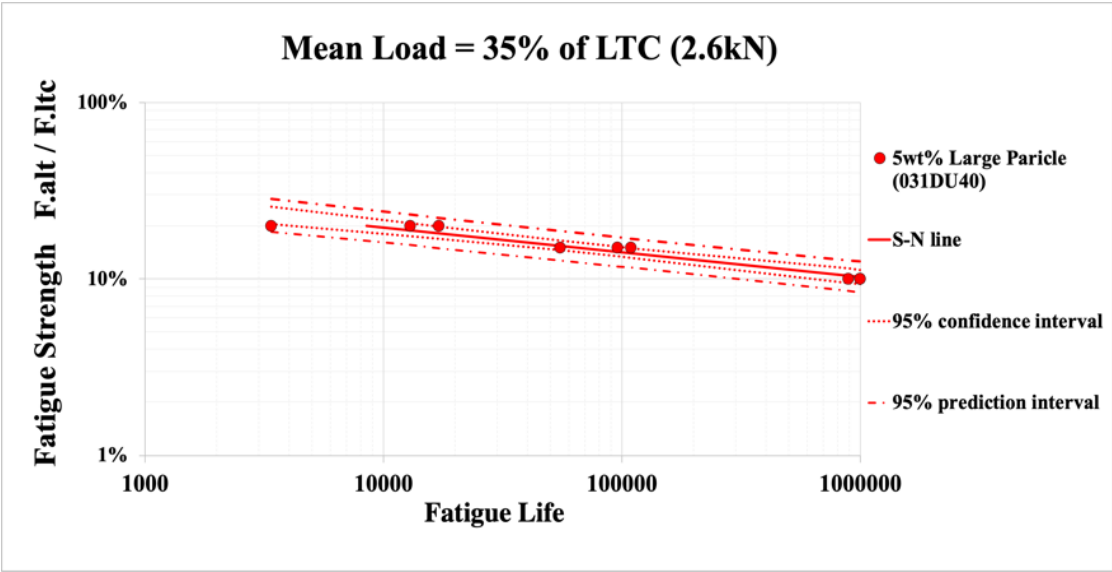


Figure 3.20 5% Concentration Large Particle (031DU40) Fatigue performance (S-N curve)

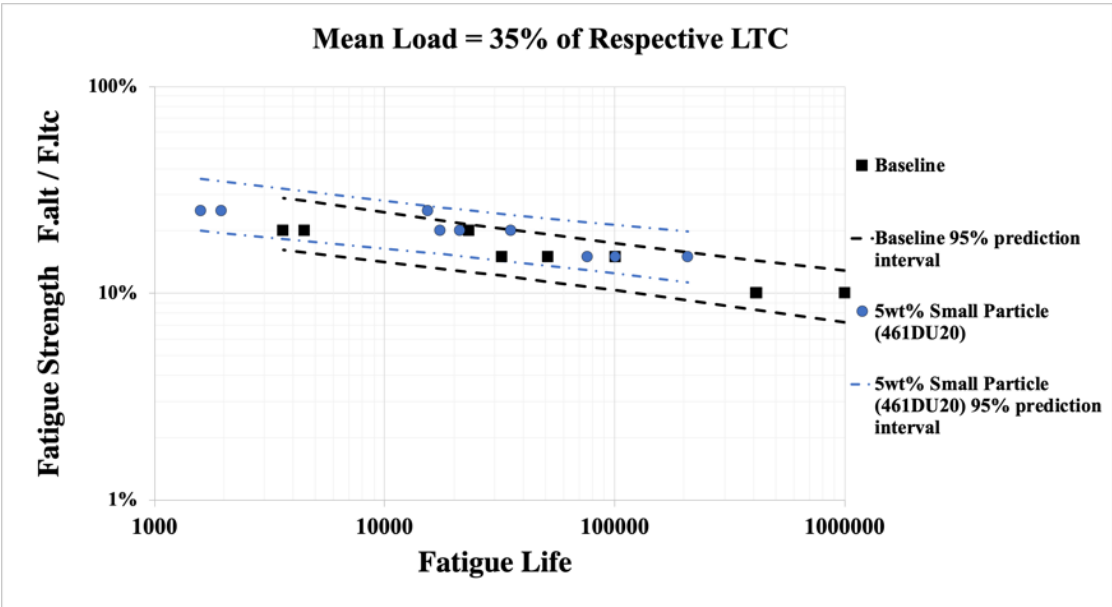


Figure 3.21 Fatigue Data for 5% Additive Concentration vs Baseline Prediction Interval (Small Particle 461DU20)

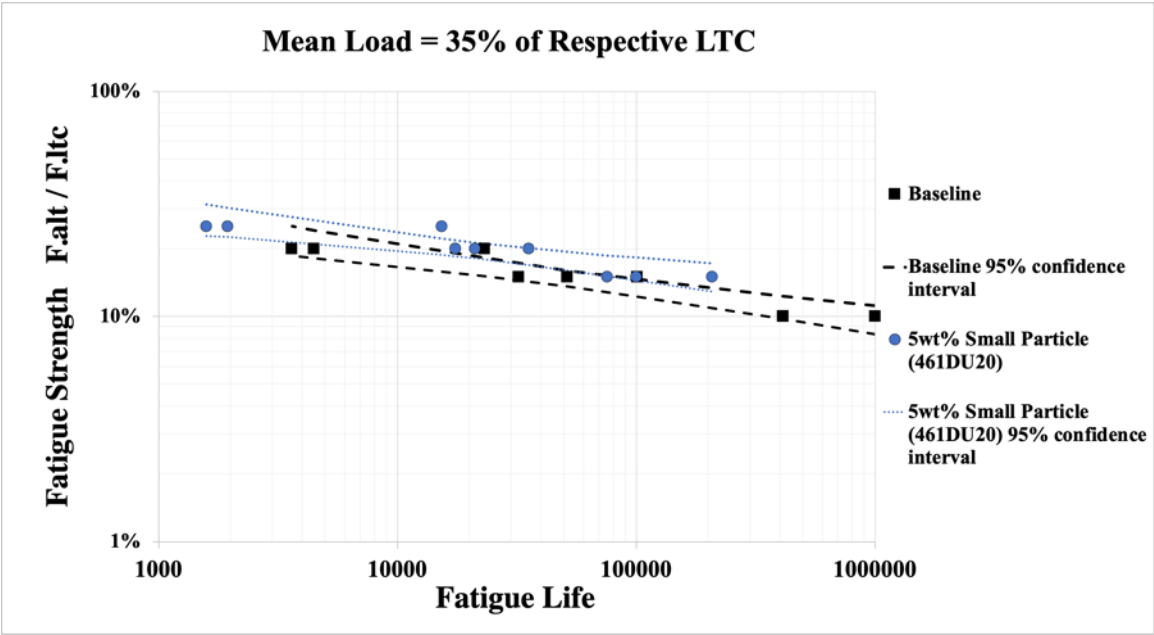


Figure 3.22 Fatigue Data for 5% Additive Concentration vs Baseline Confidence Interval Small Particle (461DU20)

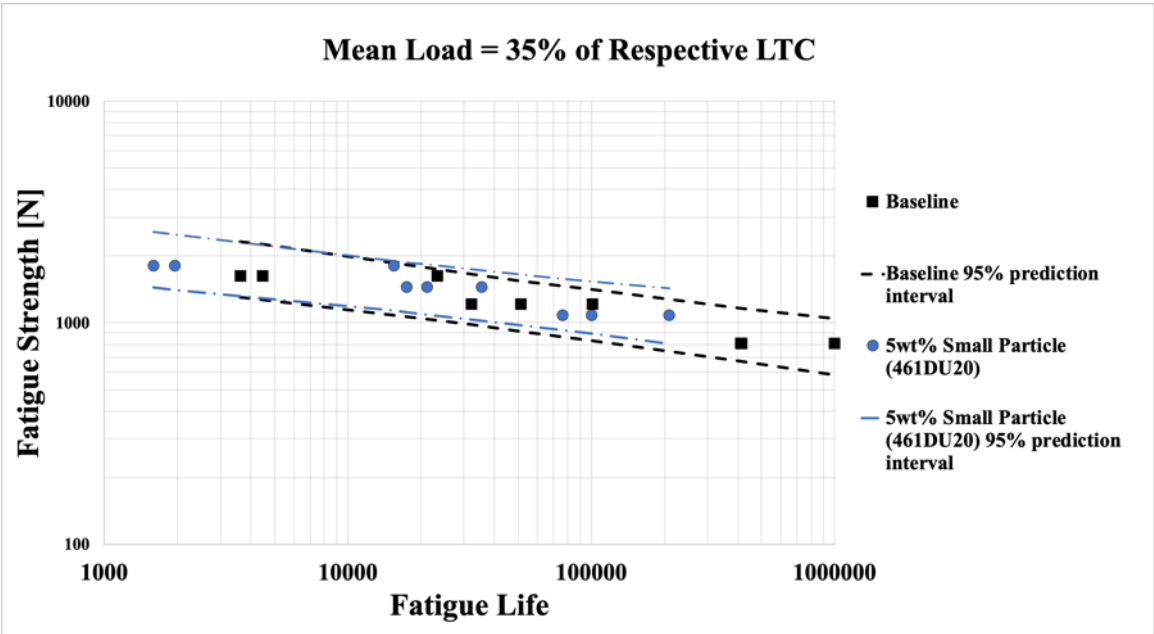


Figure 3.23 Fatigue Data for 5% Additive Concentration vs Baseline Prediction Interval (Small Particle 461DU20, non-normalized)

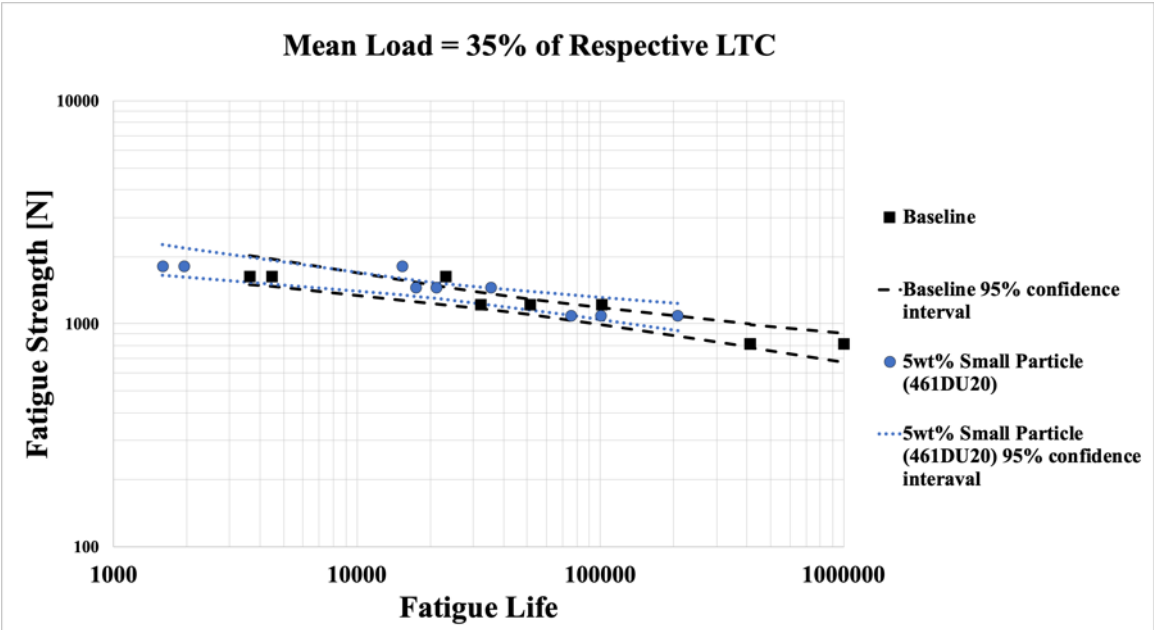


Figure 3.24 Fatigue Data for 5% Additive Concentration vs Baseline Confidence Interval (Small Particle 461DU20, non-normalized)

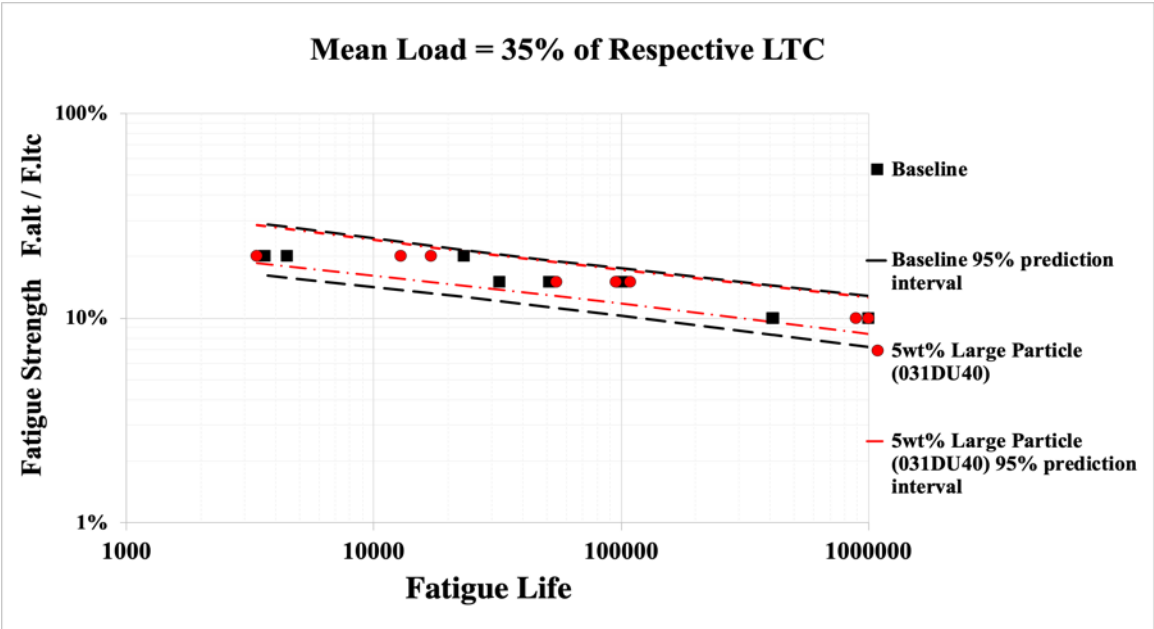


Figure 3.25 Fatigue Data for 5% Additive Concentration vs Baseline Prediction Interval (Large Particle 031DU40)

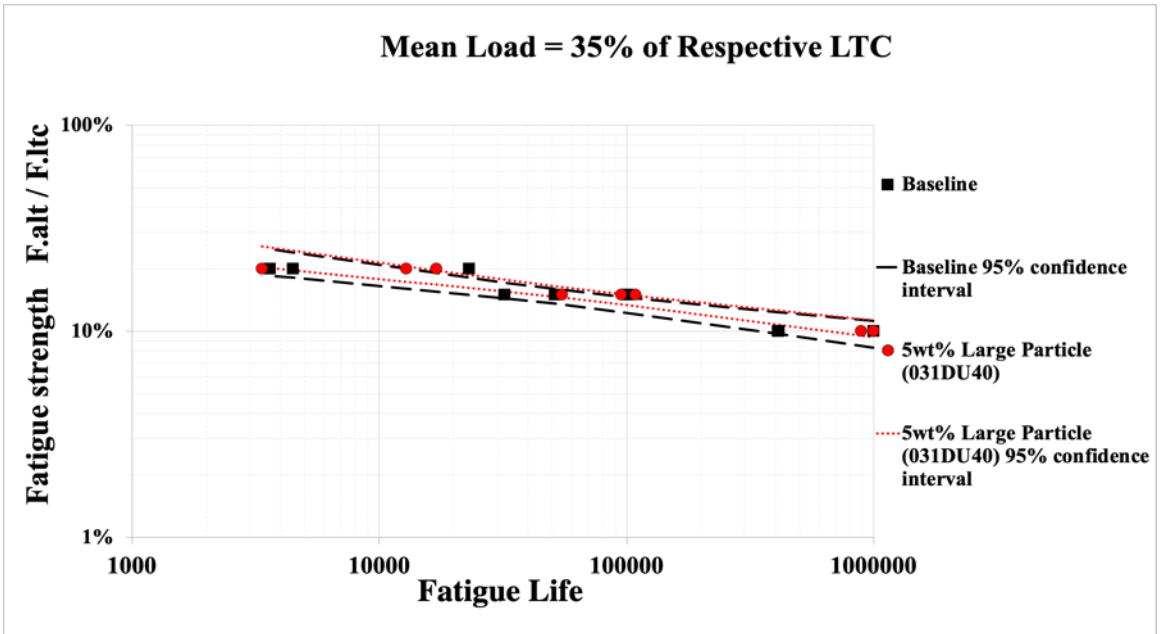


Figure 3.26 Fatigue Data for 5% Additive Concentration vs Baseline Confidence Interval (Large Particle 031DU40)

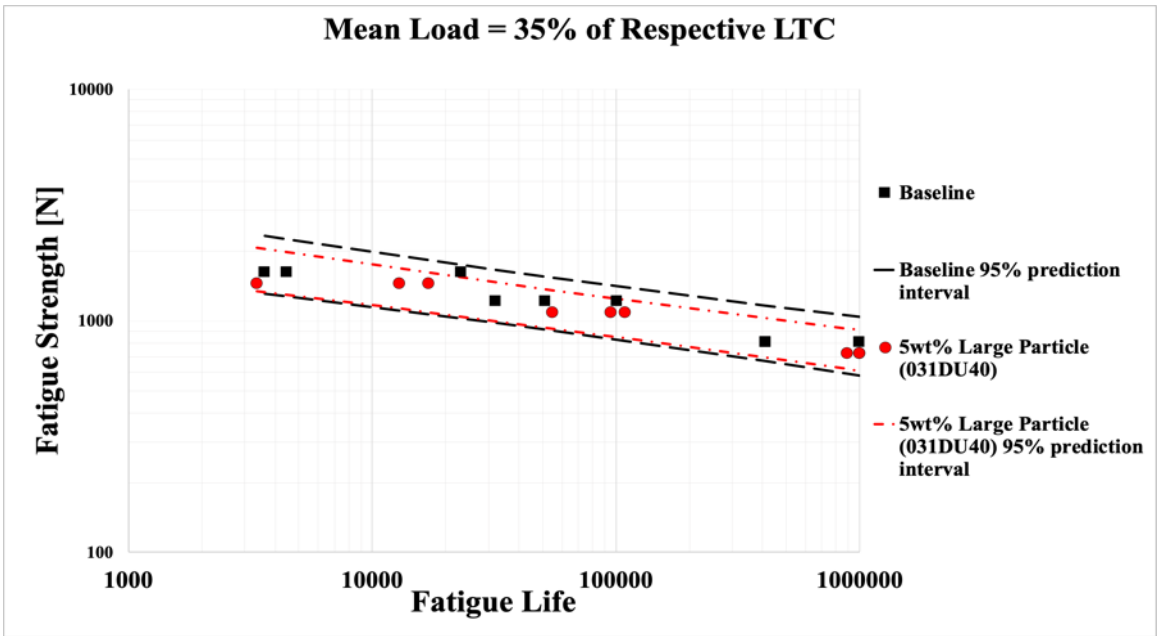


Figure 3.27 Fatigue Data for 5% Additive Concentration vs Baseline Prediction Interval (Large Particle 031DU40, non-normalized)

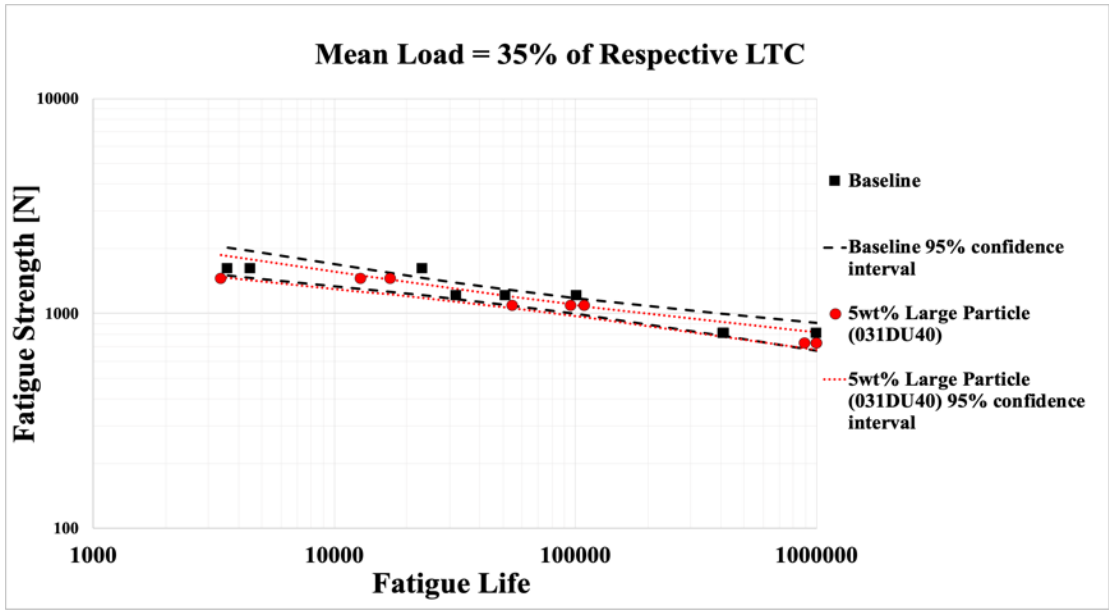


Figure 3.28 Fatigue Data for 5% Additive Concentration vs Baseline Confidence Interval (Large Particle 031DU40, non-normalized)

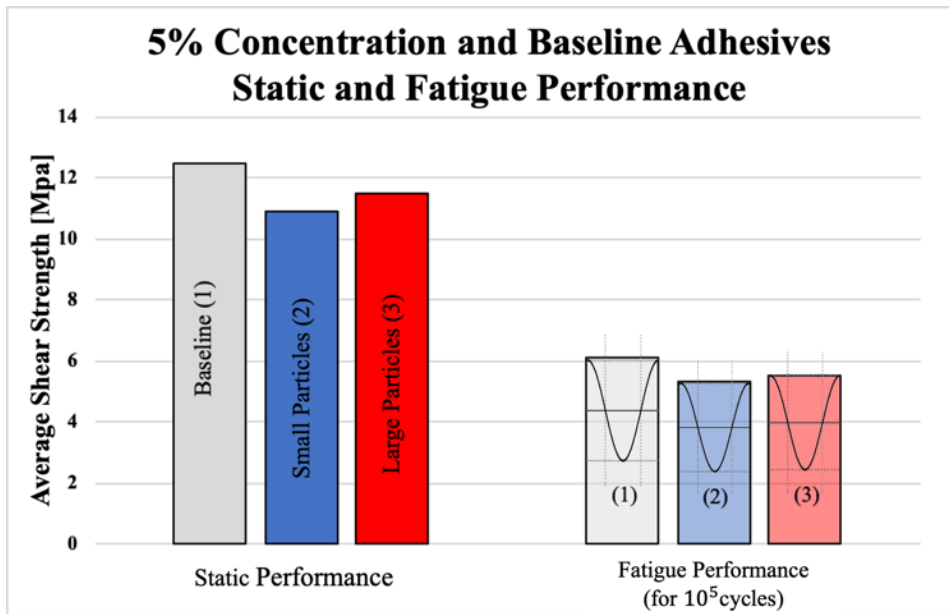


Figure 3.29 5% Concentration vs. Baseline Static and Fatigue Performance (at 10⁵ cycles)

Fatigue results for 10wt% additive concentration are shown in Figures 3.30-3.40. S-N curves were drawn for smaller (461DU20) and larger (031DU40) particles, and are shown in Figures 3.30 and 3.31, respectively. Two samples enriched with larger 031DU40 survived the 10^6 cycles mark, while the same happened for one the specimens made with the smaller 461DU20 adhesive. The two predictions bands are overlapped for the majority of their interval, Figure 3.32. The confidence intervals show partial overlap in the entire HCF field (Figure 3.33), the two adhesives have distinct S-N-lines.

The confidence interval of the enriched adhesive in Figure 3.33 does not translate to higher absolute fatigue strength: the mean and alternate stress are normalized with respect to the LTC of the enriched SLJs, which is significantly lower than for the baseline adhesive. Confidence and prediction bands for the non-normalized (absolute) fatigue results for specimens enriched with smaller 461DU20 particles are shown in Figures 3.34-3.35, respectively. The two data sets have different mean stress values, with the baseline mean stress 503N higher than the modified adhesive.

The same procedure was applied for the 10wt% larger particles (031DU40) enriched adhesive. Confidence and prediction intervals for the normalized set of data are shown in Figures 3.36-3.39, respectively. Both sets of bands overlap for the entire range. The same pattern is observed for non-normalized data sets as shown in Figures 3.27-3.28. Similarly, to the previous combination the mean stress at which the enriched specimens were tested is lower than the baseline by 100N. Finally, a summary of the joints static and fatigue performance (for 10^5 fatigue life cycles) is reported in Figure 3.40. The graph shows that the baseline is outperforming the modified adhesives in both static and fatigue performance.

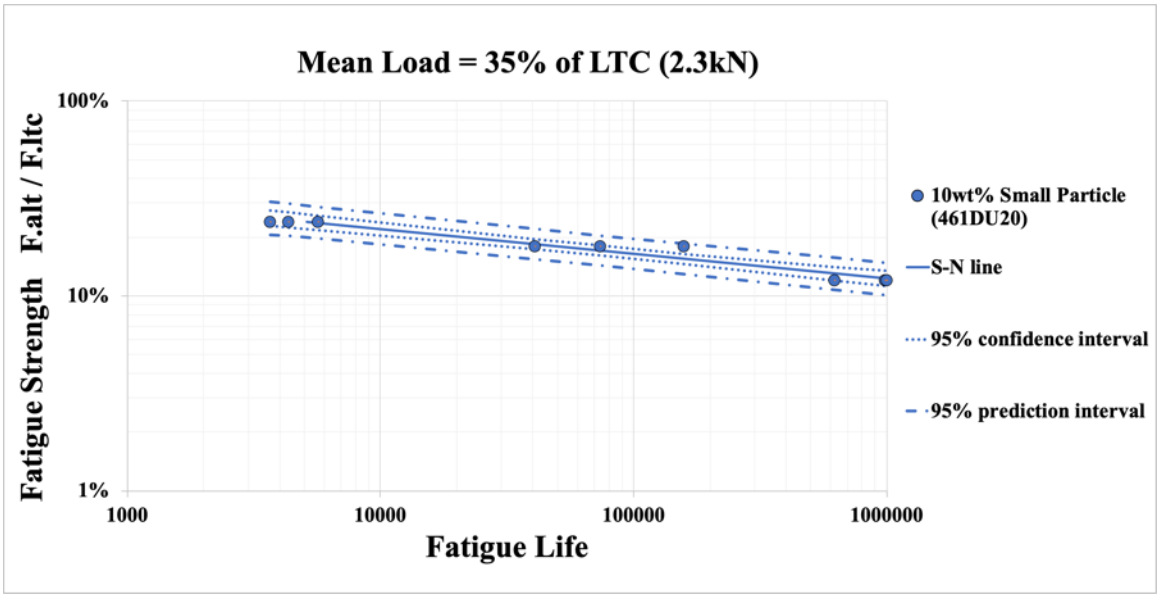


Figure 3.30 10% Concentration Small Particle (461DU20) Fatigue performance (S-N curve)

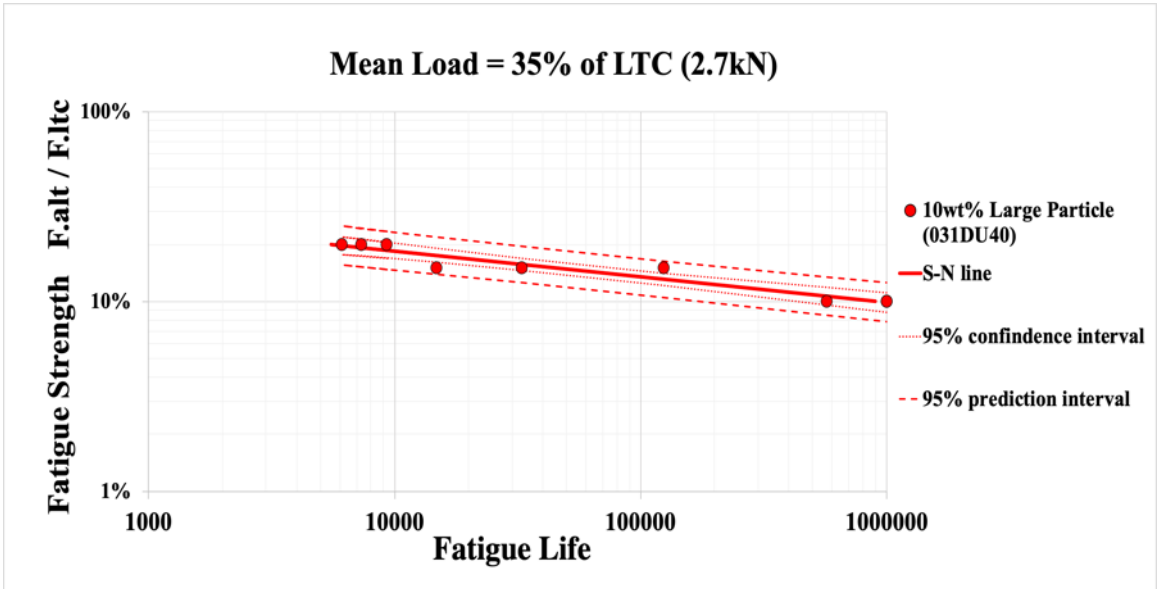


Figure 3.31 10% Concentration Large Particle (031DU40) Fatigue performance (S-N curve)

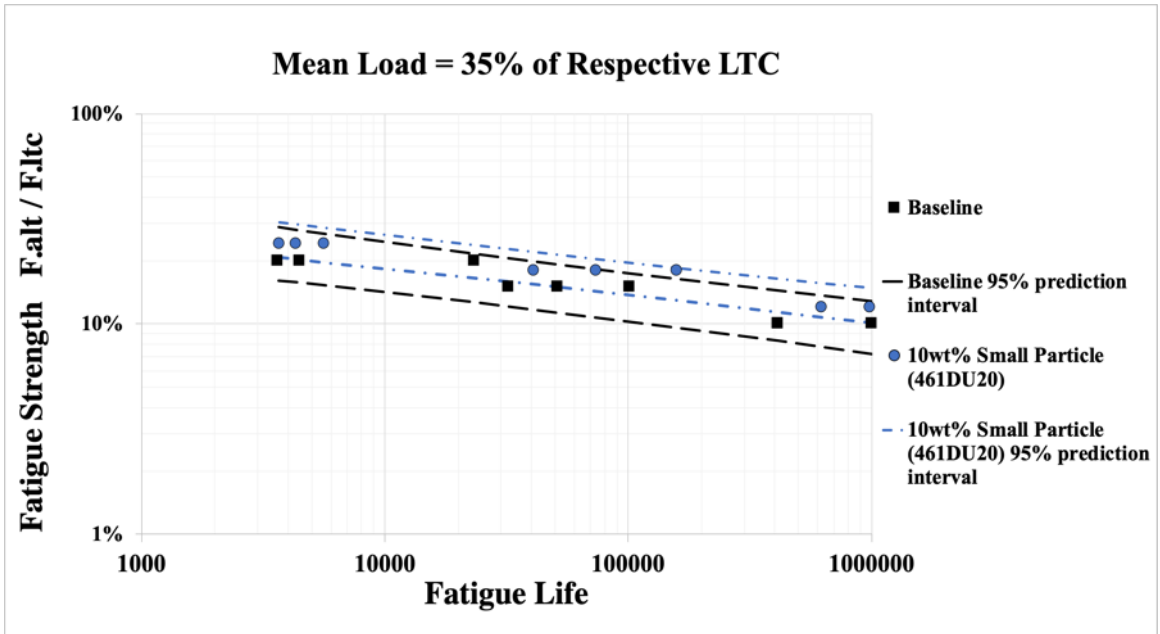


Figure 3.32 Fatigue Data for 10% Additive Concentration vs Baseline Prediction Interval (Small Particle 461DU20)

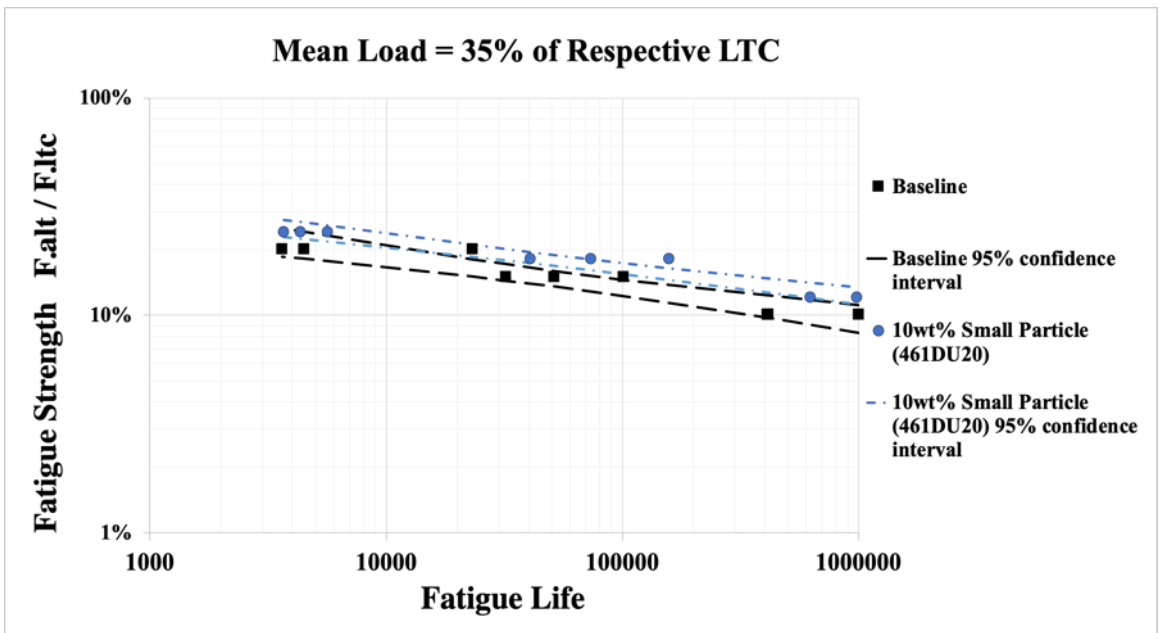


Figure 3.33 Fatigue Data for 10% Additive Concentration vs Baseline Confidence Interval (Small Particle 461DU20)

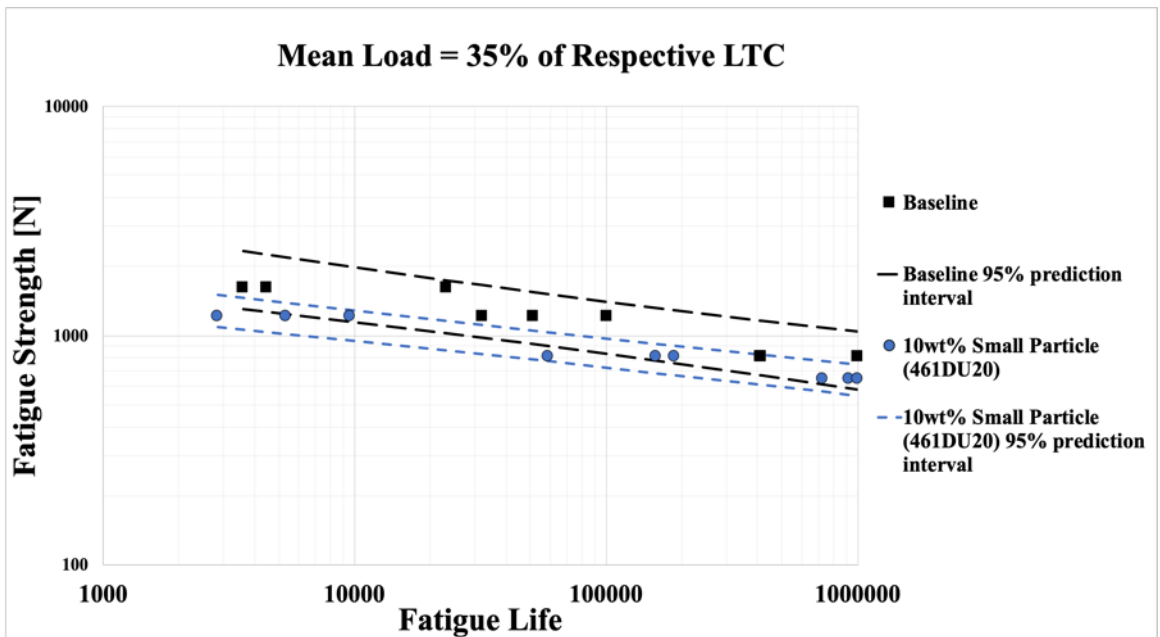


Figure 3.34 Fatigue Data for 10% Additive Concentration vs Baseline Prediction Interval (Small Particle 461DU20, non-normalized)

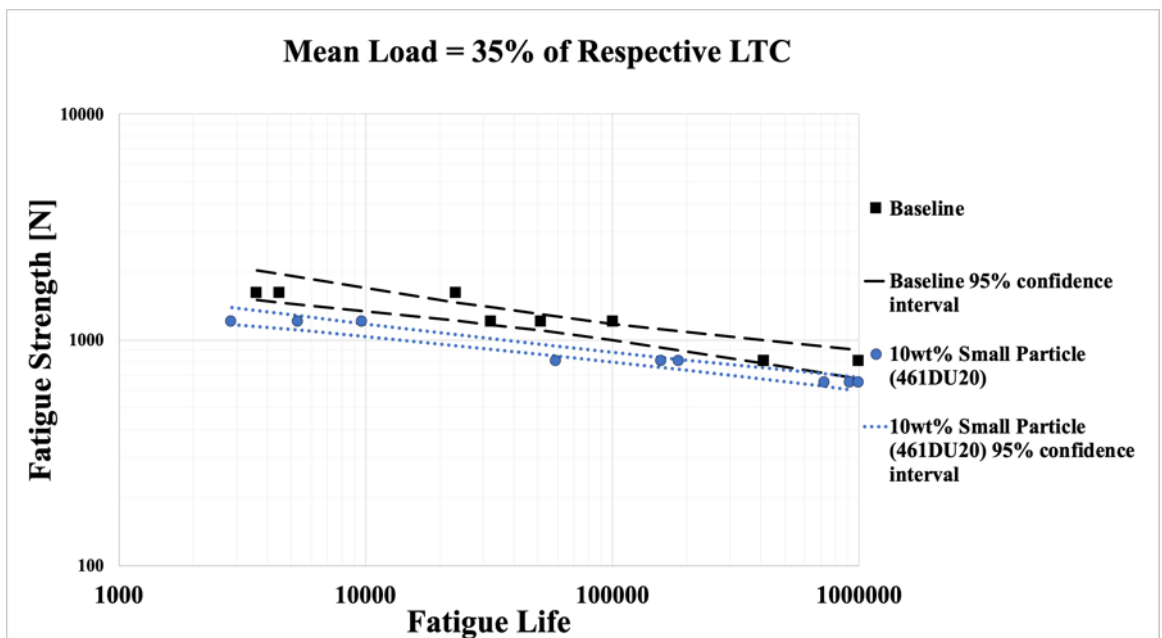


Figure 3.35 Fatigue Data for 10% Additive Concentration vs Baseline Confidence Interval (Small Particle 461DU20, non-normalized)

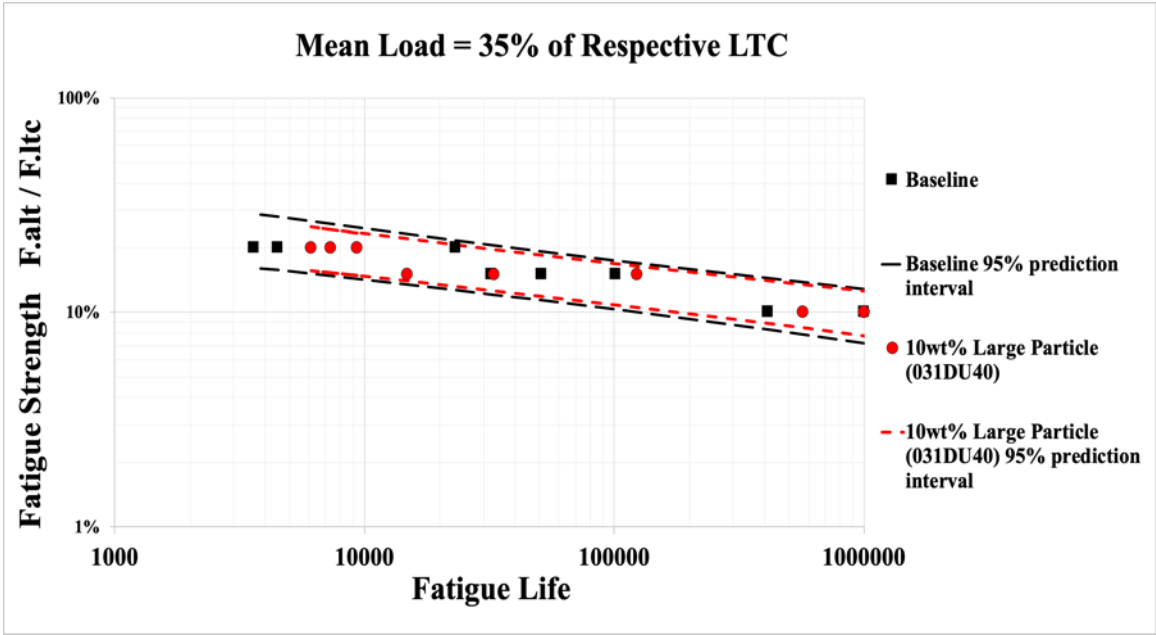


Figure 3.36 Fatigue Data for 10% Additive Concentration vs Baseline Prediction Interval (Large Particle 031DU40)

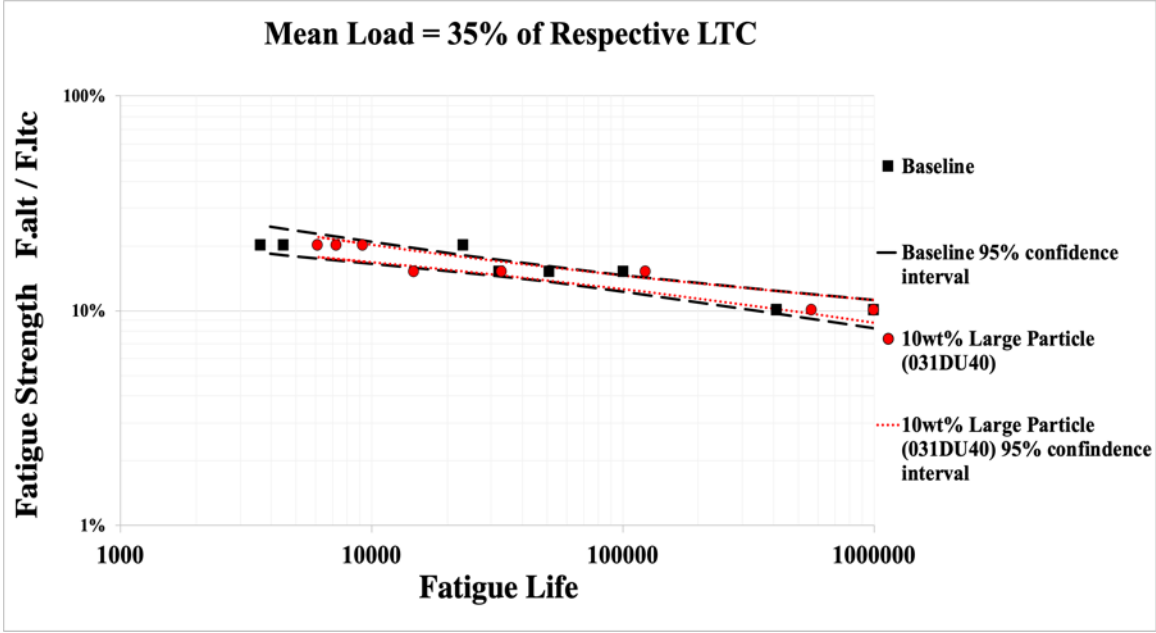


Figure 3.37 Fatigue Data for 10% Additive Concentration vs Baseline Confidence Interval (Large Particle 031DU40)

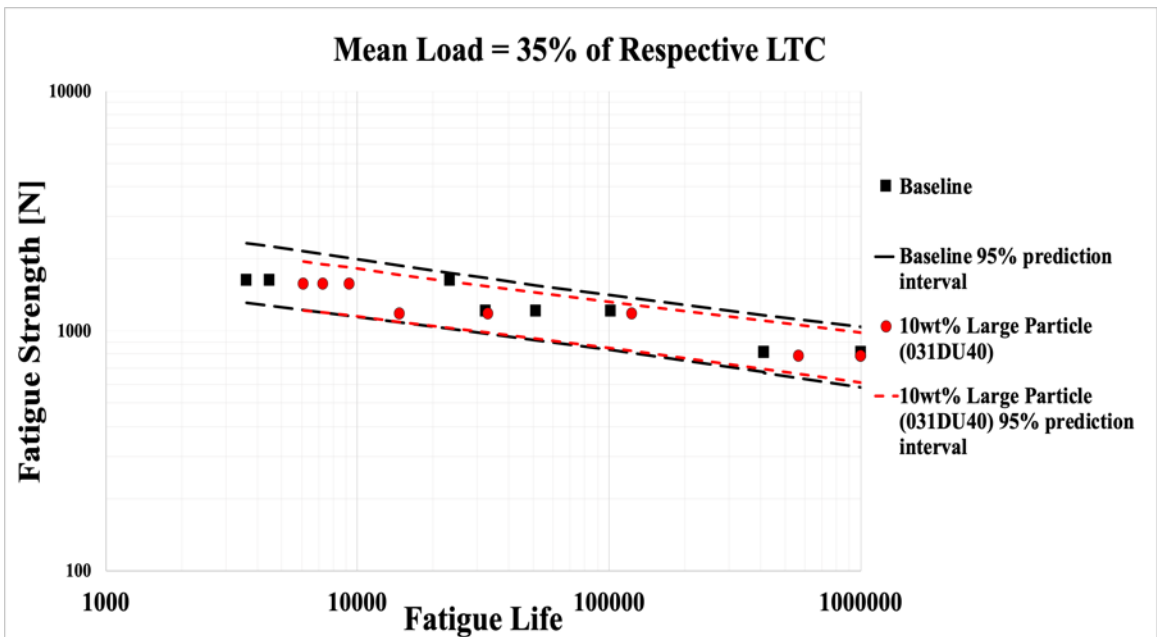


Figure 3.38 Fatigue Data for 10% Additive Concentration vs Baseline Prediction Interval (Large Particle 031DU40, non-normalized)

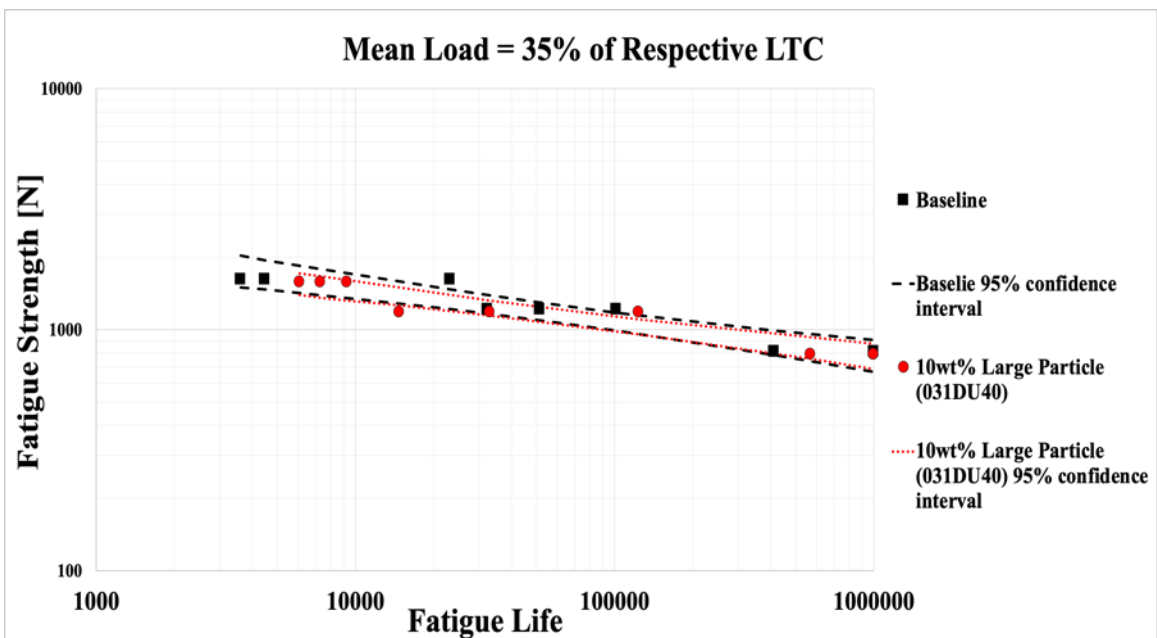


Figure 3.39 Fatigue Data for 10% Additive Concentration vs Baseline Confidence Interval (Large Particle 031DU40, non-normalized)

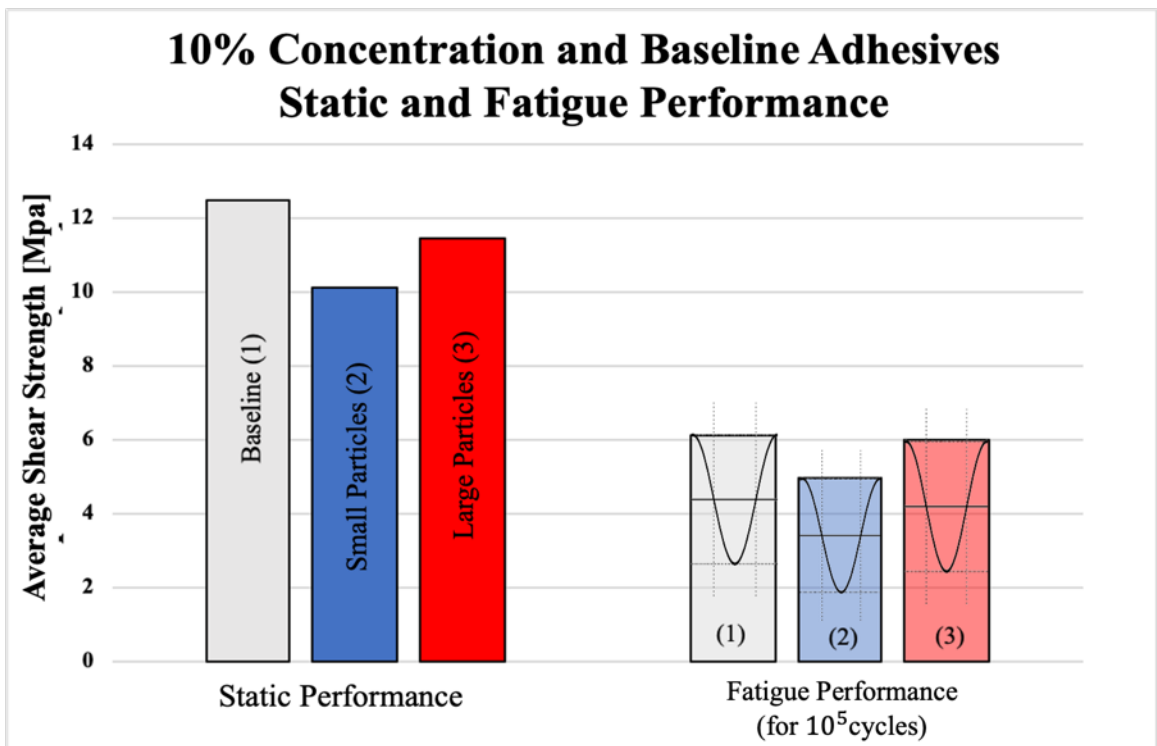


Figure 3.40 10% Concentration vs. Baseline Static and Fatigue Performance (at 10^5 cycles)

The fatigue results for 20wt% concentration specimens are reported in Figs. 3.41-3.51. S-N curves were drawn for smaller (461DU20) and larger (031DU40) particles, and are shown in Figures 3.41 and 3.42, respectively. Two samples enriched with larger particles (031DU40) survived the 10^6 cycles mark, the same happened for one the specimens made with smaller particles (461DU20) adhesive. The two predictions bands are overlapping as shown in Figure 3.43, while the confidence intervals show partial overlap in the whole HCF field (Figure 3.44). The two adhesives have distinct S-N-lines.

However, the confidence interval of the enriched adhesive in Figure 3.44 does not translate to higher absolute fatigue strength: its mean and alternate stress are significantly lower than for the baseline adhesive. Confidence and prediction bands for the non-normalized (absolute) results for samples enriched with smaller (461DU20) particles are shown in Figs. 3.45-3.46, respectively. The two data sets have different mean stress values, with the baseline mean stress being 355N higher than the modified adhesive.

The same procedure was applied for the 20wt% larger particles (031DU40) enriched adhesive. Confidence and prediction intervals for the normalized set of data are shown in Figures 3.47-3.50, respectively. The normalized set of bands overlap for the entire range. However, a different pattern is observed for non-normalized data sets as shown in Figures 3.49-3.50. Differently to the previous combination the mean stress at which the enriched specimens were tested is lower than the baseline by 60% (1.1 kN), resulting in an evident difference between the two adhesives.

Finally, a summary of the joints static and fatigue performance (for 10^5 fatigue life cycles) is reported in Figure 3.29. The graph shows that the baseline is outperforming the modified adhesives in both static and fatigue performance

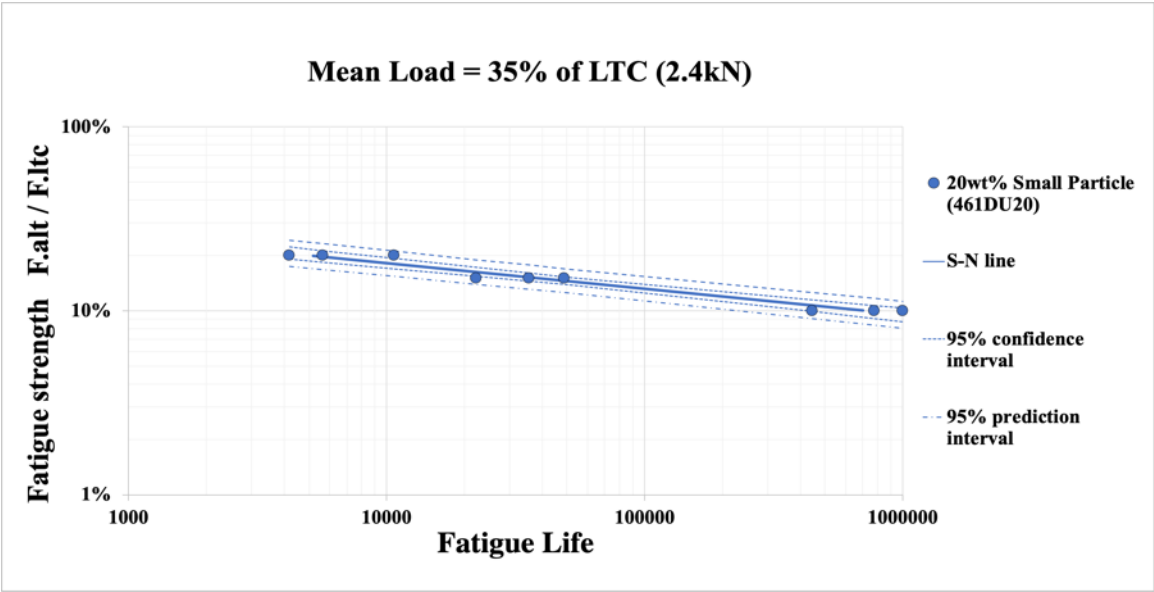


Figure 3.41 20% Concentration Small Particle (461DU20) Fatigue performance (S-N curve)

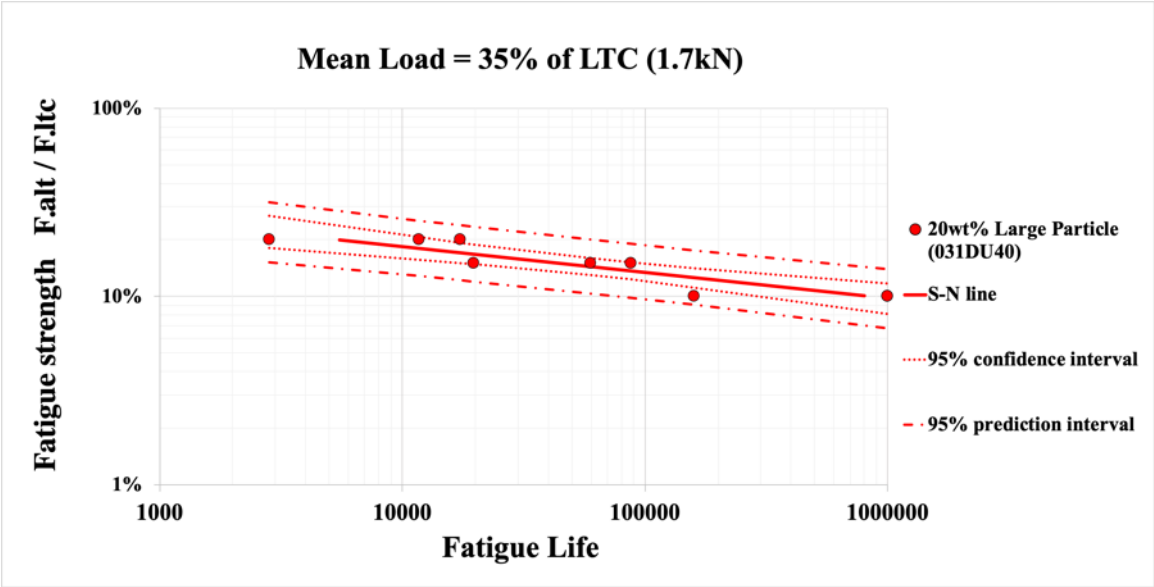


Figure 3.42 20% Concentration Large Particle (031DU40) Fatigue performance (S-N curve)

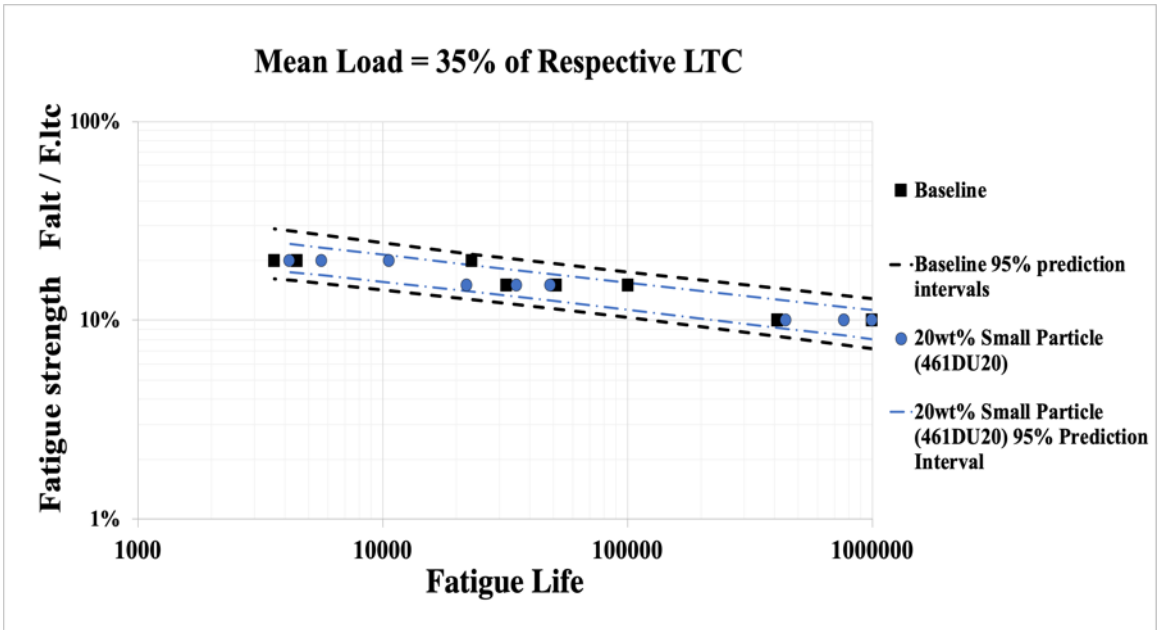


Figure 3.43 Fatigue Data for 20% Additive Concentration vs Baseline Prediction Interval (Small Particle 461DU20)

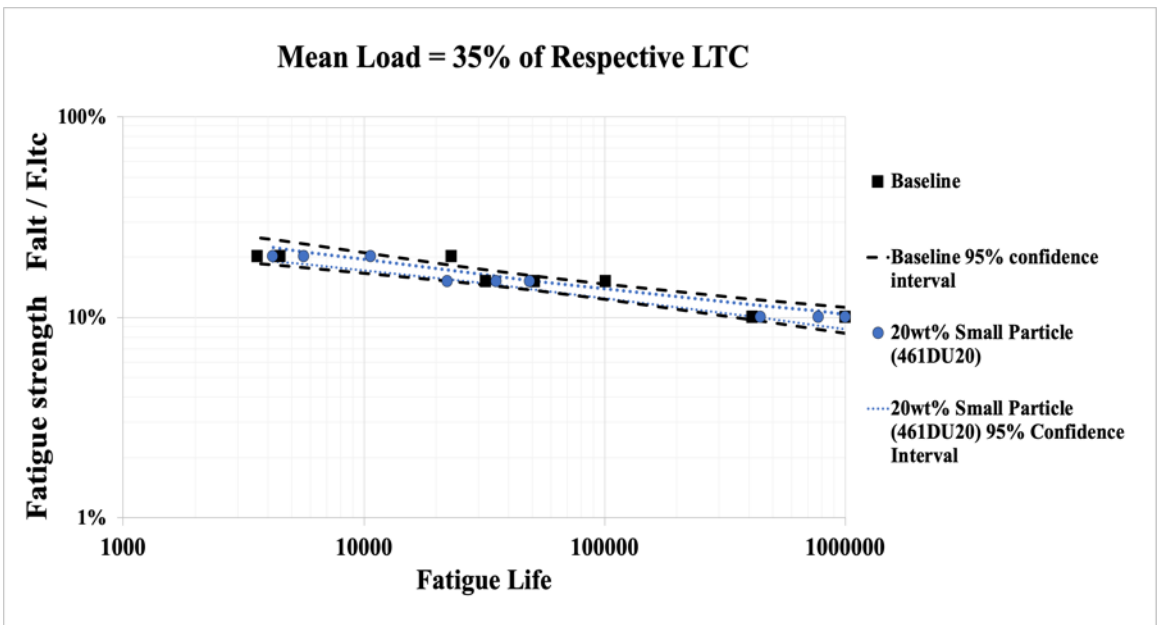


Figure 3.44 Fatigue Data for 20% Additive Concentration vs Baseline Confidence Interval (Small Particle 461DU20)

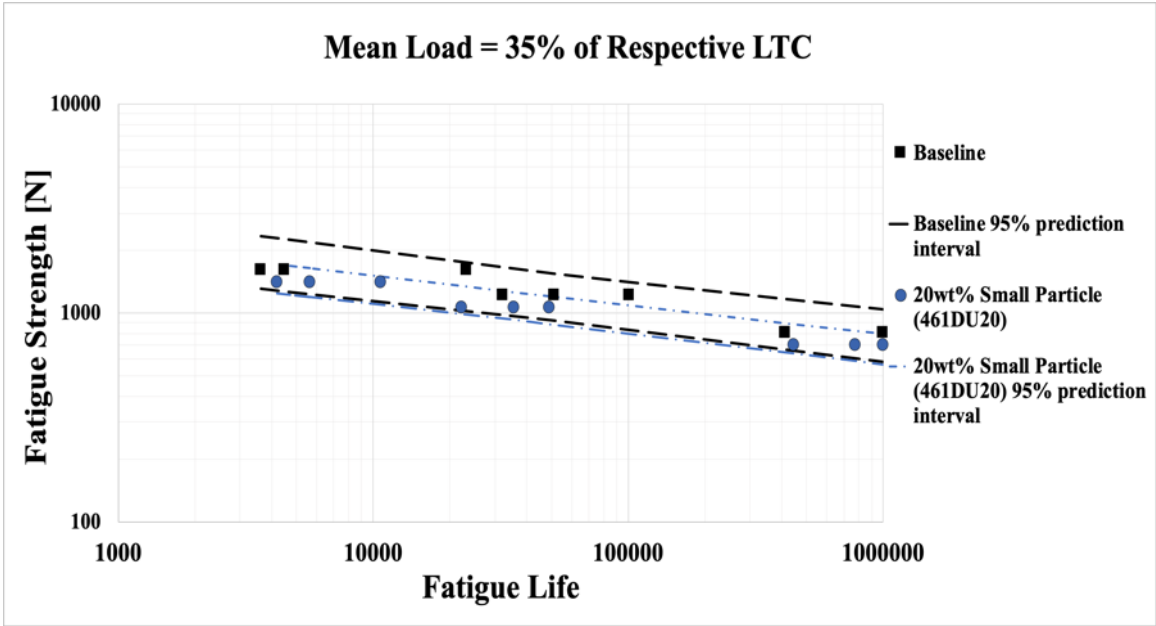


Figure 3.45 Fatigue Data for 20% Additive Concentration vs Baseline Prediction Interval (Small Particle 461DU20, non-normalized)

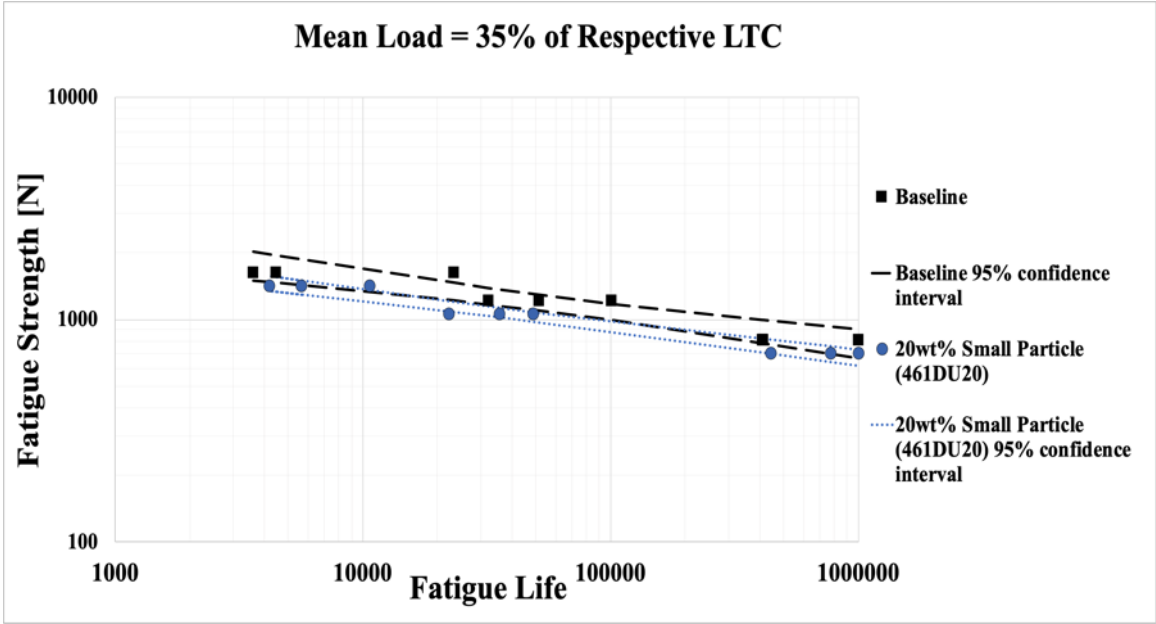


Figure 3.46 Fatigue Data for 20% Additive Concentration vs Baseline Confidence Interval (Small Particle 461DU20, non-normalized)

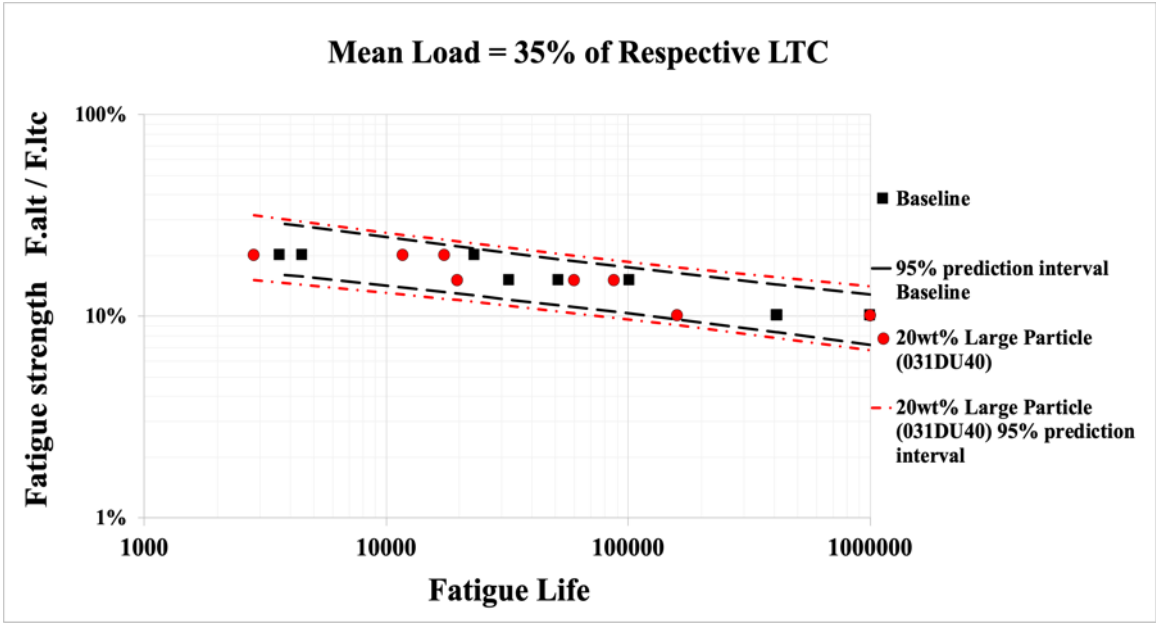


Figure 3.47 Fatigue Data for 20% Additive Concentration vs Baseline Prediction Interval (Large Particle 031DU40)

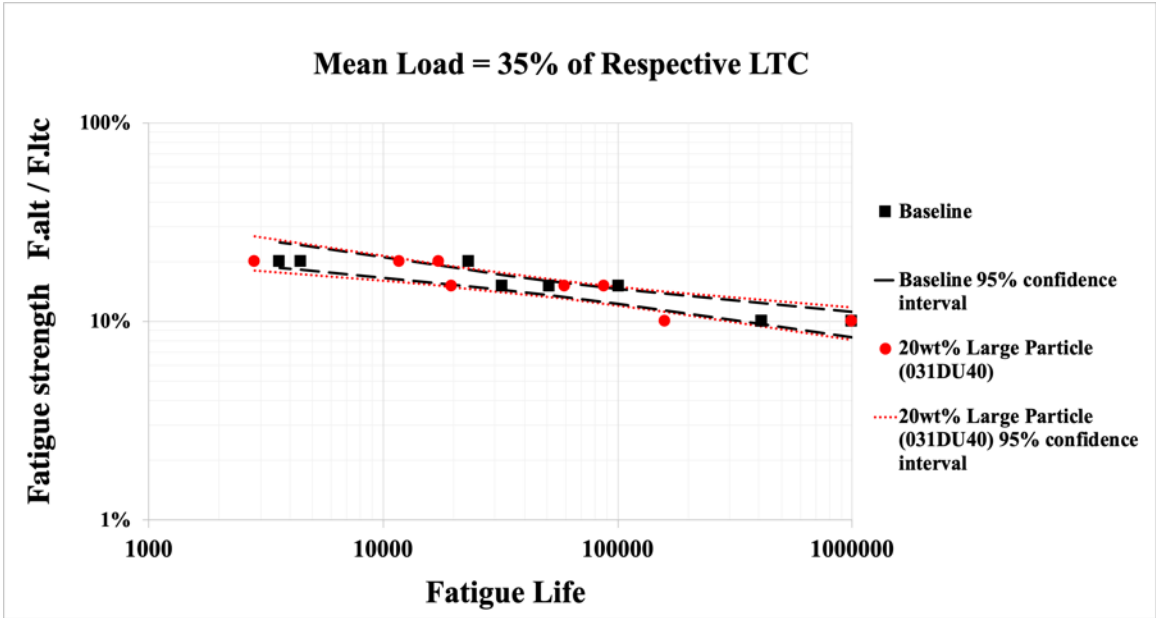


Figure 3.48 Fatigue Data for 20% Additive Concentration vs Baseline Confidence Interval (Large Particle 031DU40)

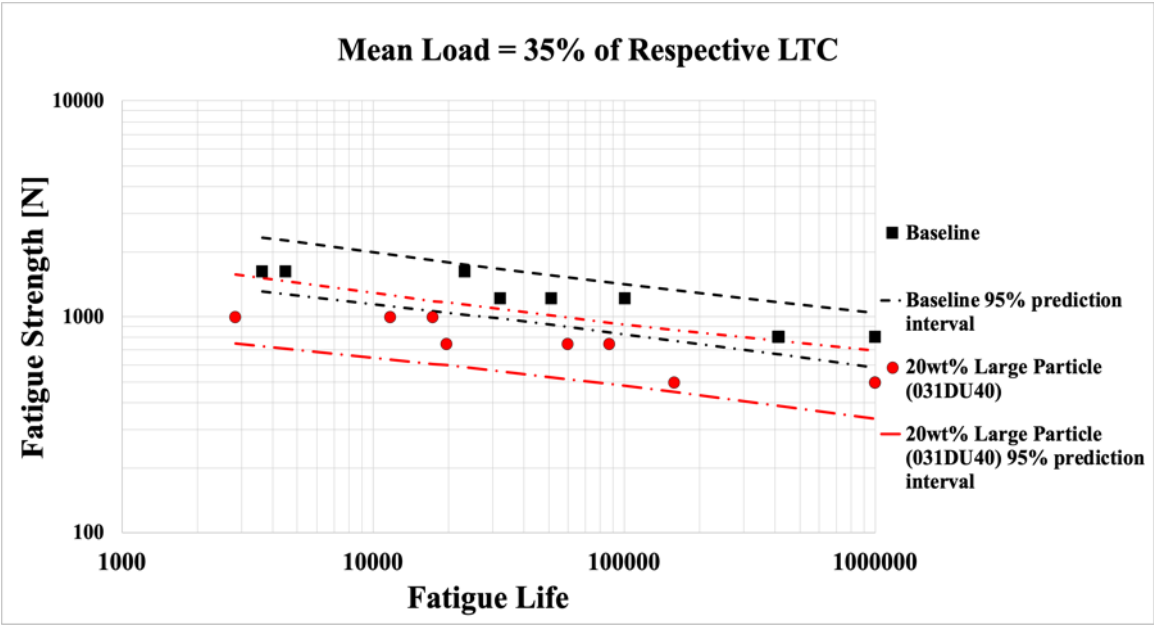


Figure 3.49 Fatigue Data for 20% Additive Concentration vs Baseline Prediction Interval (Large Particle 031DU40, non-normalized)

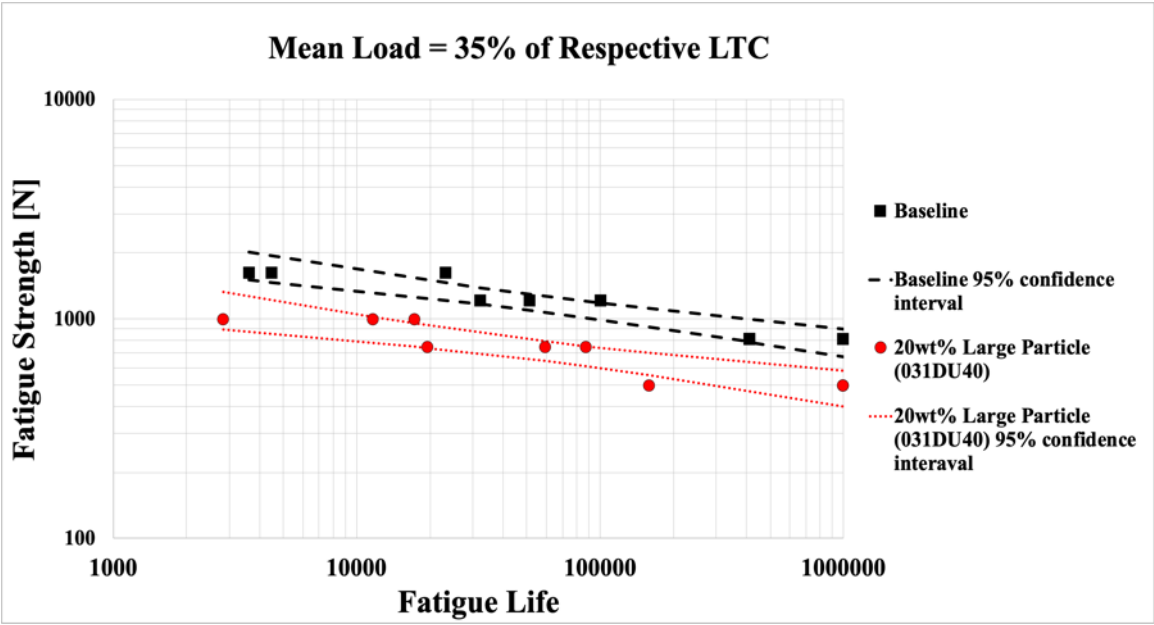


Figure 3.50 Fatigue Data for 20% Additive Concentration vs Baseline Confidence Interval (Large Particle 031DU40, non-normalized)

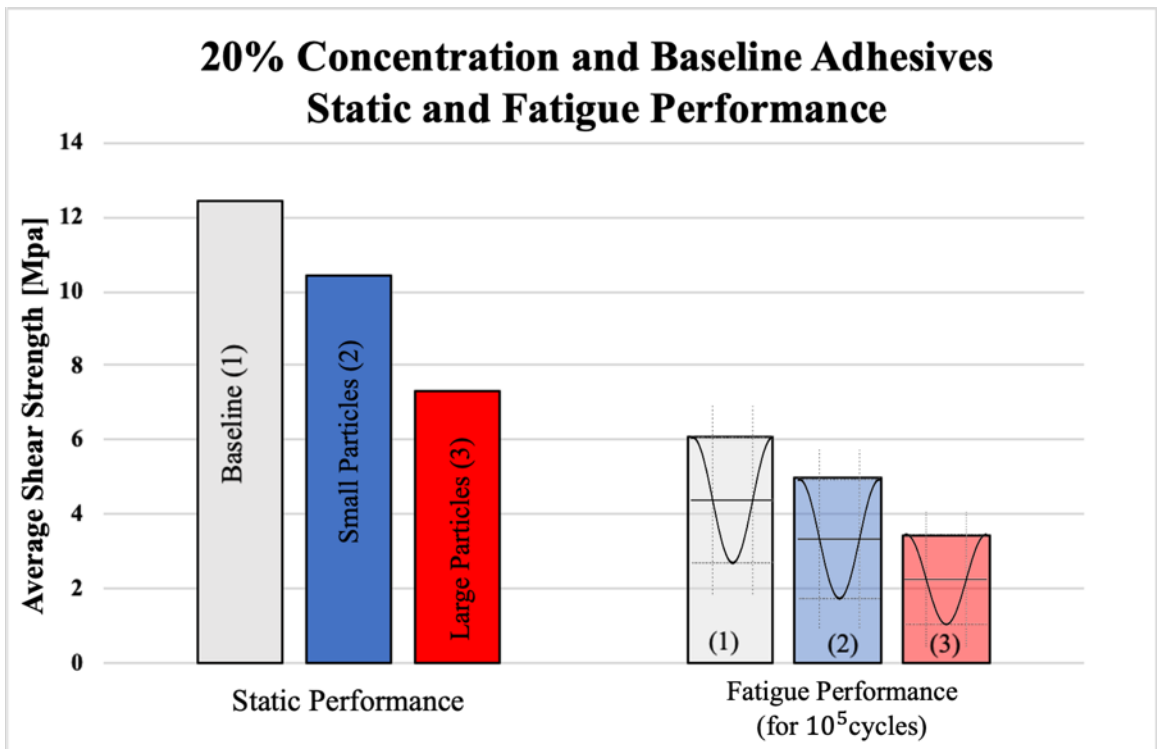


Figure 3.51 20% Concentration vs. Baseline Static and Fatigue Performance (at 10^5 cycles)

3.3 Debonding Test Data

In this section the results of the debonding tests are presented and analyzed. All the tests have been performed using a time limit of 10 minutes after which the sample has been considered survived to the test. In order to allow the workpiece to follow the desired temperature path, made by an initial ramp followed by a steady state condition, some fine tuning of the system is required. This is necessary because in induction heating processes the workpiece, the RF coil and the RF machine work like a system.

Must be stated that the steady state temperature has been set to be lower than 200°C, this choice is justified by the fact that at temperatures higher than that level the failure of the joint may be caused by the adhesive degradation and not by the effect of the particles inside the adhesive matrix. The parameters that can be used to achieve such temperature profile are the induction power and the frequency.

The induction power is responsible of the slope of the ramp and of the maximum temperature that is induced into the workpiece. The operation frequency is tuned changing the value of a series inductor present in the machine. This is necessary to operate stably at a frequency slightly below the resonance frequency of the system. A power level of 210W was used to bring the adhesive to temperature in 3 minutes. Once the target temperature was reached, the power was lowered to 150W to enter steady state conditions (Figure 3.52). Additionally, the optimal frequency was found to be equal to a range between 330-338kHz.

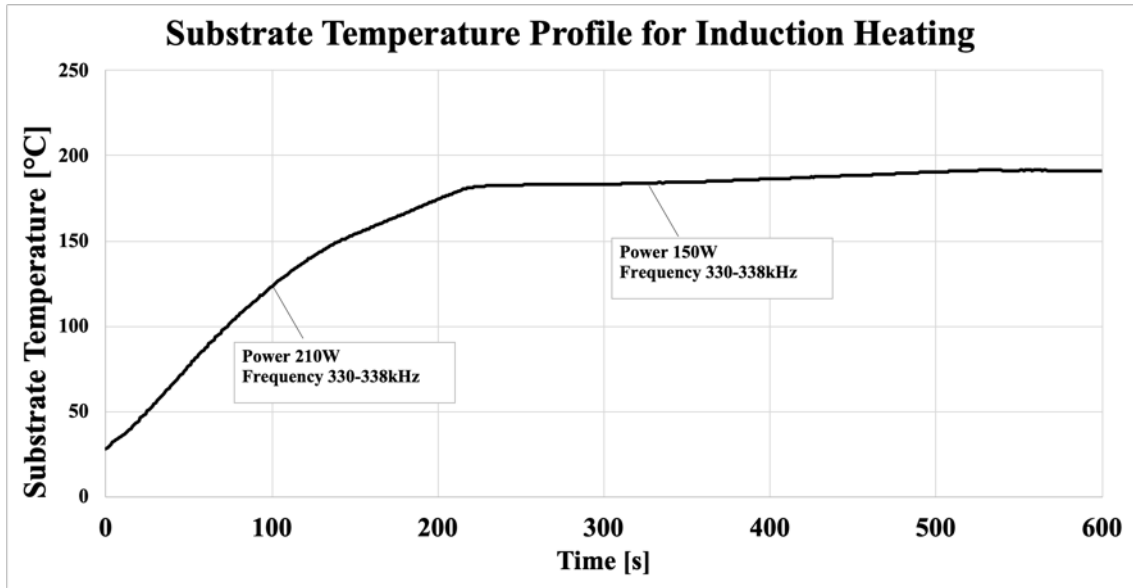


Figure 3.52 Substrate Temperature Vs Time

3.3.1 Effect of Particle Enrichment on Debonding Performance

The debonding time resulted to be highly improved by the particle enrichment, for both particles a decrease in the time and temperature to debond is registered for concentration of 10 and 20wt%. Figure 3.53 and Figure 3.54 show the temperature profiles for enriched adhesives, as well as the baseline adhesive joints. As compared to baseline joints, the debonding temperatures is significantly reduced to 91°C and 130° for the 10wt% and 20wt% additive concentration with large particle size (031DU40). The corresponding debonding temperatures for the smaller size particles are 90°C and 101°C, respectively. The baseline adhesive and the 5wt% enriched adhesives resulted to survive to the debondig test, these adhesives rare capable to maintain part of their mechanical strength when the peak temperature is 190°C.

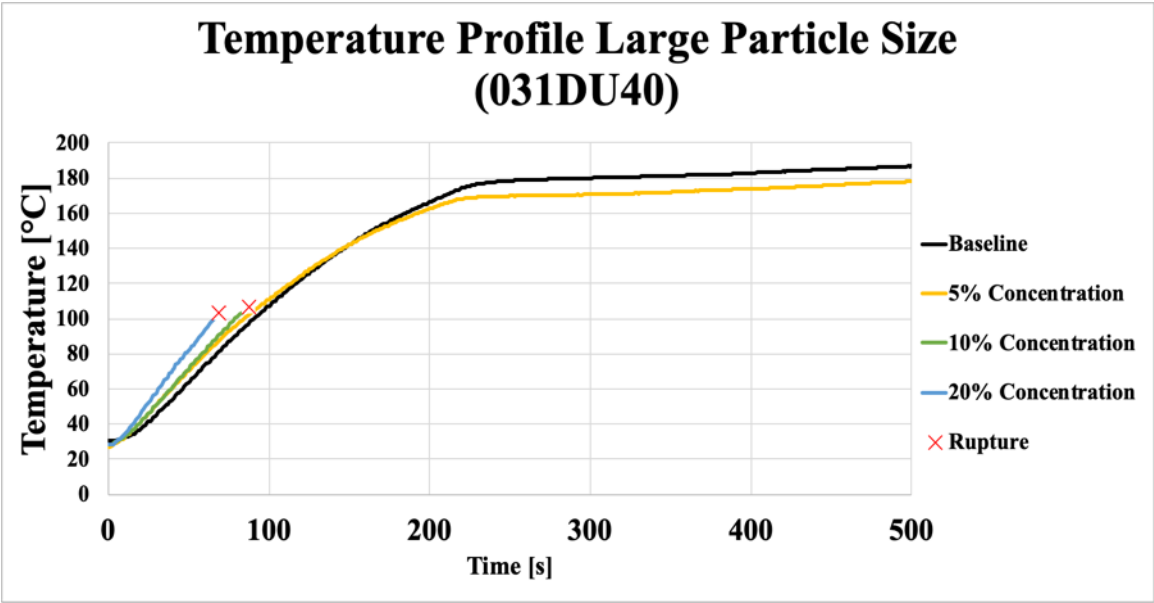


Figure 3.53 Substrate Temperature Profile for Varies Additive Concentration: Large Particles (031DU40)

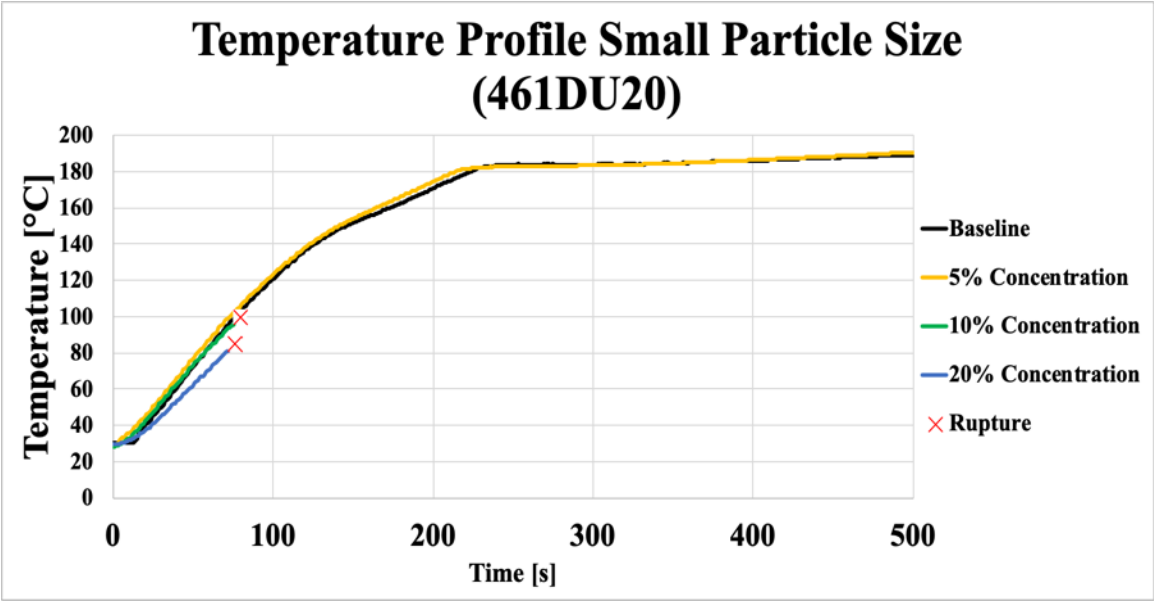


Figure 3.54 Substrate Temperature Profile for Varies Additive Concentration: Small Particles (461DU20)

This behavior suggests that the number of particles that are embedded in the adhesive matrix is not enough to allow the joint reversibility. The dependence between weight concentration and time to debond for different particles is shown in Figure 3.55. The debonding time is significantly improved when the particle concentration is 10 or 20%, and it ranges between 66 and 88 seconds for the bigger particle size (031DU40) and between 72 and 75 seconds for the smaller particle size (461DU20). Looking at the results, the particle enrichment is capable to improve the debonding capability of the adhesive.

Test data shows that additive concentration does not significantly affect the debonding time for the smaller particle size additive (461DU20). The lack of correlation between the smaller particle size concentration and the time to debond may be connected to the number of particles that are present inside the adhesive. Being the number of particles in the adhesive significantly higher when compared with the bigger particulate size and being the temperature at which the joint fails really close to the temperature at which the particles starts to expand, the joint separation can be caused by small changes in the particles volume. The debonding time of the adhesive enriched with the bigger particle size (031DU40) resulted to be highly dependent in the particle concentration. Doubling the concentration from 10 to 20wt% results in a 25% time reduction.

Test specimens made with different particle grades are characterized by different failure modes, as reported in Figure 3.55. The bigger particulate size (031DU40) results to be characterized by a partially cohesive and partially interfacial failure mode at 10wt% (CF/IF), while presents fully cohesive failure mode at 20wt% (CF). The smaller particulate size (461DU20) results to be characterized by interfacial failure mode for both 10 and 20wt% concentrations (IF).

3.3.2 Residual Strength Analysis

In this section are reported the results about the static performance of those specimens that survived the debonding test. Tests were halted after 10 minutes.

Failure did not occur for all samples made with the baseline adhesive or 5% additives concentration. The baseline adhesive retained 80% of its initial strength, and 20% performance loss is attributed to light thermal degradation. The modified adhesive joints experienced drastic load bearing capacity reduction with less than 50% of the initial strength left after that the samples were heated (Figure 3.56). The volumetric expansion of the particles is responsible for the static strength reduction.

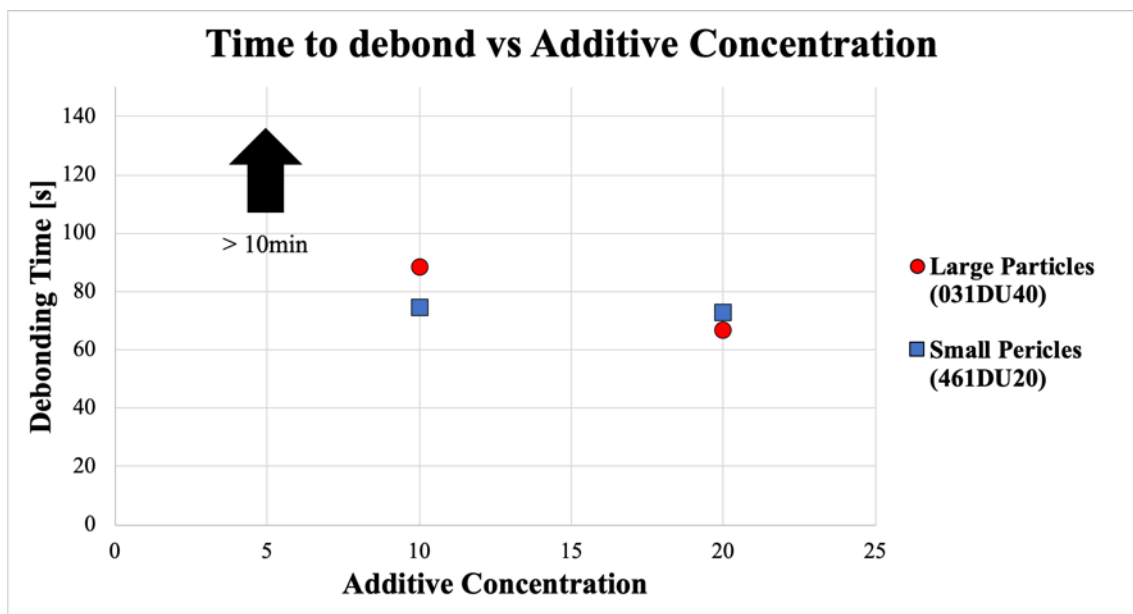


Figure 3.55 Time to Debond vs Additive Concentration

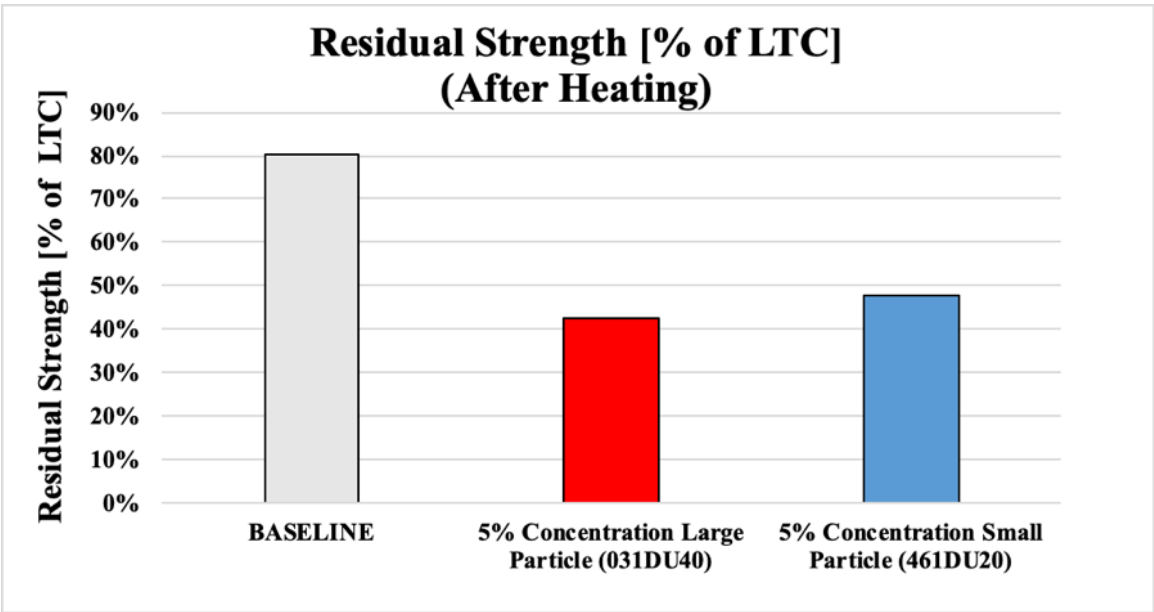


Figure 3.56 Residual Strength After Heating

CHAPTER FOUR.

CONCLUSIONS

In this study the effect of Thermally Expandable Particles (TEPs) additives to modify adhesive joint performance as well as meeting End of Life (EoL) environmental goals through debonding is investigated. Static, fatigue, and debonding performance are assessed for the use of various concentrations and particulate size of the additive to modify a commercially available epoxy-based adhesive. The use of additives caused a reduction in adhesive strength for both static and fatigue strength. The TEPs additive allowed to achieve the debonding of the substrates, using 10 or 20% concentration of additive-to-baseline adhesive. The study shows that the larger particles cause a constant decreasing trend in adhesive strength, while the strength of samples modified with smaller particles reached a saturation point after 10wt% concentration.

The time and temperature to debond were significantly decreased for particle concentrations of 10 and 20wt%, using both particle sizes. The debonding mechanics resulted to be drastically different for the two particles. The debonding time of the joints modified with bigger particle size (031DU40) were found to be highly dependent on the particle concentration with a 25% time reduction when the concentration was doubled from 10wt% to 20wt%. Suggested future work include more in-depth failure mode analysis of fractured adhesive joints with both baseline and TEPs modified adhesive.

APPENDIX A
COPYRIGHT PERMISSION LETTER

PERMISSION LETTER-THESIS STUDENTS ONLY

Giulio Piazza, 2743 Patrick Henry St. Apt.210, Auburn Hills, MI 48326

[07/01/2020]

Dear Dr. Zoepf:

I am completing a Master's thesis at Oakland University entitled: "Effect of Thermally Expandable particle additives on the Mechanical Adhesive Joint". I would like your permission to reprint in my thesis excerpt from the following:

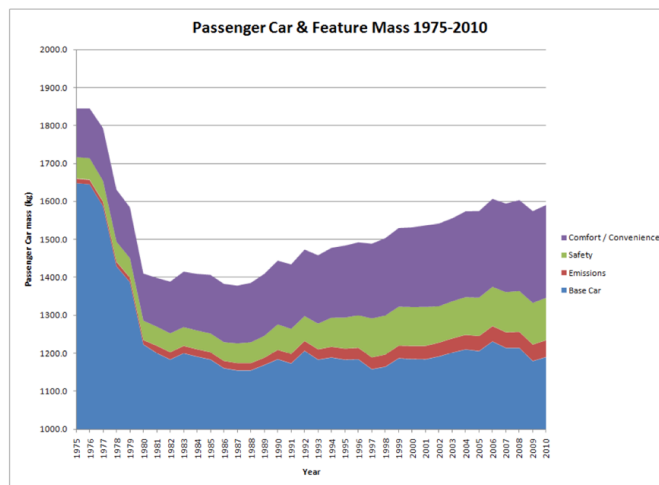


Figure 2-6: Mass of passenger cars 1975-2010 and weight attributed to Safety, Emissions and Comfort/Convenience features (Secondary mass included).

The excerpt to be reproduced is the Figure 2.6 used in your Thesis work on "Automotive Features: Mass Impact and Deployment Characterization" that I am intending to mention in the introductory chapter of my Thesis. The requested permission extends to any future revisions and editions of my thesis, including non-exclusive world rights in all languages. These rights will in no way restrict republication of the material in any other form by you or by others authorized by you. Your signing of this letter will also confirm that you own the copyright to the above-described material.

If these arrangements meet with your approval, please sign this letter where indicated below and return it to my email address giulio.piazza@oakland.edu. Thank you very much.

Sincerely,
Giulio Piazza



PERMISSION GRANTED FOR THE
USE REQUESTED ABOVE:



[Stephen M. Zoepf]

Date: 7/1/2020

REFERENCES

- [1] Modi, S., Stevens, M., and Chess, M., 2017, “Mixed Material Joining Advancements and Challenges”, Center for Automotive Research (CAR), Ann Arbor, MI.
- [2] Soo, V., 2018, “Life Cycle impact of different Joining decision on Vehicle Recycling”, Ph.D. Dissertation, The Australian National University, Canberra, Australia.
- [3] Zoepf, S., 2011, “Automotive Features: Mass Impact and Deployment Characterization”, Massachusetts Institute of Technology, Cambridge, MA.
- [4] Attanasio, M., 2018, “Effect of Electromagnetic-Sensitive particles addition on Reversibility Performances of Hot-melt Adhesives”, MS Thesis, Politecnico di Torino, Torino, Italy.
- [5] European Parliament and The European Council. Directive 2000/53/EC of the European Parliament and European Council of 18th September 2000 on End-Of-Life vehicles: “Off J Eur 2000:269(34);34-42”.
- [6] Lu, Y., Broughton, J., and Winfield, P., 2014, “A review of innovations in disbonding techniques for repair and recycling of automotive vehicle”, *The International Journal of Adhesion & Adhesives*, pp. 119-127.
- [7] Taub, A., 2006, “Technology Trends and Challenges in the 21st Century”, *Automotive Materials, MRS BULLETIN Volume 31*, pp. 336-343.
- [8] Brandon, D. and Kaplan, W., 1997, “Joining Processes, An Introduction”, ISBN 0-471-96488-3, Wiley-VCH, New York, Hoboken, NJ.
- [9] Ebnesajjad, S. and Landrock, A., 2014, “Adhesives technology handbook”, 3rd ed. William Andrew, Elsevier, London, UK.
- [10] Banea, M., Rosioara, M., and Carbas, R., da Silva, L., 2018, “Multi Material Adhesive Joints for Automotive Industry”, *Composite Part B, Volume 150*, pp.71-77.
- [11] Nassar, S., Wu, Z., Moustafa, K., and Tzlepis, D., 2015, “Effect of adhesive Nanoparticle Enrichment on Static Load Transfer Capacity and Failure Mode of Bonded Steel Magnesium Single Lap Joints”, *ASME, Volume 137*, DOI, 10.1115/1.4030081.
- [12] Ciardiello, R., Martorana, B., Lambertini, V., Brunella, V., 2017: “Iron-based Reversible adhesives: Effect of particle size on mechanical properties”, *Institution of Mechanical engineers, Vol. 232(8) 1446–1455, IMechE*, DOI: 10.1177/0954406217736552.

- [13] Banea, M., da Silva, L., Carbas, R., 2015: “Debonding on command of Adhesive joints for the automotive industry”, *International Journal of Adhesion & Adhesive*, Volume 59, pp. 14-20.
- [14] Veloso, R., 2015, “Debonding on command of Adhesive joints for the automotive industry”, MS Thesis Instituto Politecnico de Viseu, Viseu, Portugal.
- [15] Banea, M., da Silva, L., Carbas, R., Barbosa, A., Viana, G., 2018, “Effect of the water on the behavior of adhesives modified with thermally expandable particles”, *The International Journal of Adhesion & Adhesives*, Volume 91, pp. 823-840.
- [16] Hutchinson, A., Winfield, P., McCurdy, R., 2010: “Automotive Material Sustainability through Reversible Adhesives”, *Advanced Engineering Materials*, 12, N°7, pp. 646-652.
- [17] Spezzanti, G., Koricho, E., Belingardi, G., Verna, E., Matorana, B., Ngabang, B., Simioli, M., and Brunella, V., “New Joining Technologies with Hot-Melt adhesive modified with electromagnetic sensitive particles”, Laboratories preparation to industrial validation. Politecnico di Torino, Dipartimento di Ingegneria Meccanica e Aerospaziale, Torino, Italy.
- [18] ASTM, 2011: “Annual Book of ASTM Standards, section fifteen, General Products, Chemical, Specialties, and End use Products”, ASTM Volume 15.06., Adhesives
- [19] BSI, 1976: “Guide to statistical interpretation of data”, BS 2864, London.
- [20] ASTM, 1998: “ASTM Practice for statistical analysis of linear or linearized stress-life (S-N) and strain-life (ϵ -N) fatigue data', ASTM E-739-91, West Conshohocken, PA.
- [21] Schneider, C., Maddox, S., Park, G., and Abington, G., 2003: “Best Practice Guide on Statistical Analysis of Fatigue”, 13604.01/02/1157, Cambridge, UK.
- [22] Rodríguez, R., Sollero, P., and Rodrigues, M., 2011, “Stress Analysis and Failure Criteria of Adhesive Bonded Single Lap Joints”, 21st International Congress of Mechanical Engineering by ABCM, Natal, RN, Brazil, Annual Book of ASTM Standards, 13083-970, Campinas, Brazil.

- [23] Sanders, W., Gibson, L., 31 July 2002: "Mechanics of hollow sphere foams", Department of Materials Science and Engineering, Massachusetts Institute of Technology, A347 8-135, 77 Massachusetts Avenue, Cambridge, MA 02139, USA.
- [24] Pauchard, L., and Rica, S., 1998: "Contact and compression of elastic spherical shells: the physics of a ping-pong ball", Unité de Recherche associée au CNRS 1306, Associée aux Universités des Paris VI et VII, 24 rue Lhomond, 75231 Paris Cedex 05, France.
- [25] Shorter, R., Smith, J., Coveney, V., and Busfield, J., 2010, "AXIAL COMPRESSION OF HOLLOW ELASTIC SPHERES", Journal of Mechanics and Materials Structures, Volume 5, N° 5, pp. 693-705.